DEGREE PROJECT IN MECHANICAL ENGINEERING,
SECOND CYCLE, 30 CREDITS
STOCKHOLM, SWEDEN 2020

Comparison of Control Approaches for Formation Flying of Two Identical Satellites in Low Earth Orbit

HASAN BASARAN

KTH ROYAL INSTITUTE OF TECHNOLOGY
SCHOOL OF ENGINEERING SCIENCES

Comparison of Control Approaches for Formation Flying of Two Identical Satellites in Low Earth Orbit

Hasan Başaran

***Abstract*—Formation flying of satellites describes a mission in which a set of satellites arrange their position with respect to one another. In this paper, satellite formation flying guidance and control algorithms are investigated in terms of required velocity increment Δv, and tracking error for a Chief/Deputy satellite system. Different control methods covering continuous and impulsive laws are implemented and tested for Low Earth Orbit (LEO). Sliding Mode, Feedback Linearization and Model Predictive Controllers are compared to an Impulsive Feedback Law which tracks the mean orbital element differences. Sliding Mode and Feedback Linearization controllers use the same dynamic model which includes Earth Oblateness perturbations. On the other hand, Model Predictive Control with Multi-Objective Cost Function is based on the Clohessy–Wiltshire equations, which do not account for any perturbation and do not cover the eccentricity of the orbit. The comparison was done for two different missions both including Earth Oblateness effects only. A relative orbit mission, which was based on the Prisma Satellite Mission and a rendezvous mission, was implemented. The reference trajectory for the controllers was generated with Yamanaka and Ankersen's state transition matrix, while a separate method was used for the Impulsive Law. In both of the missions, it was observed that the implemented Impulsive Law outperformed in terms of Δv, 1.2 to 3.5 times smaller than the continuous control approaches, while the continuous controllers had a smaller tracking error, 2 to 8.3 times less, both in terms of root mean square error and maximum error in the steady state. Finally, this study shows that the tracking error and Δv has inversely proportional relationship.**

***Index Terms*—Aerospace, Chief, Control, Deputy, Feedback Linearization, Follower, Formation Flight, Fuel Consumption, Guidance, Leader, Model Predictive Control, Relative Orbit, Rendezvous, Sliding Mode.**

***Abstract*—Sammanfattning - Formationsflygning av satelliter innebär att en grupp satelliter flyger tillsammans och anpassar sina relativa lägen i förhållande till varandra. I detta examensarbete studerades regleralgoritmer för formationsflygande satelliter med fokus på bränsleförbrukning och positionsavvikelse genom "Chief & Deputy"-metoden. Olika reglermetoder har studerats, t.ex. Sliding Mode- och Feedback Linearization-reglering för formationsflygningsfall i låg jordbana med J_2-störning samt en Model Predictive-reglering för fall med relativ rörelse baserad på Clohessy-Wiltshire-ekvationerna. Vidare studerades en reglermetod baserad på impulsframdrivning. De fyra reglermetoderna implementerades på två olika rymduppdrag. Först ett uppdrag baserat på Prisma-satelliterna för två satelliter i relativ omloppsbana och sedan ett Rendezvous-uppdrag. Referensbanan för alla reglermetoder, utom för implusmetoden, har tagits fram med hjälp av Yamanakas och Ankersens tillståndsmatris. Resultaten visar att den implementerade impulsmetoden presterar bättre med avseende på bränsleförbrukning, medan de kontinuerliga reglermetoderna producerade mindre relativ positionsavvikelse, både med avseende på kvadratiskt medelvärde och maximalt värde.**

I. Introduction

FORMATION flying has been identified as critical technology for the 21st century by NASA, for astrophysical and Earth science missions. Formation flying missions of satellites involves the autonomous cooperation of satellites with each other to maintain the desired formation, an example can be seen in Fig. 1, which depicts the Mango and Tango satellite, [1]. The main satellite, Mango, is the one with solar panels wide open and it arranges its position with respect to the other satellite, Target, or simply Tango. In this paper a Deputy/Chief or Follower/Leader approach will be used. The Deputy is the main satellite, which arranges its own position with respect to the Chief. Which if referenced to Fig. 1 makes Mango the Deputy, and Tango the Chief.

A paradigm shift is emerging in spacecraft engineering from single and large multi-functional satellites towards cooperating groups of small satellites, forming a constellation, cluster or formation. This will enable innovative approaches in areas like Earth observation, scientific exploration or telecommunication. One of the advantages of such a system design is that if one of the satellites is lost due to a malfunction or environmental conditions, then the rest of the satellites can cover the mission of the lost satellite. In addition to that, the lost satellites, if required and without pausing the mission, can be replaced, depending on the importance of the lost satellite. Replacing a lost satellite is a simpler solution than repairing a subsystem of a big satellite. Furthermore, the physical size limits from having one single body can be avoided by allocating the mission into numerous smaller bodies. This shift from single large multi functional satellites to many small body satellites can be seen from the European Space Agency's (ESA) Proba-3 mission set to launch in 2022. Which is a sun chronograph mission in a Highly Elliptical Orbit (HEO), which utilises smaller body satellites to achieve an accuracy that would not have been possible with a single satellite mission [2]. In addition to this, combination of the TanDEM–x and TerraSAR–x missions is utilising a two satellite system with Synthetic Aperture Radar in order to capture the digital elevation of Earth and is completing the scientific mission better than if it was a single satellite. [3]. However, the mission becomes more complex when using formation flying because the mechanics in space are very different to the mechanics of everyday life. If a vehicle is desired to go faster in any direction, it would use its boosters in that direction in "Earth Physics". For example, a jet aircraft would simply increase

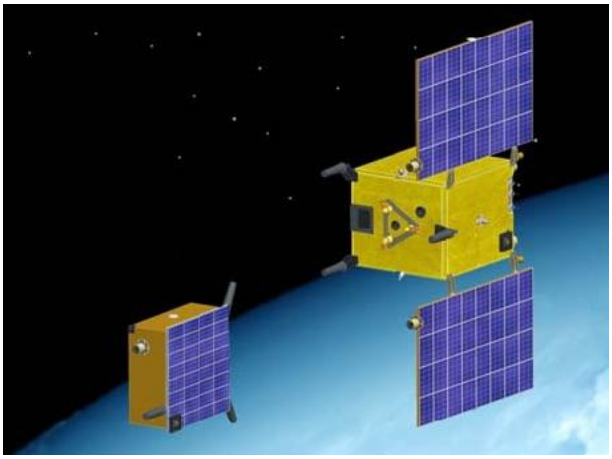

Fig. 1. An Example of Formation Flying Satellite, from Prisma Mission, taken from [1]

the thrust generated by its engine in the direction of flight, increasing the velocity of the aircraft. However, in space this story changes a little. If a satellite is required to go faster, then the best method is to first slow it down. This will lead to a decrease in its altitude and semi major axis, and in return the orbital period will decrease. The orbital period is proportional to the semi-major axis', which means it will make an orbit faster than before. A specific and an interesting case would be rendezvous mechanics. More specifically, lets assume two identical satellites having almost identical orbits with a true anomaly difference only, i.e. they only have in-plane distance differences, one leads the other one, and assume both of the orbits are circular. For this scenario let the trailing satellite be called Deputy, and the other satellite called Chief. Chief has no control application, hence, the Deputy must close the difference itself. If daily life logic is applied, to close the distance, the Deputy satellite would apply tangential thrust towards the Chief. However, the effect of it is limited. Initially, the tangential thrust will allow the Deputy Satellite to close the gap, however, in the long run this will cause the Deputy satellite to gain altitude, and to lose velocity. Furthermore, the period of the Deputy will be increased which will cause it to fall further behind. In other words, the overall effect is that the applied thrust will increase the semi-major axis of the orbit, causing the deputy to fall even more behind of the chief in the long run, even though the gap was closed initially. This illustrates that taking an everyday approach to Formation Flying does not necessarily work. Furthermore, keeping the relative motion bounded is another problem in Formation Flying because of the differences in orbit parameters, such as semi major axis, and perturbations. Numerical simulations show that if two satellites have 1 meter difference in altitude, this will cause approximately 150 meter tangential difference in 1 day for a satellite in circular orbit at 400 km altitude without any perturbation. Furthermore, if satellites are both in sun synchronous orbits with 1 degree of inclination difference at an altitude of 600 km, it will take 8 days to have 1 degrees of right ascension of the ascending node (RAAN) difference, 11 days for 1 degree of argument of periapsis difference and 18 days to have 1 degree of mean anomaly difference due to J_2 perturbation only. That means, if the relative position is not controlled, it will most definitely diverge. To solve that non-intuitive relative position arrangement the formation flying problem must be handled carefully, such as designing controllers for that purpose.

Alongside this, space debris is becoming a hazardous problem due to the risk of collisions occurring in between the debris itself. Recent research shows that even if launches into Low Earth Orbit (LEO), an orbit with altitude ranging from 200–300 km to 1600 km [4] and the most densely Debris populated area [5] is stopped, the mutual collisions in between debris will worsen the situation [5]. In other words, the particles or debris in LEO can damage the satellites due to increase in collision risks. For that purpose, the importance of formation flying with debris, or the importance of rendezvous with it in order to remove debris is a vital issue.

The Deputy must follow the Chief as planned with high accuracy, in order to achieve scientific or economic gains. In addition, it is necessary to actively reduce the number of debris and prevent collisions from getting out of control. Therefore, in this study, the effects of different relative position control methods on fuel consumption and tracking performance was investigated.

A. Brief History

Multi-satellite missions can be divided into two categories, Formation Flying and Constellations. The distinction is that in Formation Flying missions the satellites should arrange their position with respect to each or one satellite. Formation flying missions can be tracked since the beginning of 21st century. As these kinds of missions are relatively new, nearly 10 out of 25 is focused on mission *Type 1*, which is technology demonstration, and can be seen in Tab. I. The second most common type of mission is *Type 2* which is Earth Observation or Earth Science missions. *Type 3* is the least common one, which focuses on Astrophysics or other planetary missions. Afternoon Train is a formation flying mission in sun-synchronous orbit at an altitude of 705 km, where the main mission is observation of Earth. The satellites in this constellation follows the same "track" [10]. In the Gravity Recovery and Climate Experiment, named GRACE, a formation flying mission in LEO in which the satellites observe the anomalies of Earths gravity field since their launch at 2002 until 2017 [33]. Cluster II, is a formation flying mission in HEO, where the satellites form a tetrahedral, and study the magnetosphere of the Earth [34]. The Tab I generally focuses on non-CubeSat type of missions, for CubeSat specific missions, the reader is referred to [35], which covers 39 different small satellite missions, mostly CubeSat, which are either formation flying or constellation missions.

B. Mission Requirements

This part covers the orbit properties, initial conditions of the satellites and the relative orbit requirements.

In 2019, 61 launches were aimed at LEO. 36 launches were aimed at higher altitude orbits such as Geosynchronous

TABLE I
PREVIOUS MISSIONS

Mission Name	Satellite Number	Launch Year	Altitude	Mass [kg]	Mission Status	Mission Type
Operational Missions						
Cluster II [6]	4	2000	19 000 km × 119 000 km	1,180	Still Operational	2
SNAP-1 [7], [8]	1+1	2000	700 km LEO	6.5	Still Operational	1
GRACE [9]	2	2002	500 km LEO	487	Deactivated	3
A-train [10]	4	2002	705 km LEO	120–2,934	Partial Deactivation	2
Essaim [11]	4	2004	640 km LEO	120	Deactivated 2010	1
XSS-11 [12]	1+1	2005	840 km LEO	100	Deactivated 2013	1
Orbital Express [13]	2	2007	490 km LEO	224–1,090	Deactivated 2007	1
FASTRAC [14]	2	2010	640 km LEO	27	Deactivated	1
TDX [15]	2	2010	515 km LEO	1,340	Still Operational	2
Swarm [16]	3	2013	460 km to 530 km LEO	240	Still Operational	2
MMS [17]	4	2015	2,550 km × 152,900 km	1,360	Still Operational	2
Lone Star-2 [18]	2	2016	400 km LEO	4.2–54.9	Mission Failure	1
GRACE FO [19]	2	2018	490 km LEO	600	Still Operational	2
DSLWP [20]	2	2018	200 km × 9,000 km Lunar Orbit	47	Deactive	2
Proba-3 [21]	2	2022	600 km × 60,530 km	220–340	Not Operational	1
Cancelled Missions						
TechSAT21 [22]	3	N/A	550 km	100	Cancelled	2
Orion/Emerald [23]	3	N/A	LEO	15–35	Cancelled	1
FUEGO [24]	12	N/A	700 km	N/A	Cancelled	2
MAGNAS [25]	28	N/A	450 to 550 km	0.5–210	Cancelled	2
ION-F [26], [27]	3	N/A	370 km	10–15	Cancelled	1
MAX [28]	2	N/A	44,000 km × 253,000 km	570–850	Cancelled	3
XEUS [29]	2	N/A	L2 Lagragian Point	1,500–2,000	Cancelled	3
APIES [30]	19	N/A	Astroid Belts	45	Cancelled	3
Gemini [31]	2	N/A	500-700 km	80–100 kg	Cancelled	1
Darwin [32]	5	N/A	L2 Lagragian Point	N/A	Cancelled	3

Equatorial Orbit (GEO) [36]. Similarly, since 2014 the number of launches to LEO was higher than that to higher altitudes, which makes LEO a highly popular [37]–[41]. With this in mind the orbit of the satellite under investigation in this work is chosen to match that of the Prisma satellite's orbit, which is a LEO orbit with an approximate altitude of 700 km [42].

The relative orbit that was chosen is based on [42], [43]. In both of the references, the relative orbit in terms of orbital element differences are given for the Prisma Mission. The relative orbit for this study was given in Fig. 2. In this study, a perfect ellipse that has its semi-minor axis lying on the z axis, and semi-major axis lying on x axis was chosen. However, in the Prisma mission, the semi-minor axis of the relative orbit in x-z plane is not located on z axis.

The x axis denotes the radial direction, y axis denotes the tangential direction, and the z axis denotes the out of plane direction. As can be seen the in-plane relative orbit is an ellipse with a semi-major axis of 1 km, with a semi-minor axis of 500 m. The out of plane relative orbit is an ellipse with a semi-major axis of 500 m and a semi-minor axis of 300 m.

A rendezvous scenario to test the capabilities of the controllers was also selected to show that the designed controllers can be used in order to rendezvous with debris.

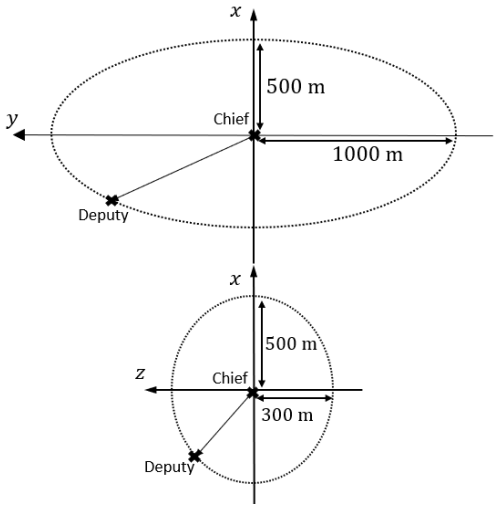

Fig. 2. The relative orbit description of the Mission based on [42], [43]

C. Vehicle

The planned vehicle that is to be used is the Swedish Space Corporation's Prisma Satellite system. Prisma consists of 2 vehicles, namely MAIN and TARGET. As the name suggests, the TARGET will be the vehicle which MAIN will arrange its position according to. However, it must be noted that both of the vehicles in this thesis will be identical with the MAIN vehicle. In other words, the Deputy and Chief will be the same as MAIN. The required specifications for the simulation purposes are shared in Tab. II.

TABLE II
FEATURES OF THE VEHICLES

	Dry Mass [kg]	Fuel Mass[kg]	I_{sp} [s]	Thrust [N]	Drag Coeff	Drag Area
Prisma [44]	143.4	11	236.8	1	2.5	1.3
C. Gas [45]	143.4	11	70	0.04	2.5	1.3

The first row of Tab. II is suitable for high-thrust applications, or impulsive controlling methods. To check the low

thrust applications, a cold gas system similar to that used in the GRACE mission was implemented with the same fuel levels as the High Thrust system and is described in the second row of Tab. II.

While the fuel mass and the structural masses for the low thrust, i.e. cold gas and high thrust cases are the same, since, the $\mathrm{I_{sp}}$, specific impulse, of the cold gas system was lower than that of Hydrazine system, that might require more fuel than that of Prisma. This could lead to errors in the analysis if the fuel consumption in terms of mass was compared. To solve that issue, the comparison was based on Δv, where Δv denotes the change in velocity consumption of the systems.

D. Scope of Thesis

In this thesis the effect of various control schemes on the fuel consumption was investigated. For that reason, the positions of each satellite was known to each other perfectly and ideally, i.e. there is no sensor noise, or an estimation algorithm. Furthermore, thrust misalignment or similar effects were ignored. The system is considered to work in a perfect manner. In addition, the system was taken as a point mass, and it was assumed that the attitude control system can arrange the satellite into the desired attitude to achieve the required thrust command produced by the formation keeping controller.

This thesis focused on the initial establishment of the relative orbit. In other words, there are scenarios where there will be error in the beginning, and the controller tries to establish the desired relative position.

In this study, only the perturbations due to the oblateness of Earth were included. For this purpose, GRACE Gravity Model 03, the GGM03S, was used. The reason behind that in the altitude investigated (approximately 700 km) the most dominant perturbation is due to Earth oblateness effects [46]. The second most dominant perturbation is drag force, due to the atmosphere was ignored [46]. Reference [47] states that if the designs of each satellite is similar in terms of aerodynamics, the decay rate of both of the orbits will be similar.

E. Thesis Structure

The thesis consists of Section II Background, where the relevant background knowledge will be explained, Section III Method, the method of the analysis and related research will be explained, and followed by Section IV Results, Section V Discussion and Section VI Conclusion with Section VII Future Work.

II. Background

A. Essentials of Astrodynamics

Primary Mass: Generally, in multi-object systems, which is gravitationally bound, main physical body is called primary.

Periapsis: The closest point to the primary on the orbit of the gravitating mass is called Periapsis.

Vernal Equinox: The date when the time lengths of day and night are almost equal and the sun passes through celestial equator of earth and moves toward north. Vernal Equinox is the time when the spring starts and it is used for inertial calculations and measurements.

Orbital Plane: The orbital plane of a gravitating mass is the geometric plane which covers the orbit of that mass.

B. Coordinate Frames

1) ECI: This frame is called Earth-Centered Inertial Frame. Origin of this frame is located at the center of the Earth. The $\hat{\boldsymbol{x}}$ axis points toward the Vernal Equinox, $\hat{\boldsymbol{z}}$ is normal to the fundamental plane and points toward the geographic north pole, and $\hat{\boldsymbol{y}}$ completes the right hand rule. This frame will be denoted as I.

2) LVLH: The Local Vertical Local Horizontal Frame, is centered at the spacecraft. The unit vector $\hat{\boldsymbol{x}}$ is pointing radially outwards from the Earth. The $\hat{\boldsymbol{z}}$ axis is perpendicular to the orbital plane, and the $\hat{\boldsymbol{y}}$ axis completes the right hand rule. This frame, overlaps with the Hill frame, and if the origin of this frame is located at Chief, will be denoted as C, if on Deputy, then will be denoted as D.

3) DCM: Direction Cosine Matrix (DCM) is a matrix that transforms the vector written in one frame to another frame. Defining the unit vector set $\boldsymbol{c}$ and $\boldsymbol{n}$, where they are orthogonal and right handed, shared in Eq. (1).

$$\boldsymbol{c} = \begin{bmatrix} \boldsymbol{c}_1 \\ \boldsymbol{c}_2 \\ \boldsymbol{c}_3 \end{bmatrix} \quad \boldsymbol{n} = \begin{bmatrix} \boldsymbol{n}_1 \\ \boldsymbol{n}_2 \\ \boldsymbol{n}_3 \end{bmatrix} \tag{1}$$

where $\boldsymbol{c}$ and $\boldsymbol{n}$ are 3 by 3 matrices. They are both resolved in the ECI frame. $\boldsymbol{c}$ is the unit vectors of the Chief LVLH frame resolved in ECI and $\boldsymbol{n}$ is the unit vectors of the ECI resolved in ECI frame. Defining The α_{ij} as the angle from $\boldsymbol{n}_j$ to $\boldsymbol{c}_i$ where i and j represents the axes, and $\boldsymbol{v}^{\mathrm{C}}$ is a vector resolved in Chief LVLH frame and $\boldsymbol{v}^{\mathrm{I}}$ is the same vector resolved in ECI frame, then the transformation can be expressed as shared in Eq. (2)

$$\boldsymbol{v}^{\mathrm{C}} = \boldsymbol{C}_{\mathrm{CI}} \boldsymbol{v}^{\mathrm{I}} \tag{2}$$

and $\boldsymbol{C}_{\mathrm{CI}}(i,j) = \cos(\alpha_{ij})$ [47].

C. Vector Notation

The position vectors was shown as $\boldsymbol{r}^{\mathrm{I}}_{\mathrm{CI}}$, which means, the position of Chief frame, which is denoted as C, with respect to the ECI, I, resolved in the ECI frame. So superscripts show the frame which the vector was resolved, subscripts show the direction of the vector. Direction Cosine Matrix (DCM), from ECI to Chief's LVLH is $\boldsymbol{C}_{\mathrm{CI}}$.

The derivative notation is $\mathrm{d_I}(.)/\mathrm{d}t$, which means, the time derivative of a vector with respect to the ECI frame.

D. Orbital Elements

1) Classical Orbital Elements: The classical orbital element set, also known as Keplerian Elements, is consisting of six elements which describes the absolute motion of an satellite around a primary. It consists of a, semi-major axis, e,

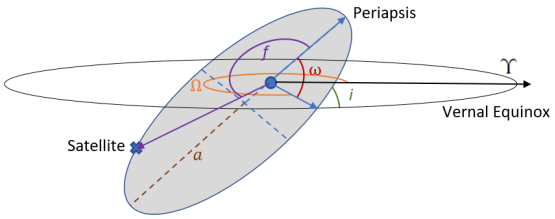

Fig. 3. Graphical illustration of orbital elements

eccentricity, i, inclination, Ω, right ascension of the ascending node, ω argument of periapsis and, M mean anomaly. The orbital elements, except, M can be seen in Fig. 3.

$$\mathbf{oe} = \{a, e, \omega, \Omega, i, M\}$$

For the unperturbed motion, all the elements except the mean anomaly is constant. The mean anomaly can be thought as the angle in between the periapsis and the location of the satellite if the orbit was circular. For the unperturbed motion, the mean anomaly changes with mean motion, $n = \sqrt{\mu/a^3}$, where μ is the standard gravitational constant of Earth.

Furthermore, there is true anomaly, which is an angle that locates the satellite in the orbit from the periapsis. In other words, it is the angle in between the vector pointing the satellite and periapsis as seen from the main focus of the ellipse. It is shown in Fig. 3 and denoted by f.

The last anomaly that will be covered is eccentric anomaly, E, taken from [48], which is the angle between the perifocal unit vector and the radius of a bounding circle at a point normal to the line of apsides at a given true anomaly.

The Keplerian equation, which creates the relation between the mean anomaly and eccentric anomaly is

$$M = E - e \sin E \tag{3}$$

Equation (3), has no closed-form solution for E when M is given. In this paper, Newton–Raphson iteration methods are used to transform anomalies, which can be found in [49]. The relation in between the true anomaly and the eccentric anomaly is

$$\cos f = \frac{\cos E - e}{1 - e \cos E} \tag{4}$$

The semi-latus rectum, p of the orbit, the magnitude of the position vector from the center of the Earth r at epoch time, period of the orbit and the magnitude of the angular moment of the vehicle h, in terms of orbital elements or in terms of each other are

$$p = a(1 - e^2) \tag{5}$$

$$r = \frac{p}{1 + e \cos f} \tag{6}$$

$$T = 2\pi\sqrt{\frac{a^3}{\mu}} \tag{7}$$

$$h = \sqrt{p\mu} \tag{8}$$

2) Differential Orbital Elements: The relative motion can both be described by Cartesian Coordinate system and orbital elements. In order to obtain the relative orbit with Cartesian Coordinate System, the differential equations for the relative motion should be solved. Of course there exist analytical solutions for the differential equations under certain assumptions, i.e. for Clohessy–Wiltshire equations shared in Eq. (46), the Chief orbit must be circular, however, they are not convenient to determine the instantaneous geometry of the relative orbit. Hence, for any of the orbital element sets, the differential orbit elements were obtained as,

$$\delta\mathbf{oe} = \mathbf{oe}_d - \mathbf{oe}_c \tag{9}$$

where sub-index d denotes the Deputy and c denotes the Chief, and $\mathbf{oe}$ denotes the orbital elements. Given $\delta\mathbf{oe}$ and $\mathbf{oe}_c$ one can find the position of the deputy by using Eq. (9).

3) Mean Orbit Elements: Under the influence of perturbations, the motion in orbital plane is divided into three, Long Periodic Motion, Short Periodic Motion and Secular Motion. The secular motion in general tends to increase with time while other motions are "relatively" bounded. The mean orbital elements covers the secular drift dynamics rather than periodic motions. Let $\mathbf{oe}(t)$ be a classical orbital element set, the osculating orbital element set is the time-dependent orbital element set, which corresponds to the Keplerian orbit which the body would follow if at time t the perturbations were cancelled [48]. The general relation can be expressed as shared in Eq. (10).

$$\dot{\mathbf{oe}}_{\text{osc}}(t) = \bar{\mathbf{oe}}(t) + \Delta\mathbf{oe}(t) \tag{10}$$

where $\bar{\mathbf{oe}}$ denotes the mean orbital elements, and the $\Delta\mathbf{oe}(t)$ corresponds to the changes in the orbital elements due to perturbations, and can be divided into long periodic and short periodic while the secular drift and the mean motion terms are handled in mean orbital elements.

The mean orbital element is introduced by Kozai [50], in 1959, to research the effect of the perturbation, specifically the effect of the gravity perturbations, on mean orbital elements. Furthermore, Brouwer [51], worked on mean Delaunay Variables and created a transformation to corresponding osculating elements . Then, Walter [52] offered an iterative solution from osculating orbital elements to mean orbital elements with using Brouwer Theory. Lydane, also worked on Brouwer's work to cover small inclinations and eccentricities [53].

E. Coordinate Transformations

1) ECI to LVLH: Let $\hat{\boldsymbol{u}}_x$,$\hat{\boldsymbol{u}}_y$,$\hat{\boldsymbol{u}}_z$ denote the unit vectors of the LVLH frame, resolved in ECI. Let C denote the Chief, then the unit vectors, by the definition of Hill frame, are shared in equation set shared in (11).

$$\hat{\boldsymbol{u}}_x^{\text{I}} = \frac{\boldsymbol{r}_{\text{CI}}^{\text{I}}}{||\boldsymbol{r}_{\text{CI}}^{\text{I}}||} \tag{11a}$$

$$\hat{\boldsymbol{u}}_z^{\text{I}} = \frac{\boldsymbol{r}_{\text{CI}}^{\text{I}} \times \boldsymbol{v}_{\text{CI}}^{\text{I}}}{||\boldsymbol{r}_{\text{CI}}^{\text{I}} \times \boldsymbol{v}_{\text{CI}}^{\text{I}}||} \tag{11b}$$

$$\hat{\boldsymbol{u}}_y^{\text{I}} = \hat{\boldsymbol{u}}_z^{\text{I}} \times \hat{\boldsymbol{u}}_x^{\text{I}} \tag{11c}$$

The DCM from ECI to Chief's LVLH is

$$\boldsymbol{C}_{\mathrm{CI}} = \left[\hat{\boldsymbol{u}}_x^{\mathrm{I}}, \hat{\boldsymbol{u}}_y^{\mathrm{I}}, \hat{\boldsymbol{u}}_z^{\mathrm{I}}\right]^{\mathrm{T}} \tag{12}$$

The position transformation from ECI to LVLH frame is by application of the DCM as shown in the Eq. (13).

$$\boldsymbol{r}_{\mathrm{DC}}^{\mathrm{C}} = \boldsymbol{C}_{\mathrm{CI}} \boldsymbol{r}_{\mathrm{DC}}^{\mathrm{I}} \tag{13}$$

Since the LVLH frame is a rotating frame, unlike ECI, velocity term requires the Transport Theorem as shown in Eq. (14)

$$\boldsymbol{v}_{\mathrm{DC}}^{\mathrm{C}} = \boldsymbol{C}_{\mathrm{CI}} \boldsymbol{v}_{\mathrm{DC}}^{\mathrm{I}} + \boldsymbol{r}_{\mathrm{DC}}^{\mathrm{C}} \times \boldsymbol{\omega}_{\mathrm{CI}}^{\mathrm{C}} \tag{14}$$

where $\boldsymbol{\omega}_{\mathrm{CI}}^{\mathrm{C}}$ is the angular velocity of the LVLH frame of Chief with respect to ECI frame, and equal to $\boldsymbol{\omega}_{\mathrm{CI}}^{\mathrm{C}} = [0, 0, h/||\boldsymbol{r}_{\mathrm{CI}}||^2]^{\mathrm{T}}$.

The opposite transformation is given in Eq. (15).

$$\boldsymbol{r}_{\mathrm{DC}}^{\mathrm{I}} = \boldsymbol{C}_{\mathrm{CI}}^{-1} \boldsymbol{r}_{\mathrm{DC}}^{\mathrm{C}} \tag{15a}$$

$$\boldsymbol{v}_{\mathrm{DC}}^{\mathrm{I}} = \boldsymbol{C}_{\mathrm{CI}}^{-1} (\boldsymbol{v}_{\mathrm{DC}}^{\mathrm{C}} - \boldsymbol{r}_{\mathrm{DC}}^{C} \times \omega_{\mathrm{CI}}^{\mathrm{C}}) \tag{15b}$$

2) Mean and Osculating Orbital Element Transformation: Brouwer created his theory in order to transfer from mean Delaunay variables to corresponding osculating elements. He divides the Hamiltonian into two parts, $\mathcal{H}_0$ as the nominal Hamiltonian which covers the two body motion, and $\mathcal{H}_1$ as the perturbed Hamiltonian, which covers the motion under perturbations. Brouwer was able to calculate those Hamiltonians which led to the calculation of the transformation from mean to osculating Delaunay orbital element set. For more information about Brouwer's theory reader can take a detailed look at [48], [51], [53].

In this paper, a first-order truncated infinite power series approximation of the Brouwer's and Lydane's theory offered by [47] was applied. Since it is a first-order truncated approximation, the same transformation can be used for either transforming from mean to osculating orbital elements or vice a versa with a sign change. Furthermore, this approximate change is expected to have error in the order of J_2. However, it was easy to implement and it does not include numerically heavy calculations. In addition to that, Schaub and Junkins [47], states that, if this transformation is used both for the Deputy and the Chief, then the error introduced is similar for both of them, and this does not cause issues for the control. The details of this method is shared in Appendix B.

3) Classical Orbital Elements to ECI: Classical Orbital elements are used to calculate the corresponding position and velocity of the satellite with respect to the Inertial frame resolved in inertial frame, which can be found in Appendix A, Section A

4) ECI to Classical Orbital Elements: The Classical orbital element transformation is shared in Appendix A, Section B. The velocity and position of a satellite with respect to ECI resolved in ECI is turned into corresponding Osculating Classical Orbital Elements.

F. Discretization of a Linear System

In Model Predictive Control (MPC), which was explained in next chapters, a discrete type of system is more desirable since a control law created by MPC based on continuous systems is generally more complex, and numerically more intense to solve.

A linear time varying continuous system is given as

$$\dot{\boldsymbol{x}}(t) = \boldsymbol{A}(t)\boldsymbol{x}(t) + \boldsymbol{B}(t)\boldsymbol{u}(t) \tag{16}$$

The solution to that equation is in the form of Eq. (17)

$$\boldsymbol{x}(t) = \boldsymbol{\Phi}(t, t_0)\boldsymbol{x}(t_0) + \int_{t_0}^{t} \boldsymbol{\Phi}(t, \tau)\boldsymbol{B}(\tau)d\tau \tag{17}$$

where $\Phi(t, t_0)$ is a State Transition Matrix (STM). The STM can be expressed in terms of continuous system's $\boldsymbol{A}$ matrix,

$$\boldsymbol{\Phi}(t, t_0) = e^{\boldsymbol{A}(t-t_0)} \tag{18}$$

For linear systems, exponential of a matrix can be calculated with inverse Laplace Transformation

$$e^{\boldsymbol{A}t} = \mathcal{L}^{-1}\{(s\boldsymbol{I} - \boldsymbol{A})^{-1}\} \tag{19}$$

G. Regulation and Tracking

The regulation problem and tracking problem are similar in nature. Simply, the difference is that, in the regulation problem a single point in a manifold is tracked, and in the tracking problem, the system tracks a trajectory, rather than a point [54].

The system given is

$$\dot{x}_1 = x_2 \tag{20}$$

$$\dot{x}_2 = f(x_1, x_2) + u \tag{21}$$

If u is designed such that, the origin is stable, then this problem tries to track the origin constantly and hence it is a regulation problem.

Defining $x_r(t)$, as the trajectory to be followed, and creating a new variable set which covers the error dynamics

$$\begin{aligned} e_1 &= x_1 - x_r \\ e_2 &= x_2 - \dot{x}_r \end{aligned} \tag{22}$$

where $\ddot{x}_r = f'(x_r)$, then

$$\begin{aligned} \dot{e_1} &= e_2 \\ \dot{e_2} &= f(x_1, x_2) + u - f'(x_r) \end{aligned} \tag{23}$$

With the system in Eq. (23), the tracking problem is turned into a regulation problem, because if the origin is an asymptotically stable equilibrium then $x(t) = x_r(t)$ holds when $t \to \infty$. Furthermore, in this paper, e_1 is taken as a vector and namely, the position tracking error, and e_2 is also taken as a vector and it is the velocity error, which can be seen in Eq. (64).

H. Equation for Relative Motion

The equations for relative motion for the tracking problem is important since, those equations can be used in both creating a reference trajectory, and can be used as the plant for the calculation of the control actuation. The literature survey showed that, the equation for relative motion can be non-linear, which covers the whole dynamics, and can be linear with some assumptions. The non-linear equations governing the dynamics and perturbations in the Hill frame are shown in Eq. (44). However, the complexity of non-linear equations does not attract designers. The linearized equation work started as early as 1960. Clohessy–Wiltshire (CW) worked on "Terminal Guidance System for Satellite Rendezvous" and they derived linear equations for relative motion for a circular reference orbit for a rotating coordinate system, also known as Hill's equations. One of the issues with CW equations is that, it is only applicable to circular or small eccentricity reference orbits [47], [48]. To solve that issue, Melton worked with time as the independent variable, and created a State Transition Matrix (STM). However, his solution is practical for values of eccentricity of 0 to 0.3 [55]. Schweighart and Sedwick worked on CW equations and came up with new linear differential equation set that covers the J_2 effects [56]. Tschauner and Hempel (TH), on the other side, worked with equations that took true anomaly as independent variable, and derived an equation set that is similar to CW equations for the elliptical orbits [48]. Lawden solved the TH equations, interestingly earlier then they have been found, for fuel optimal rocket trajectory [48]. Carter, found out that Lawden's equations were singular when true anomaly, f is multiples of π, and solved that issue, but, he introduced another singularity for circular orbits. Later, Carter published another solution, which gets rid of that singularity, but the solution that was offered was hard to implement which caused it to be little use for engineering [48], [57]. Yamanaka and Ankersen again worked on TH equations, and solved this singularity issue with a really compact solution [58], nevertheless, their solution is singular when the eccentricity is equal to one, but this is typically not a major problem. Furthermore, some thought that the Cartesian Coordinate approach for description of the relative orbit makes it harder to interpret the relative orbit. So Schaub introduced the Differential Orbital Elements, an arithmetic difference of Deputy and Chief orbital elements, to describe the relative motion [59]. Furthermore, Schaub and Alfriend introduced J_2 invariant relative orbits, where the Deputy and Chief Orbital Elements have the same rate of change under the J_2 perturbations [60]. Gim and Alfriend created the Non-Singular Orbital Element Differences and created an STM to propagate it in time which also covers J_2 perturbations with eccentricity [61].

Since it covers eccentricities that was the interest of this study with an easy to implement approach, the Yamanaka and Ankersen STM (YASTM) approach found suitable for the reference trajectory design for the Continuous Controllers. For High Thrust implementations, the method suggested by Schaub [59], where the difference in Classical Mean Orbital Elements are tracked, was used.

I. Numerical Optimization

Since different control approaches were compared in this paper, the controllers that had the best performance were required to be found. The best can be defined depending on the user, such as a controller that leads to least error, with high fuel consumption might be chosen as the best in land vehicle applications where fuel is suppliable to the system and small tracking error is desired.

The problem at hand, optimizing the controller parameters based on the total fuel consumption and tracking error, is a multidimensional non-linear problem that is not easy to solve by any algebraic means, hence, heuristic solvers were required for the problem. A heuristic solver is designed to solve problems faster than universal solvers or solve the problems that are non-solvable by the universal solver. The side effect of such design is that the some order of accuracy is lost.

Heuristic Optimizers can be divided into categories depending on different parameters. A general approach is to classify according to the rule they depend on. If a solver implements multiple iterations in order to find the solution, it is called iterative optimization. A method works with a set of solutions and tries to improve the solutions at hand, it is a Population Based Optimization. If a method implements a probabilistic theory, then it is a probabilistic optimization. Another parameter can be the innate phenomenon that the algorithm imitates. This specification mainly has two different branches, Evolutionary Algorithms, which imitates the survival of the fittest, and Swarm Intelligence Based Algorithms, which imitates the group behavior of a colony [62]. A very well known, and proven algorithm in Evolutionary Algorithm is called Genetic Algorithm (GA), which imitates Darwin's theory. The easiness of implementation to different cases and its global perspective made it famous [63]. On the other hand, in swarm based algorithms, there are two different options that are well known and widely used, Particle Swarm Optimization (PSO) and Artificial Bee Colony (ABC). PSO is based on the behavior of the fish schooling or bird flocking. The PSO, compared to other methods, specifically GA, is a faster and numerically cheaper method [64]. Likewise, ABC is a Swarm Intelligence based algorithm, which imitates the foraging behaviour of a bee colony. The main aim of this approach is to find the best location of the food, the possible solutions to the problem, depending on the food quality, or corresponding objective value [62]. According to [62], [65], the ABC is as accurate as the GA and PSO methods, and outperforms them. Similarly, [66] states that, for a specific problem it outperforms the GA in terms of convergence speed, with a similar accuracy. Further research shows that ABC's accuracy is better than the PSO, however time of convergence of PSO is better than that of ABC [67]. Considering these results, it was noticed that every optimization algorithm has their pros and cons depending on the problem. Nevertheless, the ABC algorithm was chosen due to its moderate time of convergence and high accuracy compared to the other methods at hand.

J. Controllers

The controller framework in Formation Flying can be divided into three, Multi Input Multi Output (MIMO), Leader/Follower or Chief/Deputy and Virtual Structure.

In the MIMO approach, the whole constellation of satellites and governing dynamics are treated as a single plant with multiple outputs and multiple inputs, and state space representation of this system is controlled [68].

In Virtual Structure approach, each satellite of the constellation is taken as rigid bodies that are part of a bigger virtual rigid body. The motion of the rigid body, and corresponding positions of the satellites are generated to create the reference trajectory. Then the controllers are designed as such that each satellite will track the reference [68].

In Leader/Follower, or Chief/Deputy approach, the formation flying problem of a constellation is approached with a hierarchical arrangement such that the problem is reduced into individual basis. The Chief, it can be a virtual satellite, has the reference orbit to which the Deputy should arrange itself accordingly. This approach is the most widely studied approach in the formation flying of satellites [68], and hence was implemented in this study. It must be noted that, from now on, all the control structures that was covered in this paper were based on Chief/Deputy approaches.

Controllers for the formation flight covering the Deputy/Chief structure can be divided further into three: the Continuous Control Laws, Discrete Control Laws and Impulsive Control Laws. The Continuous Control Laws work throughout the orbit, and the control is active whether best performance is achieved or not. On the other hand, the discrete control laws, is discritized, and does not calculate the control continuously. Depending on the discritization time, the control is calculated, and applied along that time. Similarly, impulsive laws does not work always, however, generally they work at the best possible time, with a high amount of thrust to optimize the fuel consumption.

In literature there were a lot of different cases of control approaches. The survey of the control laws can be found in [68] and summarized as:

- Reference [69] used the feedback linearized control law for deep space missions
- Reference [70] uses the feedback linearization with inequalities of matrices to achieve robustness
- Reference [71] combines model predictive control with feedback linearization for both orbit and attitude keeping
- Reference [72] uses the proportional and derivative (PD) feedback law and compares them with fuel optimal control law.
- References [73], [74] and [75] used modified model predictive control to control the formation flying.
- Reference [76] applies a sliding mode control approach to a low thrust satellite constellation
- References [77], [78] uses a discrete time Linear Quadratic (LQ) approach to control the relative position
- Reference [79] uses discritized LQ Regulator (LQR) to formation flying problem without radial thrust
- Reference [80] implemented an Impulsive Control Approach based on Gauss Variational Equations (GVE), shared in Eq. (26) to (31), by minimizing a cost function based on the required velocity
- Reference [81] used the Mean Orbital Element differences as reference trajectory and implemented an optimal/sub-optimal impulsive control law based on GVE
- Reference [82] focused on angular momentum and energy of the orbit to establish a relative orbit, and created an impulsive control law

Feedback Linearization's main aim is to linearize the system's dynamics by using the feedback law. This type of controller allows designer to estimate the behaviour, track the results and use the linear control theory to design controllers. However, this control requires the system to be modelled exactly, since it cancels the non-linearities of it. Comparing PD approach, feedback linearization handles the non-linearities better, and allows one to create global stabilized systems.

MPC, often called as receding horizon control, includes the minimization of a cost function with free variable as the control actuation along the specified number of time steps. In more details, the linear system is discretized with a specified time, and the states for the specified horizon is generated. In the cost function both the states and the control has its corresponding weights.

The MPC has several benefits for the control problem. First of all, it allows user to specify constraints, for example the thrust limits of the system. Furthermore, comparing with prearranged trajectories that are found again by optimal methods, the MPC can handle uncertainties better, since it is embedded to the on-board controller of the satellite, and works actively throughout the mission. Moreover, the MPC is re-configurable, which means the tuning parameters can be changed online depending on the mission requirements. However, there are disadvantages of it. The major one is that, it requires computational power, depending on the horizon of the prediction and constraints. Due to recent improvements on technology, and reformulation of the problem, it is still applicable to satellites of small size as main controller [83], [84].

On the other hand, the Linear Quadratic Regulator, is also an optimization based control algorithm, however, the system is linearized over a cost function for the infinite horizon optimization. In this approach, the system constraints are not handled, and this control approach results in a locally stable system due to linearization.

The Sliding Mode Control scheme is a very well known control method. A sliding manifold, which does not depend on the system uncertainties is designed, and the trajectory of the states are tried to converge to that manifold. The manifold is designed such that it will drive the system dynamics to the desired equilibrium point. The main advantage of the Sliding Mode Control is that it can overcome the model uncertainties, however, generally speaking, this comes with a cost of excessive fuel burn.

In impulsive control, in general, the aim is to reduce the number of impulses since the efficiency of the high thrust boosters are limited. A common approach is the use of GVE,

to calculate the best possible time to apply impulses, based on optimization or analytical solutions.

It is noticed that, most of the papers in the literature focuses on one of the above methods and does not compare the performances of each controller with other controllers. In order to lead designers to a better decision for controller design, this study was focused on implementation of different control methods and comparison of them. The reduction in fuel consumption in formation flying missions, which effects the society economically and ecologically, will lead to greener tomorrows.

K. Lyapunov Stability

Lyapunov found in 1892 that if a continuously differentiable, positive definite function $V(x)$ has its derivative as negative semi definite function, then the equilibrium point is stable. If the derivative is negative definite, then the equilibrium point is asymptotically stable.

Theorem II.1. *Given that $V(0) = 0$ and $V(\boldsymbol{x}) > 0 \; \forall \, \boldsymbol{x} \neq 0$, then $\boldsymbol{x} = 0$ equilibrium point is stable if*

- $\dot{V}(\boldsymbol{x}) \leq 0 \quad \forall \, \boldsymbol{x} \neq 0$
- $\dot{V}(0) = 0$

and asymptotically stable if the inequality of $\dot{V}(\boldsymbol{x})$ is strict. Furthermore, the equilibrium point $\boldsymbol{x} = 0$ is globally asymptotically stable if the $V(\boldsymbol{x}) \to \infty$ as $||\boldsymbol{x}|| \to \infty$.

The proof of the theorem can be found in [54]. If the derivative of the Lyapunov function is negative-semi definite, then the Lyapunov's Direct Method concludes that, the equilibrium is stable. A theorem from [47], states that, there is still possibility of the system being asymptotically stable.

Theorem II.2. *Define $\Omega = \{x | \dot{V}(\boldsymbol{x}) = 0\}$*

- *if the first non zero derivative of the $V(\boldsymbol{x})$ is odd and negative definite under subset of Ω, then the system is Asymptotically stable.*

The proof of the theorem can be found in [47].

III. Method

A. Absolute Equations of Motion

1) Non-linear Equation of Motion with J_2 Perturbation: In space, vehicles are moving under Newton's law of universal gravitation combined with perturbations. The mathematical expression of this was demonstrated at Eq. (24) [47].

$$\begin{aligned} \frac{\mathrm{d}_{\mathrm{I}}^2 \boldsymbol{r}_{\mathrm{CI}}}{\mathrm{d}\, t^2} &= \boldsymbol{f}(\boldsymbol{r}_{\mathrm{CI}}) \\ \frac{\mathrm{d}_{\mathrm{I}}^2 \boldsymbol{r}_{\mathrm{DI}}}{\mathrm{d}\, t^2} &= \boldsymbol{f}(\boldsymbol{r}_{\mathrm{DI}}) + \boldsymbol{u}^{\mathrm{I}} \end{aligned} \tag{24}$$

where $\boldsymbol{u}^{\mathrm{I}}$ is the control applied to the deputy expressed in inertial frame, and $\boldsymbol{f}$ is a nonlinear function which covers gravitational acceleration with J_2 perturbation.

$$\boldsymbol{f}(\boldsymbol{r}) = -\frac{\mu}{r^3}\left[\boldsymbol{r} - \mathrm{J}_2 \frac{3}{2}\left(\frac{r_{\mathrm{eq}}}{r}\right)^2 \begin{pmatrix} 5x\left(\frac{z}{r}\right)^2 - x \\ 5y\left(\frac{z}{r}\right)^2 - y \\ 5z\left(\frac{z}{r}\right)^2 - 3z \end{pmatrix}\right] \tag{25}$$

where μ is Standard gravitational parameter of Earth, and r_{eq} is the equatorial radius of Earth. Notice that, in this formulation $\boldsymbol{r} = [x, y, z]^{\mathrm{T}}$ is position of the satellite with respect to ECI frame resolved in ECI frame.

2) Gauss Variational Equations: Gauss' Variational Equations were used to describe the time rate of change of orbital elements under the presence of perturbations or control inputs. The derivation of it can be found in [48].

$$\frac{\mathrm{d}a}{\mathrm{d}t} = 2\frac{d_r a^2 e \sin f}{h} + 2\frac{d_\theta a^2 p}{hr} \tag{26}$$

$$\frac{\mathrm{d}e}{\mathrm{d}t} = \frac{d_r p \sin f}{h} + \frac{d_\theta[(p+r)\cos f + re]}{h} \tag{27}$$

$$\frac{\mathrm{d}i}{\mathrm{d}t} = \frac{d_h r \cos(f+\omega)}{h} \tag{28}$$

$$\frac{\mathrm{d}\Omega}{\mathrm{d}t} = \frac{d_h r \sin(f+\omega)}{h \sin i} \tag{29}$$

$$\frac{\mathrm{d}\omega}{\mathrm{d}t} = \frac{d_r p}{he} + \frac{d_\theta(p+r)}{he} - \frac{d_h r \sin(f+\omega)}{h \sin i} \tag{30}$$

$$\begin{aligned} \frac{\mathrm{d}M}{\mathrm{d}t} =& n + d_r \frac{(-2e + \cos f + e\cos^2 f)(1-e^2)}{e(1+e\cos f)na} \\ &+ d_\theta \frac{(e^2-1)(e\cos f + 2)\sin f}{e(1+e\cos f)na} \end{aligned} \tag{31}$$

where $\boldsymbol{d} = [d_r, d_\theta, d_h]^{\mathrm{T}}$ is the acceleration resolved in LVLH frame, r corresponds to radial, θ corresponds to tangential, h corresponds to the angular momentum direction.

3) Effect of J_2 on Mean Orbital Elements: To investigate the effect of the J_2 on Orbital Elements, a similar approach to Gauss' Variational Equations was done. The details of the derivation can be found in [47], [48].

$$\frac{\mathrm{d}\bar{a}}{\mathrm{d}t} = 0 \tag{32}$$

$$\frac{\mathrm{d}\bar{e}}{\mathrm{d}t} = 0 \tag{33}$$

$$\frac{\mathrm{d}\bar{i}}{\mathrm{d}t} = 0 \tag{34}$$

$$\frac{\mathrm{d}\bar{\Omega}}{\mathrm{d}t} = -\frac{3}{2}\mathrm{J}_2\left(\frac{R_e}{\bar{p}}\right)^2 \bar{n}\cos\bar{i} \tag{35}$$

$$\frac{\mathrm{d}\bar{\omega}}{\mathrm{d}t} = \frac{3}{4}\mathrm{J}_2\left(\frac{R_e}{\bar{p}}\right)^2 \bar{n}(5\cos^2\bar{i} - 1) \tag{36}$$

$$\frac{\mathrm{d}\bar{M}_0}{\mathrm{d}t} = \frac{3}{4}\mathrm{J}_2\left(\frac{R_e}{\bar{p}}\right)^2 \bar{n}\bar{\eta}(3\cos^2\bar{i} - 1) \tag{37}$$

where R_e is the Equatorial Radius of Earth, $\bar{p}$ is the mean semi-latus rectum, $\bar{\eta} = \sqrt{1-\bar{e}^2}$ and $\bar{M}_0$ is the Mean Anomaly at Epoch. When the Mean Orbital Element deviations under J_2 effect was observed, it was seen that, if $\bar{i}$, $\bar{n}$, which depends on $\bar{a}$, or $\bar{\eta}$, which depends on $\bar{e}$, of Deputy is different than that of Chief, the rate of change of mean orbital elements of Deputy are different than that of Deputy.

B. Equations of Relative Motion

The equations of relative motion was important to study the control of the deputy with respect to the chief.

1) Nonlinear Equation of Relative Motion: The equation of motion of the Chief with respect to the inertial frame is governed by Eq. (38).

$$\frac{\mathrm{d}_{\mathrm{I}}^2 \boldsymbol{r}_{\mathrm{CI}}}{\mathrm{d}t^2} = -\frac{\mu}{||\boldsymbol{r}_{\mathrm{CI}}||^3}\boldsymbol{r}_{\mathrm{CI}} \tag{38}$$

where $||.||$ is the 2-norm of the "." variable. Similarly, the dynamics of the Deputy is governed by

$$\frac{\mathrm{d}_\mathrm{I}^2 \boldsymbol{r}_\mathrm{DI}}{\mathrm{d}t^2} = -\frac{\mu}{||\boldsymbol{r}_\mathrm{DI}||^3}\boldsymbol{r}_\mathrm{DI} \tag{39}$$

introducing $\boldsymbol{r}_\mathrm{DC}$ which is the position vector of the Deputy with respect to Chief

$$\boldsymbol{r}_\mathrm{DC} = \boldsymbol{r}_\mathrm{DI} - \boldsymbol{r}_\mathrm{CI} \tag{40}$$

Subtracting Eq. (39) from Eq. (38) and plugging in Eq. (40) reveals

$$\frac{\mathrm{d}_\mathrm{I}^2 \boldsymbol{r}_\mathrm{DC}}{\mathrm{d}t^2} = -\frac{\mu(\boldsymbol{r}_\mathrm{CI} + \boldsymbol{r}_\mathrm{DC})}{||\boldsymbol{r}_\mathrm{DI} + \boldsymbol{r}_\mathrm{DC}||^3} + \frac{\mu}{||\boldsymbol{r}_\mathrm{CI}||}\boldsymbol{r}_\mathrm{CI} \tag{41}$$

The above derivative, as can be seen, is with respect to Inertial frame, however, it was more desirable to have the derivative with respect to LVLH frame of the Chief. Double Time derivative with respect to a non-inertial frame is

$$\begin{aligned}\frac{\mathrm{d}_\mathrm{I}^2 \boldsymbol{r}_\mathrm{DC}}{\mathrm{d}t} =& \frac{\mathrm{d}_\mathrm{C}^2 \boldsymbol{r}_\mathrm{DC}}{\mathrm{d}t^2} + 2\boldsymbol{\omega}_\mathrm{CI} \times \frac{\mathrm{d}_\mathrm{C} \boldsymbol{r}_\mathrm{DC}}{\mathrm{d}t} + \frac{\mathrm{d}_\mathrm{C} \boldsymbol{\omega}_\mathrm{CI}}{\mathrm{d}t} \times \boldsymbol{r}_\mathrm{DC} \\ &+ \boldsymbol{\omega}_\mathrm{CI} \times \boldsymbol{\omega}_\mathrm{CI} \times \boldsymbol{r}_\mathrm{DC}\end{aligned} \tag{42}$$

where $\boldsymbol{\omega}_\mathrm{CI}$ is the angular velocity of the orbital frame of the Chief with respect to Inertial frame. To resolve everything in chief orbital frame, the C frame, the definitions below were used.

$$\boldsymbol{\omega}_\mathrm{CI}^\mathrm{C} = [0, 0, \dot{\theta}]^T \tag{43a}$$
$$\boldsymbol{r}_\mathrm{DC}^\mathrm{C} = [x, y, z]^\mathrm{T} \tag{43b}$$
$$\boldsymbol{r}_\mathrm{CI}^\mathrm{C} = [0, 0, r_0]^\mathrm{T} \tag{43c}$$

where $\dot{\theta}$ is the magnitude of the angular velocity of the orbital frame of Chief, or the rate of change of argument of latitude. Plugging (43) with Eq. (42) into Eq. (41) reveals the nonlinear equation of relative motion without any perturbations

$$\ddot{x} - 2\dot{\theta}_\mathrm{C}\dot{y} - \ddot{\theta}_\mathrm{C} y - \dot{\theta}_\mathrm{C}^2 x = -\frac{\mu(r_\mathrm{C} + x)}{[(r_\mathrm{C} + x)^2 + y^2 + z^2]^{\frac{3}{2}}} + \frac{\mu}{r_\mathrm{C}^2} \tag{44a}$$

$$\ddot{y} + 2\dot{\theta}_\mathrm{C}\dot{x} + \ddot{\theta}_\mathrm{C} x - \dot{\theta}_\mathrm{C}^2 y = -\frac{\mu y}{[(r_\mathrm{C} + x)^2 + y^2 + z^2]^{\frac{3}{2}}} \tag{44b}$$

$$\ddot{z} = -\frac{\mu z}{[(r_\mathrm{C} + x)^2 + y^2 + z^2]^{\frac{3}{2}}} \tag{44c}$$

where, $\ddot{r}_\mathrm{C} = r_\mathrm{C}\dot{\theta}_\mathrm{C}^2 - \mu/r_\mathrm{C}^2$ and $\ddot{\theta}_\mathrm{C} = -2\dot{r}_\mathrm{C}\dot{\theta}_\mathrm{C}/r_\mathrm{C}$. In Eq. (44), the sub-index C denotes the belonging of Chief. Notice that, the differential disturbances or the control commands can be directly added to the above equations if they are resolved in the Chief's LVLH frame. Also, the $[x, y, z]$ is the position of the Deputy with respect to Chief, resolved in Chief's LVLH frame. As mentioned earlier, this equation was not used in the analysis, rather, it was used as a step to calculate Clohessy–Wiltshire Equations.

2) CW Equations: In the formation flying, the very well known Clohessy–Wiltshire (CW) equations are used, specifically for rendezvous. These equations are created by CW in the 1960s to investigate the rendezvous of spacecraft. Since they are computationally easy to solve, they are suitable to use in initial analysis. Furthermore, due to the linear structure of the equations, they seem suitable to use in optimal control problem.

The method suggested by [48] was followed, by creating a Taylor Series expansion of the Right Hand Side of Eq. (44) about the origin. The first order terms of that Taylor Series expansion was shared in Eq. (45).

$$-\frac{\mu(a_\mathrm{C} + x)}{[(a_\mathrm{C} + x)^2 + y^2 + z^2]^{1.5}} \approx n_\mathrm{C}^2(2x - a_\mathrm{C}) \tag{45a}$$

$$-\frac{\mu y}{[(a_\mathrm{C} + x)^2 + y^2 + z^2]^{1.5}} \approx -n_\mathrm{C}^2 y \tag{45b}$$

$$-\frac{\mu z}{[(a_\mathrm{C} + x)^2 + y^2 + z^2]^{1.5}} \approx -n_\mathrm{C}^2 z \tag{45c}$$

where n_C is the mean motion of the Chief, and equal to $\sqrt{\mu/a_\mathrm{C}^3}$. Removing the C subscript, and rearranging revealed the very well known CW equations

$$\ddot{x} - 2n\dot{y} - 3n^2 x = d_x \tag{46a}$$

$$\ddot{y} + 2n\dot{x} = d_y \tag{46b}$$

$$\ddot{z} + n^2 z = d_z \tag{46c}$$

where d_x, d_y, d_z are the differential forces applied to the satellites expressed in the Hill frame, and n is the mean motion of the Chief. It is easy to see that, the cross-track motion and in-plane motion does not depend on each other.

3) TH Equations: A common method to account for the eccentricity in relative motion is to change the independent variable in Eq. (44) to True Anomaly, f. To achieve that, a chain rule shared in Eq. (47) was done, where $(.)'$ denotes the derivative of a variable with respect to true anomaly. The whole transformation is shared in [48], with a normalized position vector, $\bar{\boldsymbol{r}}_\mathrm{DC}^\mathrm{C} = \boldsymbol{r}_\mathrm{DC}^\mathrm{C}/||\boldsymbol{r}_\mathrm{CI}^\mathrm{I}||$.

$$\frac{\mathrm{d}(.)}{\mathrm{d}t} = (.)'\dot{f} \tag{47a}$$

$$\frac{\mathrm{d}^2(.)}{\mathrm{d}t^2} = (.)''\dot{f}^2 + \dot{f}\dot{f}'(.)' \tag{47b}$$

The Tschauner–Hempel (TH) equations can be seen as the eccentricity extension of the CW equations, with true anomaly being the independent variable, which can be seen in Eq. (48a). Notice that, there is no perturbation included in TH equations just like CW equations [48]:

$$\begin{aligned}\bar{x}'' &= \frac{3}{k}\bar{x} + 2\bar{y}' \\ \bar{y}'' &= -2\bar{x}' \\ \bar{z}'' &= -\bar{z}'\end{aligned} \tag{48a}$$

where $k = 1 + e\cos f$. Similar to the CW equations, out of plane motion does not depend on in-plane motion.

4) Yamanaka and Ankersen STM: Yamanaka and Ankersen (YA) worked on the TH equations, to improve already created solutions by Lawden and Carter [48]. Their solution is valid for eccentricities less than 1. On the other hand, YASTM is easy to implement for numerical purposes, and covers the required eccentricity for this paper. Furthermore, if the eccentricity is taken as 0, then the solution offered by YA is the same as Hill's solution.

YA used a slightly different coordinate system than Hill, where $\hat{\boldsymbol{z}}$ axis points toward Zenith, $\hat{\boldsymbol{y}}$ axis is normal to the orbital plane and opposite the angular momentum vector, and $\hat{\boldsymbol{x}}$ completes the right handed system. In this paper, this frame was denoted as Y frame. More over, their solution is valid for the states that has the transformation in Eq. (49) and the inverse transformation in Eq. (50)

$$\tilde{\boldsymbol{r}}^{\mathrm{Y}}_{\mathrm{DC}} = \rho \boldsymbol{r}^{\mathrm{Y}}_{\mathrm{DC}} \tag{49a}$$
$$\tilde{\boldsymbol{v}}^{\mathrm{Y}}_{\mathrm{DC}} = -e\sin\theta \boldsymbol{r}^{\mathrm{Y}}_{\mathrm{DC}} + \left(1/k^2\rho\right)\boldsymbol{v}^{\mathrm{Y}}_{\mathrm{DC}} \tag{49b}$$
$$\boldsymbol{r}^{\mathrm{Y}}_{\mathrm{DC}} = 1/\rho \tilde{\boldsymbol{r}}^{\mathrm{Y}}_{\mathrm{DC}} \tag{50a}$$
$$\boldsymbol{v}^{\mathrm{Y}}_{\mathrm{DC}} = k^2(e\sin\theta \tilde{\boldsymbol{r}}^{\mathrm{Y}}_{\mathrm{DC}} + \rho \tilde{\boldsymbol{v}}^{\mathrm{Y}}_{\mathrm{DC}}) \tag{50b}$$

where $\rho = 1 + e\cos f$. The YASTM is consisting of in-plane STM and out-of-plane STM. The in-plane STM is in the form of $\Phi^{-1}_{\theta_0}$ and Φ_θ, which can be seen in Eqs. (53) and (54), respectively. Notice that, the orbital elements in $\Phi^{-1}_{\theta_0}$ should correspond to the orbital elements in initial time, t_0 and similarly, Φ_θ should have elements in time t. The overall STM is shown in Eqs. (51) and (52).

$$\begin{bmatrix} \tilde{x}_t \\ \tilde{z}_t \\ \tilde{v_x}_t \\ \tilde{v_z}_t \end{bmatrix} = \Phi_\theta \Phi^{-1}_{\theta_0} \begin{bmatrix} \tilde{x}_{t_0} \\ \tilde{z}_{t_0} \\ \tilde{v_x}_{t_0} \\ \tilde{v_z}_{t_0} \end{bmatrix} \tag{51}$$

$$\begin{bmatrix} \tilde{y}_t \\ \tilde{v_y}_t \end{bmatrix} = \Phi_{\theta-\theta_0} \begin{bmatrix} \tilde{y}_{t_0} \\ \tilde{v_y}_{t_0} \end{bmatrix} \tag{52}$$

The orbital elements in time t can be propagated by assuming Keplerian Orbit, as stated in [58]. The $\Phi^{-1}_{\theta_0}$ is

$$\Phi^{-1}_{\theta_0} = \frac{1}{1-e^2} \times \begin{bmatrix} 1-e^2 & 3e(s/\rho)(1+1/\rho) & -es(1+1/\rho) & -ec+2 \\ 0 & -3(s/\rho)\left(1+e^2/\rho\right) & s(1+1/\rho) & c-2e \\ 0 & -3(c/\rho+e) & c(1+1/\rho)+e & -s \\ 0 & 3\rho+e^2-1 & -\rho^2 & es \end{bmatrix} \tag{53}$$

where $s = \rho\sin f$ and $c = \rho\cos f$. Similarly Φ_θ is

$$\Phi_\theta = \begin{bmatrix} 1 & -c(1+1/\rho) & s(1+1/\rho) & 3\rho^2 J \\ 0 & s & c & (2-3esJ) \\ 0 & 2s & 2c-e & 3(1-2esJ) \\ 0 & s' & c' & -3e\left(s'J + s/\rho^2\right) \end{bmatrix} \tag{54}$$

where $k^2 = h/p^2$ and $J = k^2(t-t_0)$. The c' and s' are the derivatives of c and s with respect to f, respectively.

For the out-of-plane motion, there is only one transition, Eq. (55), and the matrix corresponds to $\Phi_{\theta-\theta_0}$.

$$\begin{bmatrix} \tilde{y}_t \\ \tilde{v}_{yt} \end{bmatrix} = \frac{1}{\rho_{\theta-\theta_0}} \begin{bmatrix} c & s \\ -s & c \end{bmatrix}_{\theta-\theta_0} \begin{bmatrix} \tilde{y}_0 \\ \tilde{v}_{y0} \end{bmatrix} \tag{55}$$

Since, the Y frame, as explained in the beginning of this section, is different than the Hill frame of the Chief, a DCM should be applied after implementing Eq. (49) or (50). The DCM for Hill frame to Y frame is

$$C_{\mathrm{YH}} = \boldsymbol{R}_x\left(-\frac{\pi}{2}\right) \times \boldsymbol{R}_y(0) \times \boldsymbol{R}_z\left(\frac{\pi}{2}\right) \tag{56}$$

where $\boldsymbol{R}_x$ corresponds to a DCM of rotation only around x axis, and the same applies to $\boldsymbol{R}_y$ and $\boldsymbol{R}_z$ for y and z axes. .

C. Reference Orbit

The reference orbits that are tracked were created with two different methods. One was created with YASTM, explained in Section III-B4. The second method that was covered is the orbital element differences.

For YASTM, and the Mean orbital element differences, the main issue was the decision of the initials of each method. For that purpose, solution of the CW equations with the Hill frame positions and the corresponding orbital element solution was used.

1) Reference with YASTM: In this reference method, an initial point was created as the solution of the CW equations, Eq. (57), [47]:

$$x(t) = A_0\cos(nt+\alpha) + x_{\mathrm{off}} \tag{57a}$$
$$y(t) = -2A_0\sin(nt+\alpha) - \frac{3}{2}ntx_{\mathrm{off}} + y_{\mathrm{off}} \tag{57b}$$
$$z(t) = B_0\cos(nt+\beta) \tag{57c}$$

where α and β are in-plane and out-of-plane phase angles. A_0 and B_0 are the amplitudes of the motion along x and z axis, whereas $2A_0$ is the amplitude along y axis direction. x_{off} and y_{off} are the offsets along x and y axes. As can be seen, in $y(t)$ there is a secular drift term due to x_{off}, which includes time as a multiplication. In order to have bounded motion, which is generally the desired case, the x_{off} was set to 0. This removes the secular drift term. Similarly, to have a relative trajectory that has the Chief in the center, the y_{off} was set to be 0. The phase angles and the amplitudes are specific to the mission, and affects the shape. In order to have an elliptic motion in xz plane, the phase angles should be set with a $\pi/2$ difference, which was also done in this mission. The amplitude for in-plane motion, A_0 for the Relative Orbit Mission for this study is 500 m, and B_0 is 300 m. The corresponding velocity terms are the derivatives of the Eq. (57), shown in Eq. (58):

$$\dot{x}(t) = -A_0 n\sin(nt+\alpha) \tag{58a}$$
$$\dot{y}(t) = -2A_0 n\cos(nt+\alpha) \tag{58b}$$
$$\dot{z}(t) = -B_0 n\sin(nt+\beta) \tag{58c}$$

However, since the orbit was slightly elliptic, the solution of Hill's or the CW equations will cause a secular drift due to their assumption of circular Chief orbit. To cancel that secular drift, mostly along y axis, the equation suggested by [85] was used, Eq. (59), to correct the initials. The resultant initials are, $x(0)$ is 500 m, $y(0)$ and $z(0)$ are 0 m. Similarly, $\dot{x}(0)$ is 0 m/s, $\dot{y}(0)$ is -1.0690 m/s and $\dot{z}(0)$ is 0.3181 m/s.

$$\frac{\dot{y}(0)}{x(0)} = -\frac{n(2+e)}{(1+e)^{1/2}(1-e)^{3/2}} \tag{59}$$

When the initials were created, the rest was using the YASTM approach described in Section III-B4. Then, the transformation in Eq. (15) was used to transform the reference from Chief's Hill frame to ECI frame, which is the frame of the sliding mode and feedback linearization controllers.

2) Mean Orbital Element Reference: A similar approach to the YASTM reference method was applied. This time, the solution of the CW equations, calculated with orbital elements were used, Eq. (60). This solution was taken from [47], and it is true for near circular orbits.

$$x(f) \approx \delta a - a\cos f\delta e \tag{60a}$$
$$y(f) \approx a(\delta\omega + \delta M + \cos i\delta\Omega) + 2a\sin f\delta e \tag{60b}$$
$$z(f) \approx a\sqrt{\delta i^2 + \sin^2 i\delta\Omega^2}\cos\left(\theta - \theta_z\right) \tag{60c}$$

where $\theta_z = \tan^{-1}\left(-\delta i/(\sin i\delta\Omega)\right)$ and $\delta(.)$ denotes the orbital element difference. When these solutions were created, the amplitude and the phase angles of Eq. (57) can be calculated in terms of orbital elements, Eq. (61):

$$A_0 = -a\delta e \tag{61a}$$
$$B_0 = a\sqrt{\delta i^2 + \sin^2 i\delta\Omega^2} \tag{61b}$$
$$\alpha = 0 \tag{61c}$$
$$\beta = f - \theta_z \tag{61d}$$
$$y_{\text{off}} = a(\delta\omega + \delta M + \cos i\delta\Omega) \tag{61e}$$

A major fact is that, in order to have a bounded relative motion, δa should be set to 0 [47], [48]. This also holds for eccentric orbits, hence the secular drift was prevented, and a bounded orbit was achieved. Similarly, if the Deputy was desired to have a trajectory which has the Chief as its center then the y_{off} should be set to 0, which was the case here. Equation (61) gave 3 conditions for 6 of the orbital elements. The bounded relative orbit gave the fourth condition. The fifth condition was setting the y_{off} to be zero, however, this left one degree of freedom. When the y_{off} equation was investigated, it was seen that summation of $\delta\omega$ and δM was limited. Hence, to get rid of that one degree of freedom, either δM or $\delta\omega$ was set and the other one was calculated according to the equation of y_{off}.

Even though those equations were written for osculating orbital elements, in literature it was observed that they were also used for mean orbital elements [42], [43]. When the reference orbital element differences were calculated with Eq. (60) and (61), then at each time step the reference orbital elements were created by Eq. (62).

$$\mathbf{oe}_{dd} = \mathbf{oe}_c + \delta\mathbf{oe}_r \tag{62}$$

where $\mathbf{oe}_r$ corresponds to the reference orbital element differences, and $\mathbf{oe}_{dd}$ corresponds to the desired deputy orbital elements. Then the error that should be compensated is:

$$\delta\mathbf{oe} = \mathbf{oe}_{dd} - \mathbf{oe}_d \tag{63}$$

With Eq. (63), the Gaussian Variational equations can be used, to calculate the required velocity for Deputy to have the Desired Orbital Elements.

D. Controllers

In this section, the methodology behind the controllers is explained. The controllers that were compared are, Sliding Mode Control, due to its robustness, Feedback Linearization, due to its easy design, MPC, due to its optimality and easiness of constraint implementation. For the impulsive laws, Schaub and Alfriend's method was used as a benchmark control, since it is a sub-optimal impulsive law [81].

1) System to be Controlled: For Sliding Mode and Feedback Linearization, the system that was controlled was the same system. The dynamics that are covered was described in Eq. (25). Since this dynamics are not in the error tracking form, the methodology in Section II-G, and specifically Eq. (23) were applied. The final system was:

$$\begin{aligned}\dot{\boldsymbol{e}}_1 &= \boldsymbol{e}_2 \\ \dot{\boldsymbol{e}}_2 &= f(\boldsymbol{x}_d) - f^{'}(\boldsymbol{x}_r) + \boldsymbol{u}\end{aligned} \tag{64}$$

with $f(\boldsymbol{x})$ in Eq. (25), $\boldsymbol{x}_d$ is equivalent to $\boldsymbol{r}^{\text{I}}_{\text{DI}}$, the position of Deputy resolved in inertial frame and $\boldsymbol{x}_r$ is equivalent to $\boldsymbol{r}^{\text{I}}_{\text{RI}}$, the reference position in inertial frame. Also, $\boldsymbol{e}_1 = [e_x, e_y, e_z]^{\text{T}}$ and $\boldsymbol{e}_2 = [\dot{e}_x, \dot{e}_y, \dot{e}_z]^{\text{T}}$. In other words, $\boldsymbol{e}_1$ is the position error in in ECI, and $\boldsymbol{e}_2$ is the velocity error in ECI.

In YASTM [58], it is stated that, the Deputy and the Chief has the same perturbation accelerations. For that reason, the $f'(.)$ was taken as the same as $f(.)$. Of course, the accelerations are not the same, however, the order of the error is reduced. Because, if the second derivative of the $\boldsymbol{x}_r$ was taken without perturbation, the system diverged.

2) Sliding Mode Control: As mentioned in the Background Section, in sliding mode, a sliding manifold that does not depend on the dynamics of the system was generated, and the system was forced to track that manifold. In order to achieve that, a sliding manifold was created, $S = \{\boldsymbol{e} : s(\boldsymbol{e}) = 0\}$ where $s(\boldsymbol{e}) = a\boldsymbol{e}_1 + \boldsymbol{e}_2$ with $a > 0$ and a is a scalar. On S it holds that, $a\boldsymbol{e}_1 = -\boldsymbol{e}_2$ which means that $\dot{\boldsymbol{e}}_1 = -a\boldsymbol{e}_1$. Basically, if the system was kept on $s(\boldsymbol{e})$, then it will converge to origin exponentially. Because, $\boldsymbol{e}_1$ will converge to 0, due to $\dot{\boldsymbol{e}}_1 = -\boldsymbol{e}_1$ and since on sliding manifold $-a\boldsymbol{e}_1 = \boldsymbol{e}_2$, that means $\boldsymbol{e}_2$ will be 0 as well.

To force the system to slide on the manifold, the general approach is to create a Lyapunov function based on that sliding manifold, and arrange the control such that, the Lyapunov function leads to an asymptotically stable equilibrium point. The corresponding Lyapunov function and its derivative is shared in Eq. (66).

$$V(s) = \frac{1}{2}s^2 \tag{65}$$
$$\dot{V}(s) = s\dot{s} = s(a\boldsymbol{e_2} + f(\boldsymbol{x}_d) - f'(\boldsymbol{x}_r) + \boldsymbol{u}) \tag{66}$$

where $s = s(\boldsymbol{e})$. It can be seen that, $V(s)$ is a continuously differentiable and globally unbounded positive definite function. The next step was to assure that, the derivative of it is negative definite. One of the approaches to achieve that was, to bound the derivative of the Lyapunov function from above, and force that bound to be negative at all times with the control input. The upper bound:

$$\dot{V}(s) \leq |s||a\boldsymbol{e}_2 + f(\boldsymbol{x}_d) - f'(\boldsymbol{x}_r)| + s\boldsymbol{u} \tag{67}$$

Then the control input, that forces the derivative to be negative is:

$$\boldsymbol{u} = -\left(|a\boldsymbol{e}_2 + f(\boldsymbol{x}_1) - f(\boldsymbol{x}_r)| + \boldsymbol{\mu}_0\right)\mathrm{sign}(s) \tag{68}$$

where $\boldsymbol{\mu}_0$ is a vector of length 3, with all elements greater than 0, and equal to μ_0. When the control was plugged back into the derivative in Eq. (66), the resultant Lyapunov derivative is:

$$\dot{V}(s) \leq -|s|\boldsymbol{\mu}_0 \tag{69}$$

which is negative definite, due to $\mu_0 > 0$, so the system will converge to the sliding manifold, and slide on it to origin. Furthermore, the a and μ_0 was calculated by numerical optimization methods to reduce the error and corresponding fuel consumption.

Furthermore, the approach shared can be thought as, at each of the axes, the same manifold was forced to be followed. Of course, each of the axis could be separated, however, that would introduce more parameters to be tuned.

A general problem that was faced with the above methodology is that, the sign function leads to chattering due to disturbances. In other words, when the system slides on the surface, the disturbances push it out. Even an infinitesimal push will lead application of the thrust, as a result, the chattering or induced oscillations will happen. To get rid of that problem, sign function was modeled as a saturation, sat function [54]. Then the control was modeled as

$$\boldsymbol{u} = -\boldsymbol{\mu}_0 \mathrm{sat}(s/\eta) \tag{70}$$

where η is chosen as 0.1, and function sat is shared in Eq. (71).

$$\mathrm{sat}(u) = \begin{cases} u, & \text{if} \quad |u| \leq 1 \\ \mathrm{sign}(u), & \text{if} \quad |u| > 1 \end{cases} \tag{71}$$

3) Feedback Linearization: The feedback linearization allows one to linearize the non-linear system with the aid of feedback. The advantage of this is to make the system more tractable and to make the system linear, where the theory is relatively well known. The downside is that, this requires system to be well known, i.e. if the model has errors then there might happen some stability problems. Furthermore, notice that, the most dominant disturbance in 700 km altitude was already modelled in the system.

In Feedback Linearization, it is important to have a system in the form of Eq. (72), in order to use the feedback to linearize. If the system is not turnable into such form, then there is partial feedback linearization to implement such a controller. However, since the dynamics in Eq. (64) is already in that form, the feedback linearization can be applied directly to the system [54].

$$\dot{z} = Az + B\left[\psi(z) + \gamma(z)u\right] \tag{72}$$

Considering the non-linear system given in Eq. (64). The controller,

$$\boldsymbol{u} = f^{'}(\boldsymbol{x}_r) - f(\boldsymbol{x}_d) - K_1\boldsymbol{e}_1 - K_2\boldsymbol{e}_2 \tag{73}$$

turns the system dynamics into

$$\dot{\boldsymbol{e}}_1 = \dot{\boldsymbol{e}}_2 \tag{74}$$

$$\dot{\boldsymbol{e}}_2 = -\boldsymbol{K}_1\boldsymbol{e}_1 - \boldsymbol{K}_2\boldsymbol{e}_2 \tag{75}$$

where $\boldsymbol{K}_1$ and $\boldsymbol{K}_2$ are diagonal matrices with all elements are k_1 and k_2, respectively, and, k_1 and k_2 are strictly positive and scalar. For this problem, different Lyapunov function was chosen:

$$V(\boldsymbol{e}_1, \boldsymbol{e}_2) = \frac{1}{2}\boldsymbol{e}_1^{\mathrm{T}}\boldsymbol{K}_1\boldsymbol{e}_1 + \frac{1}{2}\boldsymbol{e}_2^{\mathrm{T}}\boldsymbol{e}_2 \tag{76}$$

$$\dot{V}(\boldsymbol{e}_1, \boldsymbol{e}_2) = \boldsymbol{e}_1^{\mathrm{T}}\boldsymbol{K}_1\dot{\boldsymbol{e}}_1 + \boldsymbol{e}_2^{\mathrm{T}}\boldsymbol{K}_2\dot{\boldsymbol{e}}_2 \tag{77}$$

The Lyapunov function in Eq. (76) is a positive definite function and it is globally unbounded, since $\boldsymbol{K}_1$ matrix is a positive definite matrix. The open version, where the control in Eq. (73) was plugged in, of its derivative is in Eq. (78):

$$\dot{V}(\boldsymbol{e}_1, \boldsymbol{e}_2) = -\boldsymbol{e}_2^{\mathrm{T}}\boldsymbol{K}_2\boldsymbol{e}_2 \tag{78}$$

According to the Lyapunov theory, this is not asymptotically stabilizing control, the derivative of it is not negative definite. In other words $\dot{V}(\boldsymbol{e}_1, \boldsymbol{e}_2) = 0, \quad \forall \boldsymbol{e}_1 \neq 0$ but $\forall \boldsymbol{e}_2 = 0$. The Lyapunov's Direct Method concludes only stability of the equilibrium point, hence, Theorem II.2 shall be used. To start with, the $\Omega = \{(\boldsymbol{e}_1, \boldsymbol{e}_2) | \dot{V}(\boldsymbol{e}) = 0\}$ was calculated.

$$\Omega = \{(\boldsymbol{e}_1, \boldsymbol{e}_2) | \boldsymbol{e}_2 = 0\} \tag{79}$$

Then the first step is the calculation of the second derivative of the Lyapunov function.

$$\ddot{V}(\boldsymbol{e}) = -\dot{\boldsymbol{e}_2}^{\mathrm{T}}\boldsymbol{K}_2\boldsymbol{e}_2 - \boldsymbol{e}_2^{\mathrm{T}}\boldsymbol{K}_2\dot{\boldsymbol{e}_2} \tag{80}$$

on the subset of Ω, Eq. (80) is equal to zero, since $\boldsymbol{e}_2$ is zero. The third derivative was shared in Eq. (81).

$$\dddot{V}(\boldsymbol{e}) = -\boldsymbol{e}_1^{\mathrm{T}}\boldsymbol{K}_1^{\mathrm{T}}\boldsymbol{K}_2\boldsymbol{K}_1\boldsymbol{e}_1 \tag{81}$$

On the subset of Ω, the third derivative is the first non-zero derivative, and it is negative definite, hence the system is asymptotically stable. Since, the Lyapunov function is globally unbounded, then it is globally asymptotically stable. Furthermore, The controller gains, k_1 and k_2 are chosen again by numerical optimization.

On the other side, since there was a limit on the level of thrust, the controller implemented will not be globally asymptotically stabilizing. Furthermore, due to unmodelled perturbances, the control will not reach to origin, but expected to oscillate around it.

4) Model Predictive Control: Model predictive control covers the future states and inputs and solves the optimal control problem:

$$\min \sum_{k=0}^{N} ||\boldsymbol{x}_{k+1}||_{\boldsymbol{Q}^2} + ||\boldsymbol{u}_k||_{\boldsymbol{R}^2} \tag{82}$$

$$\text{s.t.} \quad \boldsymbol{L}\boldsymbol{x} = \boldsymbol{b}$$

$$\boldsymbol{L}^{'}\boldsymbol{x} = \boldsymbol{b}^{'}$$

where $||\boldsymbol{x}_{k+1}||_{\boldsymbol{Q}^2}$ is the weighted vector norm. Furthermore, the states corresponds to, $\boldsymbol{x}_{\mathrm{k+1}} = [x_{1_{\mathrm{k+1}}}, x_{2_{\mathrm{k+1}}}, x_{3_{\mathrm{k+1}}}, x_{4_{\mathrm{k+1}}}, x_{5_{\mathrm{k+1}}}, x_{6_{\mathrm{k+1}}}]^{\mathrm{T}}$, where the first

three elements are the positions in the Hill frame, x, y, z respectively, and the final three elements are the corresponding velocities in Hill frame. The MPC, if the plant is linear, can be turned into a linear quadratic program.

$$\begin{aligned} \min_{\boldsymbol{X}} \quad & \frac{1}{2}\boldsymbol{X}^{\mathrm{T}}\boldsymbol{H}\boldsymbol{X} \\ \text{s.t.} \quad & \boldsymbol{L}\boldsymbol{X} = \boldsymbol{b} \\ & \boldsymbol{L'}\boldsymbol{X} \leq \boldsymbol{b'} \end{aligned} \tag{83}$$

In Eq. (83), $\boldsymbol{X} = [\boldsymbol{x}_{k+1|k}...\boldsymbol{x}_{k+N+1|k}, \boldsymbol{u}_{k|k}...\boldsymbol{u}_{k+N|k}] \in \mathbb{R}^{N(n+m)\times 1}$ and $\boldsymbol{H}$ is the square weight matrix, with dimension of $N(n+m)$, where n is the dimension of the states, m is the dimension of the control and N is the horizon of the MPC. Furthermore, $\boldsymbol{L} \in \mathbb{R}^{Nn\times N(n+m)}$ and $\boldsymbol{b} \in \mathbb{R}^{Nn\times 1}$. The dimensions of $\boldsymbol{L'}$ and corresponding $\boldsymbol{b'}$ depends on the constraints chosen by the user. A new notation is introduced here, which is, $\boldsymbol{x}_{k+1|k}$. That corresponds to, state at $k+1$ that is estimated at kth time, similarly for $\boldsymbol{u}_{k+1|k}$, the control input for $k+1$ step estimated at kth step. In other words, $\boldsymbol{X}$ vector is consisting of future states and control.

If the numerical capability of the hardware is limited there can be two horizons in the MPC, prediction horizon and control horizon. If the states until the horizon are included in the cost function without considering the corresponding control, it is prediction horizon. If control is applied as well, then it is control horizon. For this study, only the control horizon was considered, N.

The constraint matrices, $\boldsymbol{L}$ and $\boldsymbol{b}$ are representing the system dynamics. The system dynamics covered in this MPC is the discritized version of the Hill or CW equations using the approach shared in Section II-F.

a) Discretization of CW Equations: In order to apply the discretization shared in Section II-F, a state space representation was created, shared in Eq. (84). The main purpose of this discritization was to turn $\dot{\boldsymbol{x}}(t) = \boldsymbol{A}\boldsymbol{x}(t) + \boldsymbol{B}\boldsymbol{u}(t)$ into discrete equivalent $\boldsymbol{x}[k+1] = \boldsymbol{A}_d\boldsymbol{x}[k] + \boldsymbol{B}_d\boldsymbol{u}[k]$, where $\boldsymbol{A}$ and $\boldsymbol{B}$ are the state space matrices of the continuous system and $\boldsymbol{A}_d$ and $\boldsymbol{B}_d$ are of the discrete system. To begin with, the state space representation in continuous time was created using Eq. (46) which gives Eq. (84).

$$\begin{bmatrix} \dot{x}_1 \\ \dot{x}_2 \\ \dot{x}_3 \\ \dot{x}_4 \\ \dot{x}_5 \\ \dot{x}_6 \end{bmatrix} = \begin{bmatrix} 0 & 0 & 0 & 1 & 0 & 0 \\ 0 & 0 & 0 & 0 & 1 & 0 \\ 0 & 0 & 0 & 0 & 0 & 1 \\ 3n^2 & 0 & 0 & 0 & 2n & 0 \\ 0 & 0 & 0 & -2n & 0 & 0 \\ 0 & 0 & -n^2 & 0 & 0 & 0 \end{bmatrix} \begin{bmatrix} x_1 \\ x_2 \\ x_3 \\ x_4 \\ x_5 \\ x_6 \end{bmatrix} + \begin{bmatrix} 0 & 0 & 0 \\ 0 & 0 & 0 \\ 0 & 0 & 0 \\ 1 & 0 & 0 \\ 0 & 1 & 0 \\ 0 & 0 & 1 \end{bmatrix} \begin{bmatrix} u_x \\ u_y \\ u_z \end{bmatrix} \tag{84}$$

where x_1, x_2, x_3 corresponds to x, y and z positions in Hill frame, and x_4, x_5 and x_6 corresponds to velocities in the same axes. The next step was the calculation of the State Transition Matrix, $e^{\boldsymbol{A}(t-t_0)}$, or $\boldsymbol{A}_d$ with Eq. (19), the final form was shared in Eq. (85).

$$e^{\boldsymbol{A}t} = \begin{bmatrix} 4-3c(nt) & 0 & 0 & \frac{s(nt)}{n} & \frac{2-2c(nt)}{n} & 0 \\ -6nt+6s(nt) & 1 & 0 & \frac{-2+2c(nt)}{n} & \frac{4s(nt)}{n}-3t & 0 \\ 0 & 0 & c(nt) & 0 & 0 & \frac{s(nt)}{n} \\ 3ns(nt) & 0 & 0 & c(nt) & 2s(nt) & 0 \\ -6n+6nc(nt) & 0 & 0 & -2s(nt) & -3+4c(nt) & 0 \\ 0 & 0 & -ns(nt) & 0 & 0 & c(nt) \end{bmatrix} \tag{85}$$

where c is cosine function and s is the sine function. n is mean motion and t is the time. The $\boldsymbol{B}_d$ was calculated via using Eq. (17) which gives Eq. (86).

$$\boldsymbol{B}_d = \int_{t_0}^{t} e^{A(t-\tau)}\boldsymbol{B}d\tau = \begin{bmatrix} \frac{2s((nt/2)^2)}{n^2} & -\frac{2(s(nt)-nt)}{n^2} & 0 \\ \frac{2(s(nt)-nt)}{n^2} & \frac{8s((nt/2)^2)}{n^2}-1.5t^2 & 0 \\ 0 & 0 & \frac{2s((nt/2)^2)}{n^2} \\ \frac{s(nt)}{n} & \frac{4s((nt/2)^2)}{n} & 0 \\ \frac{-4s((nt/2)^2)}{n} & \frac{4s(nt)}{n}-3t & 0 \\ 0 & 0 & \frac{s(nt)}{n} \end{bmatrix} \tag{86}$$

b) Calculation of Constraints and Weights of MPC: The MPC has 5 different matrices and weights in total, namely $\boldsymbol{H}$, $\boldsymbol{L}$, $\boldsymbol{b}$, $\boldsymbol{L'}$ and $\boldsymbol{b'}$. The $\boldsymbol{L}$ and $\boldsymbol{b}$ are due to system dynamics, $\boldsymbol{L'}$ and $\boldsymbol{b'}$ are due to the system constraints or mission constraints. The $\boldsymbol{H}$ corresponds to the weights of the problem.

The $\boldsymbol{L}$ and $\boldsymbol{b}$ were obtained by creating the system dynamics for the whole horizon, which can be seen in (87) to (89). Notice that, in Eq. (87) the $[k+n|k]$ notation was dropped since everything was calculated at kth step.

$$\boldsymbol{x}_{k+1} = \boldsymbol{A}_d\boldsymbol{x}_k + \boldsymbol{B}_d\boldsymbol{u}_k \tag{87}$$

$$\boldsymbol{x}_{k+2} = \boldsymbol{A}_d\boldsymbol{x}_{k+1} + \boldsymbol{B}_d\boldsymbol{u}_{k+1} \tag{88}$$

$$\vdots$$

$$\boldsymbol{x}_{k+N+1} = \boldsymbol{A}_d\boldsymbol{x}_{k+N} + \boldsymbol{B}_d\boldsymbol{u}_{k+N} \tag{89}$$

Equation (87) can be plugged into Eq. (88), then this application can be done for the rest of the equations. The final form of the dynamical constraint, which reveals the $\boldsymbol{L}$ and $\boldsymbol{b}$ matrices is:

$$\begin{bmatrix} \boldsymbol{A}\boldsymbol{x}_k \\ \boldsymbol{A}^2\boldsymbol{x}_k \\ \vdots \\ \boldsymbol{A}^N\boldsymbol{x}_k \end{bmatrix} = \begin{bmatrix} \mathbf{I}_{n\times n} & 0 & \dots & 0 & -\boldsymbol{B} & 0 & \dots & 0 \\ 0 & \mathbf{I}_{n\times n} & \ddots & \vdots & -\boldsymbol{A}\boldsymbol{B} & -\boldsymbol{B} & 0 & 0 \\ \vdots & \ddots & \ddots & \vdots & \vdots & \ddots & \ddots & 0 \\ 0 & \dots & 0 & \mathbf{I}_{n\times n} & -\boldsymbol{A}^{\mathrm{N}-1}\boldsymbol{B} & \dots & -\boldsymbol{A}\boldsymbol{B} & -\boldsymbol{B} \end{bmatrix} \times \begin{bmatrix} \boldsymbol{X} \end{bmatrix} \tag{90}$$

where Eq. (90) is in the form of $\boldsymbol{b} = \boldsymbol{L}\boldsymbol{X}$, and $\mathbf{I}_{n\times n}$ denotes the identity matrix with dimension of n, the dimension of the

states. Furthermore, $\boldsymbol{L}^{'}$ and $\boldsymbol{b}^{'}$ were obtained by investigating the limitations of the system, specifically thrust saturation, $\mathrm{T_{max}}$. All the accelerations at each time step, shall be smaller than that of $\mathrm{T_{max}}/m_k$. It must be noted that, while that acceleration limitation was implemented, the mass was taken as constant and equal to the first time step mass. The constraint that was implemented is:

$$-\mathrm{T_{max}}/m_k \leq \begin{bmatrix} u_{\mathrm{k}} \\ u_{\mathrm{k+1}} \\ \vdots \\ u_{\mathrm{k+N-1}} \end{bmatrix} \leq \mathrm{T_{max}}/m_k \tag{91}$$

To translate this into linear programming, which can only take less than or equal to constraint, the left hand side of the non-equality was multiplied with -1 and implemented. Furthermore, in [86], it is found that, to enforce stability, a constraint set that enforces the final state set to be close to the equilibrium point, namely $\boldsymbol{x}_r$ is suggested to be implemented, and this condition is

$$|\boldsymbol{x}_{k+N} - \boldsymbol{x}_{r,k+N}| \leq d \tag{92}$$

where d is greater than equal to 0. The value of d is chosen by numerical trial-and-error, and different errors and values corresponding to different d values are enlisted in the Results Section.

The linear program in Eq. (83) is suitable for regulation problems. To account for tracking, the cost function was changed to, $\frac{1}{2}(\boldsymbol{X} - \boldsymbol{X}_r)^T \boldsymbol{H}(\boldsymbol{X} - \boldsymbol{X}_r)$, where $\boldsymbol{X}_r$ denotes the reference states, with 0 control in Eq. (93).

$$\boldsymbol{X}_r = [\boldsymbol{x}_{r_{\mathrm{k+1}}}, \boldsymbol{x}_{r_{\mathrm{k+2}}}, ..., \boldsymbol{x}_{r_{\mathrm{k+N+1}}}, 0, ..., 0] \tag{93}$$

When the terms purely depending on $\boldsymbol{X}_r$ are removed in the cost function, since they do not depend on minimization parameters, the new formulation of the cost function is given in Eq. (94).

$$J = \frac{1}{2}\boldsymbol{X}^T \boldsymbol{H} \boldsymbol{X} + \boldsymbol{f}\boldsymbol{X} \tag{94}$$

where $\boldsymbol{f} = -(\boldsymbol{X}_r^T(\boldsymbol{H} + \boldsymbol{H}^T))/2$.

According to [87], the system should be normalized so that the cost function is meaningful. If not normalized, then it must be done in the weight matrix. To normalize the states, the current reference trajectory at the beginning of the MPC optimization, $\boldsymbol{x}_{r_k}$ was used. For positions, norm of the first three elements of the reference, was used, denoted as $||\boldsymbol{x}_{r,p_k}||$ and for velocity, the norm of the last three elements of the reference vector at time k was used, denoted as $||\boldsymbol{x}_{r,v_k}||$, in Eq. (95). The square was added because, the multiplication of the states vector with the weight matrix was done twice for the each element. For the Rendezvous mission, the reference consisted of zeros. For that purpose, the initial reference trajectory for the Relative Orbit Mission was created and constantly used to normalize the weight matrix in the Rendezvous mission, so that the controllers in both of the missions will have similar performances.

$$\boldsymbol{P} = \begin{bmatrix} I_{3\times3}\frac{q}{||\boldsymbol{x}_{r,p_k}||^2} & 0_{3\times3} \\ 0_{3\times3} & I_{3\times3}\frac{q}{||\boldsymbol{x}_{r,v_k}||^2} \end{bmatrix} \tag{95}$$

The final form of the weight matrix $\boldsymbol{H}$ is

$$\boldsymbol{H} = \begin{bmatrix} \boldsymbol{P} & 0 & \dots & \dots & \dots & 0 \\ 0 & \ddots & \ddots & & & \vdots \\ \vdots & \ddots & \boldsymbol{P} & \ddots & & \vdots \\ \vdots & & \ddots & \boldsymbol{I}_{m\times m}\frac{r}{||\boldsymbol{u}_k^{\max}||^2} & \ddots & \vdots \\ \vdots & & & \ddots & \ddots & 0 \\ 0 & \dots & \dots & \dots & 0 & \boldsymbol{I}_{m\times m}\frac{r}{||\boldsymbol{u}_k^{\max}||^2} \end{bmatrix} \tag{96}$$

where q and r are the weights of the control acceleration and the states.

c) Model Predictive Control Framework: It is noticed that, a single cost function did not cover the whole domain of the trajectory, due to performance issues. For that reason, a Multi Objective Cost Function, with different weights were adapted. The idea behind that was, if the tracking error was high, automatically, the effect of it in the cost function was high as well, which reduces the price of the control effort, and allows the MPC to choose a higher consumption trajectory. However, when the error was reduced, this time the control effort dominated the cost function, and hence, the control effort was forced to be small, which introduces, relatively high amplitude steady state oscillations due to perturbations. To prevent that, a tracking error triggered switching cost function was applied. The initial weight of the states was set to be q_1 and the final weight of the states was q_2, similarly, for control, r_1 and r_2 were implemented. The tracking error was calculated as $||\boldsymbol{x}_k - \boldsymbol{x}_{r_k}||$, and if this value was less than k which is the switching error, the weight of the r was decreased, and set to be r_2.

In [87], it is stated that, to tune the system, the value for q should be kept as 1, and the value of r should be smaller than 1, e.g. 0.1. Basically, the tuning should be done with r_1 and r_2 rather than q_1 and q_2. The investigations showed that:

- r_2 affects the maximum error proportionally and fuel consumption inversely proportional in the steady state hence should be small
- r_1 affects the root mean square error proportionally, and affects the fuel consumption inversely proportional, should be an average value
- d affects proportionally the root mean square error as well, with smaller effect compared to r_1
- Switching error k, affects the root mean square error with a small effect compared to r_1

The first tuning was done to r_2 since it mostly affects the maximum error in the steady state in a proportional way. On the other hand, the r_1 dominated the root mean square error since the initial error where r_1 was used, was high. If r_1 was chosen small, then there was an increase in the fuel consumption, with a decrease in root mean square error. Furthermore, if r_1 was chosen big, while r_2 kept small, this time, the fuel consumption around the switching increased, and hence, the overall consumption went slightly up. For that reason, after trial-and-error, r_1 was kept as 0.05, while

r_2 was kept as 10^{-5}. When r_1 and r_2 are set, the next parameter was d. The various values of d did not effect the final maximum error at all due to disturbances effecting on the system, however, it effected the root mean square error and fuel consumption. It is seen that, d proportionally affects the root mean square error and inverse proportionally fuel consumption, however, the effect of it, compared to r_1 was small. Concerning different values of d, it was chosen as 2. For the switching error, k, if it was a small value, then again due to disturbances, the system might never reach it and switching of the cost function might not happen. Furthermore, if k was chosen a high value then the switch might occur early and might cause a better root mean square error with higher fuel consumption. Again implementing a trial-and-error, it was found that, k being 10 m suited for the performance purposes. The various parameters used in MPC are:

- q_1 is 1
- q_2 is 1
- r_1 is 0.05
- r_2 is 10^{-5}
- d is 2 m
- k is 10 m

The control horizon for MPC was chosen considering [83], [84] and [88]. References [83], [84] suggest that 15–30 thrust application in each orbit is enough for the stability, which corresponds to 24 control horizon and 33 prediction horizon with 240 s of discritization time. On the other hand, [88] suggests that half of the orbit should cover 30 thrust, and which corresponds to around 90 s of discritization time and 30 as the control horizon. Furthermore, [88] states that the onboard controllers can solve the optimization problem in 90 s.

When the initial tests were run, it was noticed that, when half of the orbit was discretized with shorter time, the performance of the system increased as expected. In other words, if the total time that was covered by the controller was kept constant while reducing the discritization time, the performance was increased. For that reason, a similar approach to [88] was implemented. The discretization time was set as 50 s and Control Horizon was set as 60 steps.

d) Stability of Model Predictive Control: The Model Predictive Control is based on solving an optimal control problem for a finite horizon, and implementing the first control of the solution at each time step. This approach makes it a non-linear control, hence to prove the stability, Lyapunov Stability Framework will be used.

Theorem III.1. *$J^*(\boldsymbol{x}_k) = \min_{\boldsymbol{u}} \sum_{i=0}^{N-1} ||\boldsymbol{x}_{k+i}||^2_Q + ||\boldsymbol{u}^2_{k+i}||_R$, where R and Q weight matrices are positive definite, and 0 is an equilibrium point with $\boldsymbol{u} = 0$. If the problem is initially feasible at $k = 0$, then $\lim_{k\to\infty} \boldsymbol{x}_k \to 0$ and $\lim_{k\to\infty} \boldsymbol{u}_k \to 0$, where $\boldsymbol{x}_k = 0$ and $\boldsymbol{u}_k = 0$ is an equilibrium point, $\forall k$* [89]

Proof. At time k, the control structure is $\eta_k = [u_k, u_{k+1}, ..., u_{k+N-1}]$ and assuming that η_{k+1} leads to equilibrium point of 0 where $\eta_{k+1} = [u_{k+1}, ..., 0]$. Then the difference of minimum cost functions at k and $k+1$ is,

$$J^\star(\boldsymbol{x}_k) - J^\star(\boldsymbol{x}_{k+1}) \geq \langle \boldsymbol{x}_k, Q\boldsymbol{x}_k \rangle + \langle \boldsymbol{u}_k, R\boldsymbol{u}_k \rangle \tag{97}$$

The above equation also holds for $k+1$ to $k+N-1$ since it reached the equilibrium point. From Eq. (97), the cost function is monotonically non-increasing function. By the definition of the cost function, which is quadratic and hence always greater than 0, and hence , bounded from below, that means the $J^*(\infty)$ or J^*_∞ is a finite value. Then summing the both sides of the Eq. (97) from zero to infinity reveals,

$$\infty \geq J^*(0) - J^*(\infty) \geq \sum_{k=0}^{\infty} [||\boldsymbol{x}_k||^2_Q + ||u_k||^2_R] \tag{98}$$

The right hand side of the Eq. (98) is an infinite sum and it goes to finite value, that means at infinity, the inside of the sum should reach 0. Since, $Q, R > 0$, then the only solution is $x \to 0$ and $u \to 0$ as $k \to \infty$. □

In the above theorem, without losing the generalization, the equilibrium condition is taken as 0. In the YASTM, if the eccentricity is 0, then the solution converges to Hill's solution. Furthermore, the reference trajectory $\boldsymbol{x}_r$ is created by taking input accelerations as 0, that means $\boldsymbol{x} = \boldsymbol{x}_r$ is an equilibrium point. For that reason, this stability theorem holds for the Reference Tracking as well. However, in the above theorem the disturbances were not included. As a result an oscillatory steady state error is expected due to perturbation effects.

Furthermore, if the cost function is changed at finite time, and the first optimization problem leads to $\boldsymbol{X}_{\text{final}} \in \Omega$. If this Ω is feasible for the new cost function, then the system under the second MPC with new cost function, will be asymptotically stable as well.

5) Impulsive Control Law: To compare the performances of the controllers, an Impulsive Law offered by [81] was used. It uses the Gauss Variational Equations, Eqs. (26) – (31), to regulate the tracking error of mean orbital elements at the best possible point of the orbit. The mean orbital element rate of change can be calculated based on Gauss' Variational Equations

$$\dot{\boldsymbol{\alpha}}_{\text{mean}} = \left[\frac{\partial \boldsymbol{\alpha}_{\text{mean}}}{\partial \boldsymbol{\alpha}}\right]^T \frac{\mathrm{d}\boldsymbol{\alpha}}{\mathrm{d}t} \tag{99}$$

where $\mathrm{d}\boldsymbol{\alpha}/\mathrm{d}t$ is the Gauss Variational Equations. [81] states that, the Jacobian $\partial\boldsymbol{\alpha}_{\text{mean}}/\partial\boldsymbol{\alpha}$, is basically an identity matrix with off diagonal elements being in the order of J_2. Hence, it is stated that, an assumption of that Jacobian being equal to Identity matrix can be done

$$\dot{\boldsymbol{\alpha}}_{\text{mean}} \approx \dot{\boldsymbol{\alpha}} = \boldsymbol{B}(\boldsymbol{\alpha}_{\text{mean}})\boldsymbol{u} \tag{100}$$

where $\boldsymbol{B}(\boldsymbol{\alpha}_{\text{mean}})$ corresponds to the Gauss Variational Equations with mean orbital elements. Furthermore, when Eq. (100) is used to calculate the required corrections to get rid of the tracking errors, the error will be on the order of J_2. When the magnitude of corrections goes to zero, the error introduced by the unity Jacobian will also go to zero [81].

In this control approach, the mean orbital elements will be corrected by pairs at the best possible time, $[i, \Omega]$, $[M, \omega]$ and $[a, e]$. The only undesired coupling is between i, Ω and ω. Notice that in this section, all the orbital elements are mean orbital elements.

a) Correction of $[i, \Omega]$*:* When Gauss Variational Equations are observed, it is seen that, both i and Ω's rate of change depend on the true anomaly and out-of-track acceleration.

$$\delta i = (r\cos\theta)/h\Delta v_h \tag{101}$$
$$\delta\Omega = (r\sin\theta)/(h\sin i)\Delta v_h \tag{102}$$

Then calculating the best possible true anomaly is by dividing Eq. (102) by Eq. (101). Then doing some algebraic manipulation and taking the arctangent of the result reveals the critical true anomaly.

$$\theta_{\text{crit}} = \text{atan}(\delta\Omega\sin i/\delta i) \tag{103}$$

When Eq. (101) and (102) is squared summed and rooted, the magnitude of the required Δv_h correction is found.

$$\Delta v_h = (h/r)\sqrt{\delta i^2 + \delta\Omega^2\sin^2 i} \tag{104}$$

As mentioned earlier, this correction causes a perturbing effect on ω. To get rid of this caused error, the magnitude of the drift will be calculated. To do so, Eq. (102) is manipulated and Δv_h is calculated in terms of $\delta\Omega$, and plugged in Eq. (30), shared in Eq. (105).

$$\delta\omega(\Delta v_h) = -\cos i\,\delta\Omega \tag{105}$$

This drift will be included in the correction of ω and M.

b) Correction of $[\omega, M]$*:* The Ω and M are corrected at perigee and apogee. They are corrected with radial thrusting. For the ease of readability, the GVE equations are shared here, for changing velocity at the Perigee, Δv_{r_p} and Apogee, Δv_{r_a}.

$$\delta\omega = (1/he)\left[-p(\Delta v_{r_p} - \Delta v_{r_a})\right] - \delta\Omega\cos i \tag{106}$$
$$\delta M = (\eta/(he))\left[(p - 2r_p e)\Delta v_{r_p} - (p + 2r_a e)\Delta v_{r_a}\right] \tag{107}$$

Where, r_p and r_a corresponds to the magnitude of the position at Perigee and Apogee, respectively. To calculate the magnitudes of corresponding Δv_{r_p} and Δv_{r_a}, the identities below are used.

$$p = a(1 - e^2) \tag{108a}$$
$$r_a = a(1 + e) \tag{108b}$$
$$r_p = a(1 - e)h/p = na/\eta \tag{108c}$$

When Eq. (108) is combined with Eq. (106) and (107), with algebraic manipulations, the Δv_{r_a} and Δv_{r_p} are calculated.

$$\Delta v_{r_p} = -(na/4)\left\{\left[(1 + e)^2/\eta\right](\delta\omega + \delta\Omega\cos i) + \delta M\right\} \tag{109}$$

$$\Delta v_{r_a} = -(na/4)\left\{\left[(1 - e)^2/\eta\right](\delta\omega + \delta\Omega\cos i) + \delta M\right\} \tag{110}$$

As mentioned earlier, the coupling in Ω and ω is included, and corrected at apogee and perigee.

c) Correction of $[a, e]$*:* a and e are corrected at the Perigee and Apogee as well, with Δv_{θ_a} and Δv_{θ_p}. The corresponding GVE are in Eq. (111) and (112).

$$\delta a = (2a^2/h)\left[(p/r_p)\Delta v_{\theta_p} + (p/r_a)\Delta v_{\theta_a}\right] \tag{111}$$
$$\delta e = (1/h)\left[(p + r_p + r_p e)\Delta v_{\theta_p} + (-p - r_a + r_a e)\Delta v_{\theta_a}\right] \tag{112}$$

Again applying algebraic manipulations reveals the magnitudes of the Δv.

$$\Delta v_{\theta_p} = (na\eta/4)\left[\delta a/a + \delta e/(1 + e)\right] \tag{113}$$
$$\Delta v_{\theta_a} = (na\eta/4)\left[\delta a/a - \delta e/(1 - e)\right] \tag{114}$$

d) Rocket Equations: In this section, some of the fundamentals of Rocket Equations that are used was given. As given in Tab. II, the level of thrust was known, and the corresponding specific impulse, I_{sp}. However, the amount of fuel burnt was not known. To calculate fuel burnt, Eq. (115) was used, which derived from Newton's second law by ignoring the perturbing effects.

$$T_{\text{tot}} = \frac{\text{d}\,m}{\text{d}\,t}V_{\text{eff}} \tag{115}$$

where V_{eff} denotes the "effective" exhaust speed and $V_{\text{eff}} = \text{I}_{\text{sp}}\,\text{g}_0$. where g_0 is the nominal gravitational acceleration and it is 9.81 m/s^2. Since T_{tot}, total thrust applied, and I_{sp} are known, $\dot{m}$ can be calculated by using Eq. (115).

Eq. (116) is created by assuming air drag is not existing, and only acceleration is coming from Eq. (115), i.e. thrust is applied.

$$m\frac{\text{d}\,V}{\text{d}\,t} = -\frac{\text{d}\,m}{\text{d}\,t}V_{\text{eff}} \tag{116}$$

Separating the variables to corresponding derivatives and integrating reveals the equation

$$\Delta V = -\text{I}_{\text{sp}}\text{g}_0\ln\left(\frac{m_f}{m_0}\right) \tag{117}$$

where m_f denotes the final mass after the thrust is applied, and m_0 denotes the initial mass. Since time rate of change of mass is linear, $m_f = m_0 + \Delta t\,\dot{m}$ can be written. Putting that into Eq. (117) and solving for time change reveals Eq. (118)

$$\Delta t = \frac{m_0(\text{e}^{\frac{-\Delta v}{\text{I}_{\text{sp}}\text{g}_0}} - 1)}{\dot{m}} \tag{118}$$

Equation (118) is useful to calculate the thrusting time for a given $\Delta\, v$.

e) Control Structure: It is stated that, the error throughout the orbit does not deviate too much, hence, at the beginning of each orbit, the error is calculated.

$$\bar{\mathbf{oe}}_{dd} = \bar{\mathbf{oe}}_c + \delta\bar{\mathbf{oe}}_r \tag{119}$$
$$\delta\bar{\mathbf{oe}} = \bar{\mathbf{oe}}_{dd} - \bar{\mathbf{oe}}_d \tag{120}$$

where $\bar{\mathbf{oe}}_{dd}$ is the desired Deputy mean orbital elements, calculated as described in Section III-C2, and $\delta\mathbf{oe}_r$ is the reference Differential Orbital Elements. Subscript c denotes the Chief, subscript r denotes the reference and d denotes the Deputy. Then, critical Argument of Latitude, θ_{crit} was calculated by Eq. (103). The required Δv's were calculated by Eqs. (104), (109), (110), (113) and (114). Since the specific impulse and maximum thrust capabilities of the thrusters were known, the required time to apply each Δv was calculated by Eq. (118).

Since the point of applications are known beforehand, i.e. θ_{crit}, apogee and perigee, the time of application can be

calculated. It is known that, the effect of most of the thrusting scheme depends on sinusoidal functions, due to GVE. To increase the efficiency, the ideal point of thrust, such as exact location of perigee or apogee, is held in the middle of the thrusting time. For example, if the satellite will be at Perigee at $t = 3000$ s, and the thrusting time is calculated as $\Delta t = 20$ s, then at time 2990 s the thrusting will start and will end at 3010 s. To calculate the time that satellite will reach the desired true anomaly, the Keplerian orbit was assumed, and the time of thrusting was updated at each 200 s in order to reduce the error due to perturbations.

E. Reference Feeding

The controller frames were requiring different reference trajectories resolved in different frames. In details, Sliding Mode Controller and Feedback Linearization requires reference position in ECI frame, MPC requires reference positions in Chief's LVLH Frame and Impulsive Control requires the reference orbit in orbital elements differences.

In Feedback Linearization, Sliding Mode and MPC, the reference position was created by, as mentioned earlier, YASTM, which was in Hill's frame, and can be directly feedable to MPC. To turn it to ECI frame, the transformation, explained in Section II-E1 was used.

For the Impulsive Control, the reference mean orbital element differences were created by Eq. (60), and the approach in Eq. (120) was implemented to calculate the required corrections.

F. Tuning

In order to have a meaningful comparison, the controller were tuned, specifically Feedback Linearization Controller and Sliding Mode Controller. The tuning here was done by the means of numerical optimization.

The objective value of the numerical optimization was covering both the tracking error and the fuel consumption. In order to get rid of the effect of units, the total fuel, was 11 kg and the tracking error, if controller was not tuned for example, can be orders of km, tracking error and fuel consumption were normalized. The tracking error is relative error, normalized with the magnitude of the reference, in Eq. (121). The fuel consumption, was normalized as well, with the total fuel onboard.

$$\boldsymbol{e}_t(t) = \left| \frac{\boldsymbol{r}^{\mathrm{I}}_{\mathrm{DI}}(t) - \boldsymbol{r}^{\mathrm{I}}_{\mathrm{RI}}(t)}{\boldsymbol{r}^{\mathrm{I}}_{\mathrm{RI}}(t)} \right| \tag{121}$$

where $\boldsymbol{e}_t$ is the normalized relative tracking error and $r^{\mathrm{I}}_{\mathrm{RI}}$ is the reference to be tracked . For the relative fuel consumption, Eq. (122) was implemented.

$$c_f = 1 - \frac{m_{\mathrm{final}} - m_{\mathrm{structure}}}{m_{\mathrm{fuel}}} \tag{122}$$

Concerning the fuel consumption and tracking relative error, the Cost function of the numerical optimization problem was given in Eq. (123).

$$\min_{\text{control params}} \quad J = \sqrt{\frac{\sum_{t_0}^{t_f} \boldsymbol{e}_t^2(t)}{t_f - t_0}} + r\, c_f \tag{123}$$

where r is the weight of the fuel consumption. Notice that, a root mean square (RMS) approach for the relative tracking error was implemented. The need to add r as a multiplication constant for c_f was due to the fact that, even though both of the parts in cost function was normalized, the relative error was slightly bigger. To compensate the order of fuel consumption, r was set to be 3.5 .

Furthermore, while Tuning, the most dominant perturbation in the altitude of 700 km, which is J_2 perturbation, was considered in the numerical simulations as shared in Eq. (25).

In addition, in both of the control algorithms that was tuned, the cold gas thrust system that is shared in Tab. II was used.

1) ABC Algorithm: As mentioned earlier, the ABC algorithm imitates the forging behavior of a bee colony. The food locations represents possible solutions to the optimization problem. The bees are the agents that tries and decides the quality, or fitness of the possible solution. There are three different bees, employed bees which seeks the neighbour hood of the solution and tries to find a new and better solution, onlooker bees which choose a food source depending on its quality and seeks new and better solution, and scout bees, which randomly seeks through the region if a food source's limit is reached [62]. The ABC algorithm can be summarized as:

- Initialize the food sources
- Evaluate the quality of the food source
- Repeat
  - Employed bees work on their food sources
  - Onlooker bees work on specific food source
  - Scout bees seeks new food sources
  - Memorize the best solution
- Repeat until the Maximum Cycle is reached

In the Employed bee phase, the bees search a new solution, v_i in the neighbourhood of the food location, x_i, and checks the quality of the new solution with the current solution. If the new solution is better, then they memorize the new solution's location. The new solutions are generated by random function

$$v_{ij} = x_{ij} + \phi_{ij}(x_{ij} - x_{kj}) \tag{124}$$

where subscript k is element of the the size of the employed bees, and j is element of the dimension of the problem. The k should be different than the current index i. Furthermore ϕ_{ij} is a random number in between $[-1, 1]$. When the Employed bees searched through the food locations, the Onlooker bees start their search. They choose a food location depending on its fitness value calculated as in Eq. (125). When the food location is decided, Onlooker bees do the same search as shared in Eq. (124).

$$p_i = \frac{\mathrm{fit}_i}{\sum_{n=1}^{\mathrm{SN}} \mathrm{fit}_n} \tag{125}$$

where SN denotes the size of the onlooker bees or the Employed bees, since they are equal. If the both Onlooker bees or the Employed bees cannot improve the solution at hand until a specified limit, then the food source is depleted, and it is removed from the memories of the bees. Then the

Employed bee of the food source becomes a Scout bee, and Scout bees seek new food locations based on Eq. (126).

$$x_i^j = x_{\min}^j + \text{rand}[0,1](x_{\max}^j - x_{\min}^j) \tag{126}$$

where $x_{\min}^j$ and $x_{\max}^j$ denotes the lower and upper bounds of the parameter of j [62].

2) Parameters of ABC: The parameters to be set in ABC are that, Limit, Maximum Cycle, Size of The Colony and the initialization range of the parameters. It is stated in [90], that the ABC algorithm is robust with respect to the colony size, hence it does not require fine tuning with the colony size. In other words, colony size can be a free variable, hence it was set as 50. The dimension of the problem for the both of the controller tuning cases was 2, k_1 and k_2 for the Feedback Linearization and a and μ_0 for the Sliding Mode Controller. It is stated that, the limit for each parameter should be set dimension of the problem times the colony size, hence it was set to be 100.

For the initialization of parameters, it is said that, if the global minimum is in the middle of the range, then the optimization algorithms does locate it easily. However, for the ABC algorithm, [90], since there are Scout bees that seeks the entire region, the ABC algorithm is less sensitive to initialization problems compared to other algorithms. Furthermore, while specifying the initial range, the trial-and-error method is used. It is noticed that, if the gains are approximately 10^{-2}, they reveal better fuel consumption with slightly higher error than gains around order of 10^0. Hence the range is set to be 0.1 to 10^{-8} for Feedback Linearization, 1 to 10^{-8} for Sliding Mode Controller.

The maximum cycle number in [90] is 10^4. However, due to numerical intensity of the problem at hand, the maximum cycle number was taken as 10^3. Furthermore, the convergence of the minimization problem, by investigating the history of the objective value of the solutions, was observed in order to conclude that the minimization is converged to a value.

In the initialization phase of the ABC, algorithm randomly generates the food source location. To speed up the process, a gain set, or food location, found by trial-and-error was added to the food sources.

G. Test Scenarios

In order to compare the performances of the controllers, different scenarios was applied. The Mango Satellite's orbital elements are 7,078,137 m of semi-major axis, 0.00547 of eccentricity, 198.98 degree of argument of perigee, 23.1 degree of right ascension of the ascending node, 98.2 degrees of inclination. The mean anomaly was set to be 0.

The covered mission is similar to that of the Prisma Satellite's mission shared in reference [42]. This mission has Δa of 0 m, Δe as 0.7064 $\times 10^{-4}$, $\Delta\omega$ of 0.0199 $\times 10^{-4}$ deg, $\Delta\Omega$ of 0.1393 $\times 10^{-4}$, Δi of 0.4008 $\times 10^{-4}$ deg and ΔM of 0 deg as it is reference mean orbital element difference.

When the Gauss Variational Equations based on mean orbital elements and J_2 perturbations are investigated, it was found that, if orbital elements of Deputy a, e, i were different than that of Chief, then J_2 perturbances effect were different which causes a drift in the relative position. As a result, the test scenarios was based on differences in those orbital elements as errors. The initial errors for the test scenarios are shared in Tab. III.

TABLE III
TEST SCENARIO ERRORS IN TERMS OF ORBITAL ELEMENT DIFFERENCES

Errors	1	2	3	4
δa [m]	100	0	0	100
δe [–]	0	0.00001	0	0.00001
$\delta\omega$ [deg]	0	0	0	0
$\delta\Omega$ [deg]	0	0	0	0
δi [deg]	0	0	0.001	0.001
δM [deg]	0	0	0	0.001

Relative Orbit mission can be seen in Fig. 2. In X-Y plane, it is an ellipse with semi-major axis of 1 km with semi-minor axis of 500 m, in X-Z plane semi major axis of 500 meters and semi-minor axis of 300 m.

IV. RESULTS

In this section, various control approaches shared in Method was tested with the initial conditions in Section III-G. The numerical solvers for simulations involving Sliding Mode and Feedback Linearization was an adaptive Runge–Kutta (4,5) method. On the other hand, since Impulsive Law, and MPC requires the time to be known to apply thrust, Runge–Kutta 4 with step size of 1 s was implemented. In all the control laws except Impulsive Control Law offered by Schaub and Alfriend [81], the cold gas system was used.

As mentioned earlier, the numerical simulations, except optimization, and investigation of effects of the gains, the results are obtained by using the GRACE Gravity Model 03, which includes the oblateness effect of the Earth. This is achieved by using HPOP for Matlab created by Mahooti [91].

Most of the comparison in the results were done for Δv, which presents how much fuel is consumed, Root Mean Square Error (RMSE) which shows the averaged error throughout the simulation. Additionally, it shows also the performance of the tracking error. If a controller converges to the reference fast, then the RMSE of this scenario is small. The last parameter that was used is, maximum error in the steady state. Since there exist perturbations, it is expected to have oscillations in the steady state. Furthermore, if precision is important in a mission, one of the vital parameters would be maximum error, hence, taken as a performance parameter.

This part starts with the results of the numerical optimization, then continues with the results of the each control method. Finally, the comparison of each controller was shared.

A. Tuning

The gain tuning for Feedback Linearization and Sliding Mode Controller was achieved with ABC by only considering the most dominant effect on 700 km altitude. The maximum cycle of the ABC was set, as mentioned before, as 10^3 iterations for both of the controllers. Furthermore, the cold gas system is implemented for the optimization. The resultant

controller gains are shared in Tab. IV. For tuning, the Chief is located to the orbit shared in Section III-G. Furthermore, the initial errors are corresponding to combination of error case 1 to 3 in Tab. III. The simulations were done for 2 orbit time.

TABLE IV
THE RESULTS OF THE NUMERICAL OPTIMIZATION

Sliding Mode Gains		Feedback Lin. Gains	
a	0.001349	k_1	0.000003865
μ_0	0.2460	k_2	0.002887

The convergence history of the numerical optimization is shown in Fig. 4.

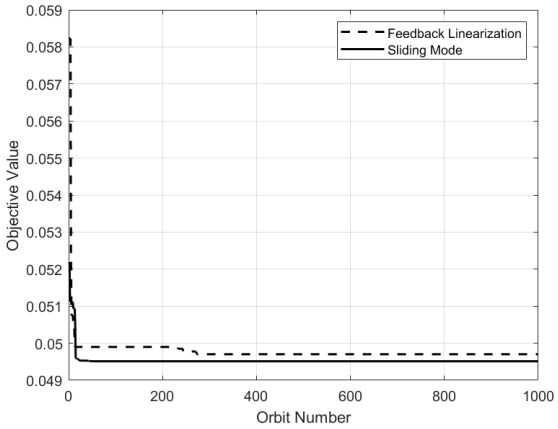

Fig. 4. The Objective Value Histories of the Numerical Optimization

It was seen that, after 200 iterations, the numerical optimization algorithm converged to a value, which corresponds to the local minimum. Furthermore, the numerical optimization algorithm was run twice to conclude that it was a local minimum. Moreover, the initial gains seemed to speed up to process, since the solutions for the controllers converged to the real value fast. Additionally, the numerical solvers for the simulations inside the numerical optimization was chosen as variable step Runge–Kutta solver (4-5).

B. Feedback Linearization

It was seen that, the gains of the controller plays an important role on the fuel consumption and error tracking, as expected. If the gains were set to a high value, then it was observed that the fuel consumption was high, however, tracking error was low. The results of the various control gains are shared in Tab. V. The gains were set such that the damping ratio of the system was the same in all of the cases. The initial error for the tests was the combination of the first three error cases shared in Tab. III, and the analysis were done for a time of 5 orbits.

TABLE V
VARIOUS GAINS FOR FEEDBACK LINEARIZATION, HOLDING THE DAMPING RATIO CONSTANT

	High		**Medium**		**Low**	
	k_1	k_2	k_1	k_2	k_1	k_2
Gain Level	0.02	0.57	0.01	0.4	0.0025	0.2
Δv [m/s]	5.52		3.88		2.05	
RMSE [m]	22.97		19.65		15.10	
Max. Error [m]	0.0083		0.012		0.023	

In Tab. V, as the gains were decreased, the fuel consumption, i.e. the Δv was decreased, from left column to right column. Correspondingly, the maximum error of the system, after the system reaches its equilibrium, is increased. On the other hand, the RMSE is decreased towards lower gains. The reason behind that is, when the gains are increased, the system becomes more agile, while, the damping of the system held constant. In other words, based on a mass-damper-spring system, the damper of the system is held constant, while the spring became more stiff. The overall effect is that, the system cannot damp efficiently, and hence oscillations to the system is introduced, which increases the RMSE.

C. Sliding Mode Control

A similar gain analysis for the Sliding Mode was done in this part. Notice that the investigation here was done for 5 orbits. In Sliding Mode Control, the created manifold $s(\boldsymbol{e})$, governs the dynamics. For that reason it is noticed that a dominates the performance. If a was chosen to be large, then the system was forced to converge to the origin rapidly. This means that the possibility of reaching the saturation limit of the thrusting capability and therefore making the system unstable, or introducing oscillations since, the system dynamics became faster, was increased. If a was chosen small, it is noticed that the system spent slightly more fuel. In other words, it was thought that system travels unnecessary routes and spent fuel while doing so. On the other hand, μ_0 forces system to converge to the sliding manifold, and dominate the perturbances. If μ_0 was chosen small, i.e. on the order of 10^{-3}, then system might have problems to converge to the sliding manifold. This was believed to be due to the fact that, the upper bound in Lyapunov derivative was set to be strict.

The investigation of the gains were done in 3 steps while using the initial error as the combination of the first three error cases shared in Tab III. First, the optimal a was used and μ_0 was varied, which can be seen in Tab. VI.

TABLE VI
VARIOUS GAINS FOR SLIDING MODE, USING OPTIMAL SLIDING MANIFOLD, a = 0.0013

	High	Medium	Low	Very Low
μ_0	0.5	0.1	0.05	0.001
Δv [m/s]	0.58	0.57	0.54	21
RMSE [m]	13.59	13.43	13.55	69142
Max. Error [m]	0.15	0.22	0.38	164481

As can be seen in Tab. VI, the increase in the μ_0, resulted in higher fuel consumption or Δv, however, the maximum error in the steady state region was smaller. Furthermore, the

system followed the same sliding manifold in a good fashion, hence, the RMSE did not change too much. The Very Low case showed that the system diverged, or an unstable system, therefore, it was not considered for the above comments. Briefly, when optimal sliding manifold was used, μ_0 affected the maximum error inversely proportional, and fuel consumption proportionally.

For the second investigation, a faster converging system, i.e. a sliding manifold with higher a was investigated, which can be seen in Tab. VII.

TABLE VII
VARIOUS GAINS FOR SLIDING MODE, USING BIG COEFFICIENT SLIDING MANIFOLD, $a = 0.013$

	High	Medium	Low	Very Low
μ_0	0.5	0.1	0.05	0.001
Δv [m/s]	2.11	2.17	2.21	22
RMSE [m]	15.31	15.35	15.42	104459
Max. Error [m]	0.014	0.037	0.086	256247

When Tab. VI and Tab. VII were compared, it was noticed that the maximum errors of higher a were lower, however the corresponding fuel consumption was higher. For non-optimal and larger coefficient sliding manifold, increase in μ_0 corresponded to a decrease in the fuel consumption, maximum error and the RMSE. The reason behind that was, decrease in μ_0 introduced oscillations, which required further fuel consumption as well. This was the believed to be the reason, why increase in a increased the RMSE. However, on the optimal sliding manifold case, it was noticed that the decrease in μ_0 did not cause any oscillations, hence the fuel consumption did not increase.

For the third investigation, a slower manifold was chosen.

TABLE VIII
VARIOUS GAINS FOR SLIDING MODE, USING SMALL COEFFICIENT SLIDING MANIFOLD, $a = 0.0003$

	High	Medium	Low	Very Low
μ_0	0.5	0.1	0.05	0.001
Δv [m/s]	0.84	0.82	0.84	16
RMSE [m]	21.96	21.27	22.10	17912
Max. Error [m]	0.30	0.39	0.50	44991

As mentioned earlier, gain a dominates the dynamics, since the observations for the previous investigations could not be made for the VIII, except, the maximum error decreasing with an increase in μ_0. Furthermore, it was observed that, RMSE was increased with a decrease in a, comparing Tab. VI and VIII, since the dynamics of the system was forced to be slower.

D. Model Predictive Control

In this section, the effects of various parameters in MPC was shown based on Δv, RMSE and the maximum error in the steady state. The analysis was done for 5 orbits, with the combination of the first three error cases in Tab. III. Initially, the performance of a single cost function was shown, by varying the weight of the input. Then, the effect of d, the final state condition, and k, switching error, (which can be seen in Section III-D4c), was investigated. Finally, the effect of r_1 and r_2 was shown.

When the input weight was decreased for single cost function application, as can be seen in Tab. IX, the RMSE and maximum error were decreased, with an increase in fuel consumption. It was decided that, if the maximum error is desired to be low, with a lower fuel consumption, then the combination of a high and low input weights with separate cost functions for different region of trajectory was desired. In details, when the error is high, r will be high, and when the error is small, then r will be small as well, which will be acquired with a switching cost function system.

TABLE IX
RESULTS OF DIFFERENT INPUT WEIGHTS FOR MPC FOR SINGLE COST FUNCTION, FOR $d = 2$

	High	Medium	Low	Very Low
r	1	0.01	0.0001	0.00001
Δv [m/s]	0.48	0.54	0.58	0.59
RMSE [m]	30.31	15.24	14.11	14.06
Max. Error [m]	6.57	1.34	0.34	0.30

The next step was, to show the effect of k, the switching error, and d. To achieve that, two combination of the r_1 and r_2 were compared, for different values of the d and k.

TABLE X
THE RESULTS OF VARIOUS k VALUES, FOR $r_1 = 0.05, r_2 = 5 \cdot 10^{-5}$ AND $d = 2$

	Very Low	Low	Medium	High
k	1	5	10	15
Δv [m/s]	0.50	0.50	0.50	0.51
RMSE [m]	17.44	17.39	17.41	17.45
Max. Error [m]	0.32	0.32	0.33	0.32

TABLE XI
THE RESULTS OF VARIOUS k VALUES, FOR $r_1 = 1, r_2 = 1 \cdot 10^{-5}$ AND $d = 2$

	Very Low	Low	Medium	High
k	1	5	10	15
Δv [m/s]	0.48	0.47	0.47	0.47
RMSE [m]	30.31	28.86	28.86	28.88
Max. Error [m]	6.57	0.30	0.30	0.30

As can be deduced from the Tab. X and XI, it was seen that, the k, switching error, had limited effect, compared to r. Because, from very low to high value, the RMSE and fuel consumption changed slightly. In addition to that, when the Tab. XI's first column was observed, the maximum error was different than the other cases, which was dominated by r_2 which was set to be the same for all. The reason behind that was, the cost function never switched. So it was easy to see that, if k is set to a small value, then switch might not happen. Briefly, the k has a limited effect on fuel consumption, RMSE and quite negligible effect on maximum error. If k is chosen small, then the system may never switch inbetween cost functions.

TABLE XII
THE RESULT OF VARIOUS d, FOR $r_1 = 1, r_2 = 1 \cdot 10^{-5}$ AND $k = 10$

	Off	Low	Medium	High
d	0	0.1	1	2
Δv [m/s]	0.48	0.47	0.47	0.47
RMSE [m]	30.71	28.72	28.79	28.86
Max. Error [m]	0.28	0.30	0.30	0.30

The Tab XII corresponds to a High r_1 case. Notice that, if the condition related to d was not implemented, corresponds to the Off column, the performance of the system degraded, i.e the RMSE and fuel consumption increased. The decrease in d corresponded to smaller RMSE, and higher fuel consumption. However, once implemented the effect of the constraint becomes limited, for example, from Medium to High, or Low to Medium cases, the changes in both RMSE and fuel consumption were small.

TABLE XIII
THE RESULT OF VARIOUS d, FOR $r_1 = 0.05, r_2 = 5 \cdot 10^{-5}$ AND $k = 10$

	Off	Low	Medium	High
d	0	0.1	1	2
Δv [m/s]	0.51	0.50	0.50	0.50
RMSE [m]	17.24	17.39	17.41	17.41
Max. Error [m]	0.31	0.32	0.32	0.32

Similarly, Tab. XIII corresponds to small RMSE scenario with small r_1. In this scenario, again the implementation of d decreased the fuel consumption, with a slight increase in RMSE. Change in d, similar to k, in both cases, did not effect the performance significantly.

TABLE XIV
THE COMPARISON OF DIFFERENT VALUES OF r_2, FOR $r_1 = 1$ $d = 2$, $k = 10$

	High	Medium	Low	Very Low
r_2	0.5	0.01	0 .005	$1 \cdot 10^{-5}$
Δv [m/s]	0.48	0.48	0.48	0.47
RMSE [m]	29.95	28.88	28.86	28 .86
Max. Error [m]	5.25	1.34	0.41	0.30

To investigate the effect of switching cost function methodology, Tab. XIV was created, and was compared with Tab. IX. As can be seen, all the Δv and RMSE of the Tab XIV were close to High case of Tab. IX. The reason behind that was, the most of the fuel consumption and RMSE were due to the initial error which was covered by the cost function with r_1. Additionally, r_2 dominates the steady state error. As a result, it was obvious that, the switching cost function methodology, without increasing the fuel consumption too much, decreased the maximum error. On the other hand, different values of r_1 for a constant r_2 were shared in Tab. XV. The fuel consumption decreased with an increase in RMSE, when r_1 was increased. However, it was noticed that, the switching may also increase the fuel consumption, which can be seen in the High column of Tab. XV. From, Medium to High, even though the RMSE was increased, the fuel consumption stayed constant. It was observed that, at High case, the second cost function spent more fuel than the other cases so that the maximum error could be small like others. In addition, as mentioned earlier, the maximum error in steady state did not change when r_2 held constant.

TABLE XV
THE COMPARISON OF DIFFERENT VALUES OF r_1 FOR $r_2 = 1 \cdot 10^{-5}$, $d = 2, k = 10$

	High	Medium	Low	Very Low
r_1	5	0.5	0.01	0.0001
Δv [m/s]	0.48	0.48	0.52	0.58
RMSE [m]	40.20	25.22	15.24	14.11
Max. Error [m]	0.30	0.30	0.30	0.30

Briefly, it was observed that, the d and k has limited effects compared to r_1 and r_2. Generally, r_1 dominated the RMSE and fuel consumption while r_2 dominated the maximum error in steady state.

E. Impulsive Control Law

The Impulsive Law offered by Schaub and Alfriend [81] was implemented, and in this part, it was compared with the results shared in [81], to show that the controller was implemented correctly. The orbit used in [81] corresponds to an orbit with 7555 km of semi-major axis, 0.05 of eccentricity, 48 degrees of argument of perigee, 20 degrees of right ascension of the ascending node, 10 degrees of inclination with 120 degrees of initial mean anomaly which are mean orbital elements. The initial errors of 100 m in mean semi-major axis, 0.05 degrees of error in mean inclination, and -0.01 degrees of error in mean right ascension of the ascending node was used. There were two comparison cases, one implementation with no thrusting limit, i.e. all the control commands in terms of Δv can be applied directly, and with thrusting limit, i.e. thrust saturation at 1 N. As can be seen from Tab XVI, both of the implementations of [81], were able to converge to the reference in 4 orbit. However, the total Δv consumption stated in [81] is 6.46 [m/s] for the same problem. The total Δv consumption for the case without thrusting limitation was 4.9% higher and with thrusting limitation was 5.4% higher. This means, the implementation was not perfect, however, it is believed that, this is inevitable. Because, most definitely, the reference and implementation used different methods at some parts of the application, which caused the error.

TABLE XVI
FINAL ORBITAL ELEMENT ERROR AND VELOCITY CHANGE FOR 4 ORBITS

Orbital Elem. Error	With Thrust Limit	Without Thrust Limit
δa [m]	-5.922 $\times 10^{-5}$	1.3026×10^{-3}
δe	-1.378×10^{-10}	-2.0445×10^{-7}
$\delta \omega$ [rad]	-1.505×10^{-6}	-7.4293×10^{-6}
$\delta \Omega$ [rad]	1.888×10^{-7}	2.9388×10^{-7}
δi [rad]	-7.356×10^{-9}	-2.1437×10^{-7}
δM [rad]	1.378×10^{-6}	4.7059×10^{-6}
Δv [m/s]	6.7684	6.8014

F. Relative Orbit Mission

In this part, the performances of each controller was obtained for the Prisma mission like relative orbit mission.

Orbital elements of the Chief satellite was shared with different error cases in Section III-G and compared, an example result can be seen in Figs. 5 and 6. The comparison was based on Δv, RMSE, maximum error in the steady state, and settling time. In this study, settling time is used as the time it takes for controller to clear 90% of the initial error.

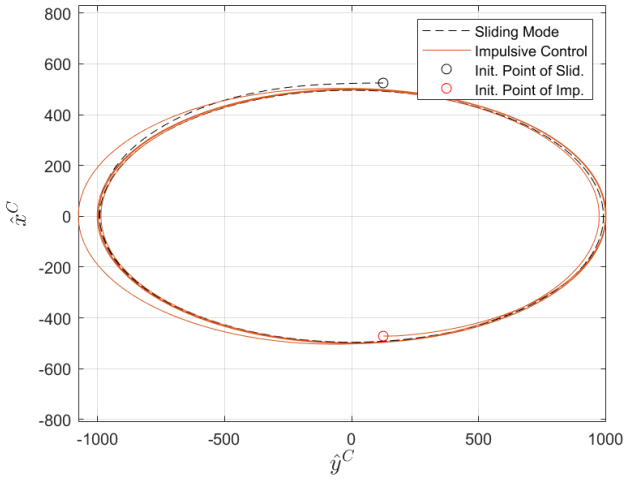

Fig. 5. Relative Orbit Mission, with Initial Error Case 4, with Respect to LVLH Frame of Chief x and y axis

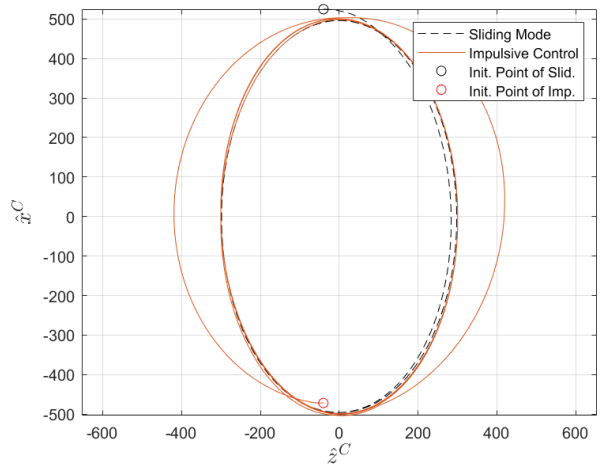

Fig. 6. Relative Orbit Mission, with Initial Error Case 4, with Respect to LVLH Frame of Chief x and z axis

The impulsive control law was used as a benchmarking method. However, since it uses a different type of reference method, i.e. mean orbital element difference, it required further effort to calculate the reference error. In order to compare the tracking error of the Impulsive Control Law with others, a reference was created by the same means as the other controllers, which introduced some numerical errors.

It was observed that, in all the cases, the Impulsive Law, in terms of Δv outperformed the designed controllers, near 2 to 3.5 times less Δv usage. On the other hand, RMSE wise,

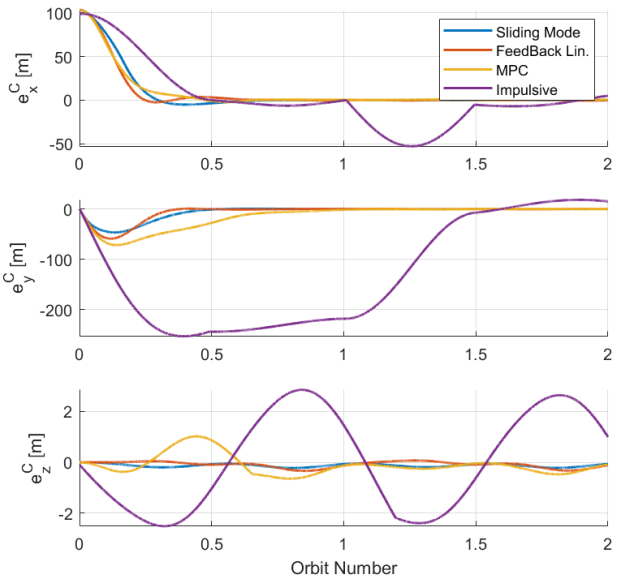

Fig. 7. The Tracking Errors in LVLH Frame of Chief for Relative Orbit Mission Case 1

it gave approximately 3 to 5 times higher errors. The Sliding Mode Controller had the largest Δv for all the cases, with lowest RMSE (for three cases out of four), and minimum error in steady state. Its settling time was the second best among all the controllers after Feedback Linearization.

The Feedback Linearization controller, had the smallest Δv for two cases out of four among the designed controllers and had the second lowest RMSE, for three out of four cases. Its maximum error in the steady state region was the second lowest among all controllers.

The MPC, on the other hand, had the least Δv for two cases out of four compared to designed controllers. However, it produced the highest RMSE and maximum error for all the cases, but still better than the Impulsive Law. Its settling time was the third among all the other controllers. The details of each controller can be found in below subsections for Relative Orbit Mission.

1) Case 1: This case consists of an initial error in the semi-major axis of the Deputy. This scenario was chosen because the difference in semi-major axis causes the two satellites having different periods, and having different J_2 effects.

As can be seen, from Fig. 7, all the controllers except Impulsive Control Law, converged to the reference trajectory in almost half an orbit.

TABLE XVII
THE COMPARISON OF THE VARIOUS CONTROLLER PERFORMANCES FOR RELATIVE ORBIT MISSION CASE 1 FOR 5 ORBITS

	Δv [m/s]	RMSE [m]	Max Error [m]	Settling Time [s]
Sliding Mode	0.69	17.94	0.23	2248
Feedb. Linear.	0.57	17.44	0.57	1760
MPC	0.59	21.95	0.84	3825
Impulsive	0.20	109.47	27.95	8837

Again from Fig. 7, all the controllers had change in y axis even though initially it was zero. This was due to the initial error in x axis, or error in semi-major axis. This causes satellites to have different periods, hence, one falls behind of the other. Furthermore, the Feedback Linearization was the fastest controller to close the error, which can be both deduced from Tab. XVII and Fig 7. When Tab. XVII was investigated, it was seen that, Sliding Mode had the highest Δv, which is 3.5 times higher than that of the Impulsive Law, and had the second lowest RMSE, which is 6.1 times lower than that of the Impulsive Law. The MPC had the second highest Δv, which is approximately 3 times higher than that of the Impulsive Law, with the highest RMSE among designed controllers, 5 times lower than that of the Impulsive Law. The lowest Δv belonged to Feedback linearization, which is 2.9 times higher than that of the Impulsive Law, with the lowest RMSE, 6.3 times lower than that of Impulsive Law.

2) Case 2: This case consists of an initial error in the eccentricity. The eccentricity, again, causes different drift rates in orbits of chief and deputy, due to J_2 effect.

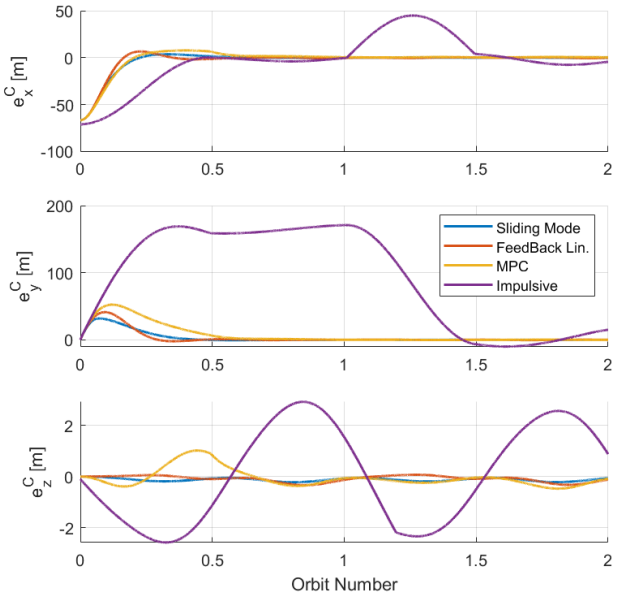

Fig. 8. The Tracking Errors in LVLH Frame of Chief for Relative Orbit Mission Case 2

As can be seen in Fig. 8 the designed controllers, were able to converge to the reference trajectory in half an orbit except Impulsive Control. The difference in x axis, again caused drift in y axis for all the controllers. When Tab. XVIII and Fig. 8 were investigated, it was seen that, the error due to eccentricity introduced a change in x axis of the LVLH frame, approximately 0.6 times that of Case 1. As expected, almost all the control effort, with RMSE was decreased, approximately 0.5 to 0.7 times.

From Tab. XVIII, The Sliding Mode consumed the highest amount of Δv among all the controllers, and also, has the smallest RMSE with smallest maximum error. Compared to the Impulsive Control law, it consumed approximately 3.4 times higher Δv, however, the RMSE of it is only 8.3 times lower than that of the Impulsive Law. The second highest fuel consumption is obtained with Feedback Linearization. The Δv of it is approximately 2.9 times higher, however, its RMSE is 7.8 times lower than that of the Impulsive Law. The MPC, on the other hand, has the lowest Δv consumption among the designed controllers, where it has 2.8 times higher Δv consumption, with 5.9 times lower RMSE than that of the Impulsive Law.

On the other hand, all the controllers, have outperformed the Impulsive control law in terms of maximum error in the steady state, and settling time.

TABLE XVIII
THE COMPARISON OF THE VARIOUS CONTROLLER PERFORMANCES FOR RELATIVE ORBIT MISSION CASE 2 FOR 5 ORBITS

	Δv [m/s]	RMSE [m]	Max Error [m]	Settling Time [s]
Sliding Mode	0.47	9.44	0.23	1844
Feedb. Linear.	0.40	9.96	0.57	1559
MPC	0.39	13.20	0.84	3093
Impulsive	0.14	78.14	29.13	8855

3) Case 3: In this case, the initial error in inclination, i, was investigated. The initial error in inclination was set to 0.001 degrees.

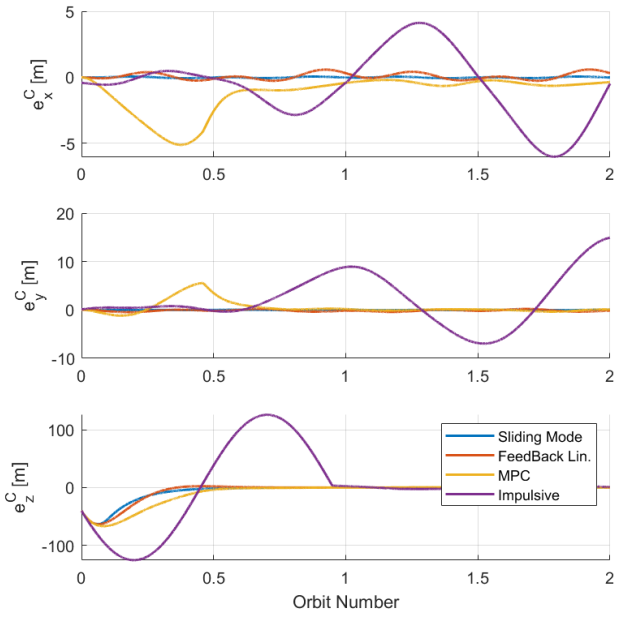

Fig. 9. The Tracking Errors in LVLH Frame of Chief for Relative Orbit Mission Case 3

As can be seen in Fig. 9, all the controllers were able to reduce the 50 m of z difference caused by the inclination difference in half of an orbit except the Impulsive Law. It took almost 1 orbit to reduce the z error.

From Tab. XIX, Sliding Mode controller had the highest Δv consumption and with the lowest RMSE and maximum

error. However, its settling time was slightly higher than Feedback Linearization. Its Δv was 3.1 times higher than that of Impulsive Control Law, and its RMSE was 4.2 times lower than that of the Impulsive Law. On the contrary, MPC this time had the second highest Δv with highest maximum error. Its settling time was the highest in the designed controllers. Its Δv was 3 times higher, and its RMSE was 3.1 times lower than those of the Impulsive Control Law. Feedback Linearization, had the lowest Δv, with medium RMSE and medium maximum error in steady state. Its settling time was the best. Additionally, its Δv was 2.3 higher and RMSE was 3.9 times lower than those of the Impulsive Control Law.

TABLE XIX
THE COMPARISON OF THE VARIOUS CONTROLLER PERFORMANCES FOR RELATIVE ORBIT MISSION CASE 3 FOR 5 ORBITS

	Δv [m/s]	RMSE [m]	Max Error [m]	Settling Time [s]
Sliding Mode	0.46	10.03	0.23	2382
Feedb. Linear.	0.35	10.76	0.57	1891
MPC	0.45	13.50	0.84	3226
Impulsive	0.15	41.64	125.83	5623

4) Case 4: In this case, the combination of all the scenarios was implemented with an additional mean anomaly error.

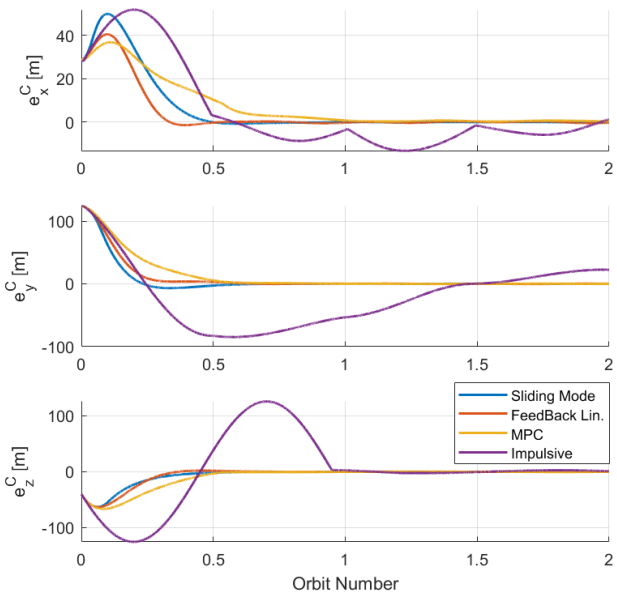

Fig. 10. The Tracking Errors in LVLH Frame of Chief for Relative Orbit Mission Case 4

From the Fig. 10 all the designed controllers were able to converge to the reference trajectory almost in half of an orbit except the Impulsive Law. The Impulsive control was able to get rid of the error in z axis in almost one orbit. The error in y axis, introduced due to error in x axis, was not able to be cancelled until the next orbit.

TABLE XX
THE COMPARISON OF THE VARIOUS CONTROLLER PERFORMANCES FOR RELATIVE ORBIT MISSION CASE 4 FOR 5 ORBITS

	Δv [m/s]	RMSE [m]	Max Error [m]	Settling Time [s]
Sliding Mode	0.77	20.62	0.23	2018
Feedb. Linear.	0.56	21.08	0.57	1634
MPC	0.52	24.96	0.84	2886
Impulsive	0.31	55.31	28.42	8056

The results of the Error Case 4 was shared in Tab. XX. The lowest Δv belongs to MPC, with the highest RMSE, maximum error, and settling time. Compared to the Impulsive Law, it had 1.7 times higher Δv consumption with 2.2 times less RMSE than those of the Impulsive Law. The second lowest Δv, which was 1.8 times higher than that of the Impulsive Law, corresponded to Feedback Linearization, with the second best RMSE, which was 2.6 times lower than that of the Impulsive Law. Additionally, its settling time was the lowest among designed controllers. The Sliding Mode had the highest Δv among the designed controllers, which is 2.5 times higher than that of the Impulsive Law, and the best RMSE, which is 2.7 times lower than that of the Impulsive Law.

G. Rendezvous Mission

In this part, the performances of each controller for the rendezvous mission was shared for the same error scenarios for the same orbit. This time, the transformation from mean orbital element difference to LVLH frame relative orbit was easier to obtain, basically, consisting of zeros. Hence, the comparison here is valid for all the controllers in the list.

1) Case 1: All the controllers, except the Impulsive Control Law, reached the reference trajectory perfectly. From Tab. XXI, the highest Δv usage again, was on Sliding Mode Controller, with the second smallest RMSE. Its Δv was 2.6 times higher, however, the RMSE of it was 6.6 times lower than those of the benchmark method. The second highest fuel consumption was for Feedback Linearization Controller, which was approximately 2.2 times higher than that of the Impulsive Control Law. The RMSE of the Feedback Linearization law on the other hand, was the best among all the controllers and it was 6.7 times lower than that of the Impulsive Law. The MPC had the best Δv consumption, 1.9 times higher than that of the Impulsive Law with the highest RMSE, which was 6.1 times lower than that of the Impulsive Law, among the designed controllers. As can be seen, the settling time and RMSE had the exact same ranking.

When the Fig. 11, all the designed controllers was able to get rid of the error in near half of orbit.

TABLE XXI
THE COMPARISON OF THE VARIOUS CONTROLLER PERFORMANCES FOR RENDEZVOUS SCENARIO ERROR CASE 1 FOR 5 ORBITS

	Δv [m/s]	RMSE [m]	Max Error [m]	Settling Time [s]
Sliding Mode	0.50	16.61	0	2139
Feedb. Linear.	0.42	16.36	0	1692
MPC	0.37	17.94	0	2170
Impulsive	0.19	109.94	0.91	8783

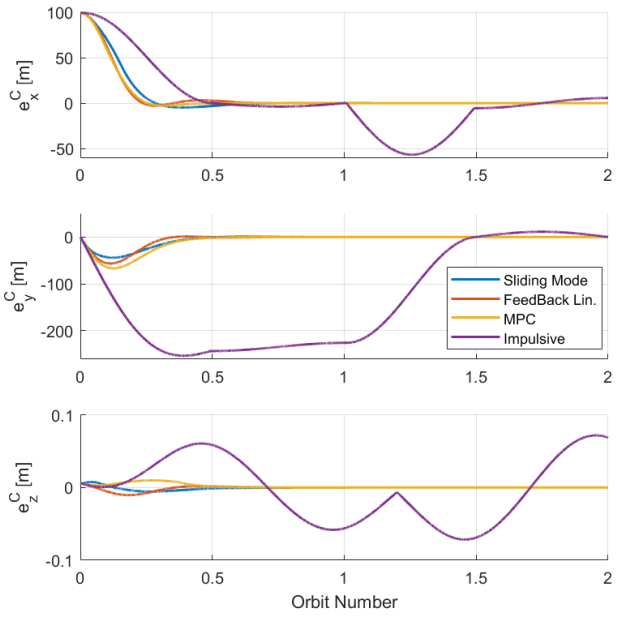

Fig. 11. The Tracking Errors in LVLH Frame of Chief for Rendezvous Mission with Error Case 1

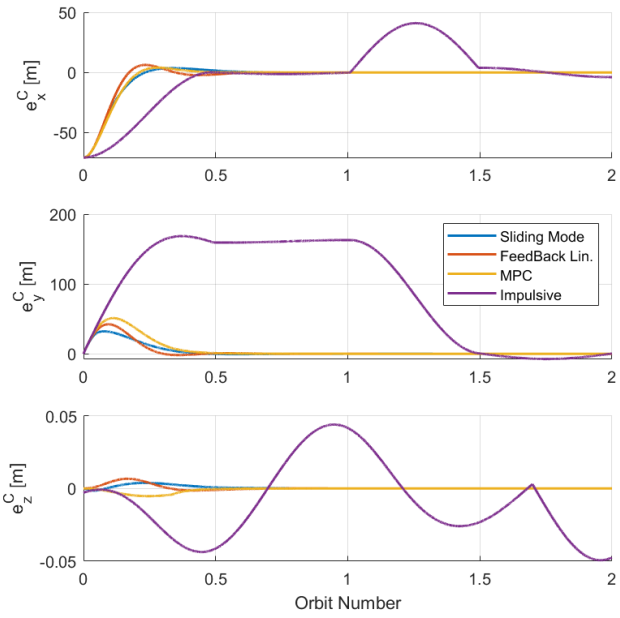

Fig. 12. The Tracking Errors in LVLH Frame of Chief for Rendezvous Mission with Error Case 2

2) Case 2: In this case, an initial eccentricity error was considered, which corresponded to an initial x axis error in the LVLH frame. When two satellites were at the same exact position, the effect of J_2 was the same, hence, there was no final oscillation in the response, which leads to no final error. From Tab. XVIII, the highest Δv consumption was on Sliding Mode, with approximately 2.5 times higher than that of the Impulsive Controller. Whereas, the RMSE was the best among the designed controllers which corresponded to 7.5 times lower than that of the Impulsive Control. The Feedback Linearization had the second highest Δv, 2.2 times higher and the RMSE of it was 7.2 times lower than those of the Impulsive Control. The MPC, this time had the lowest fuel consumption among the designed controllers, approximately 1.9 times higher than that of the Impulsive Law. The corresponding RMSE was 6.1 times lower than that of the Impulsive Law. For the convergence time, the trend as follow, the shortest time was obtained with Feedback Linearization, then Sliding Mode, and finally MPC.

TABLE XXII
THE COMPARISON OF THE VARIOUS CONTROLLER PERFORMANCES FOR RENDEZVOUS SCENARIO ERROR CASE 2 FOR 5 ORBITS

	Δv [m/s]	RMSE [m]	Max Error [m]	Settling Time [s]
Sliding Mode	0.33	10.13	0	1910
Feedb. Linear.	0.29	10.57	0	1579
MPC	0.25	12.43	0	2110
Impulsive	0.13	75.86	0.52	8769

As can be seen in Fig 12, designed controllers were able to converge to the reference in less than half of an orbit, whereas the Impulsive Law converged to reference in nearly 1.5 orbits.

3) Case 3: In this case, the effect of initial error in inclination was investigated. Again, all the designed controllers had 0 final error. As can be seen from Tab. XXIII, the same ranking occurred as of error case 2 for all the parameters. The minimum fuel consumption was achieved with MPC, which was 1.4 times higher than that of the Impulsive Law, with 2.3 times smaller RMSE. The Feedback Linearization had the second lowest Δv, which was 1.5 times higher than that of the Impulsive Law, and the RMSE was 2.7 times lower than that of the Impulsive Law. The Sliding Mode had the highest Δv, 1.9 times higher than that of the Impulsive Law and lowest RMSE, 2.8 times lower than that of the Impulsive Law. The settling time trend was observed here as well.

TABLE XXIII
THE COMPARISON OF THE VARIOUS CONTROLLER PERFORMANCES FOR RENDEZVOUS SCENARIO ERROR CASE 3 FOR 5 ORBITS

	Δv [m/s]	RMSE [m]	Max Error [m]	Settling Time [s]
Sliding Mode	0.27	10.01	0	2356
Feedb. Linear.	0.21	10.74	0	1893
MPC	0.20	11.98	0	2227
Impulsive	0.14	27.58	5.90	2624

From Fig. 13, all the controllers got rid of the initial error in z axis caused by inclination difference in approximately half an orbit. Furthermore, it was noticed that, the Impulsive Law, had a slightly different starting error along x axis. This was due to the fact that the two methods had different initialization procedure. However, this error was quite small, hence the Δv due to this error was ignored.

4) Case 4: In this case, the combination of all the previous error cases with additional mean anomaly error was investi-

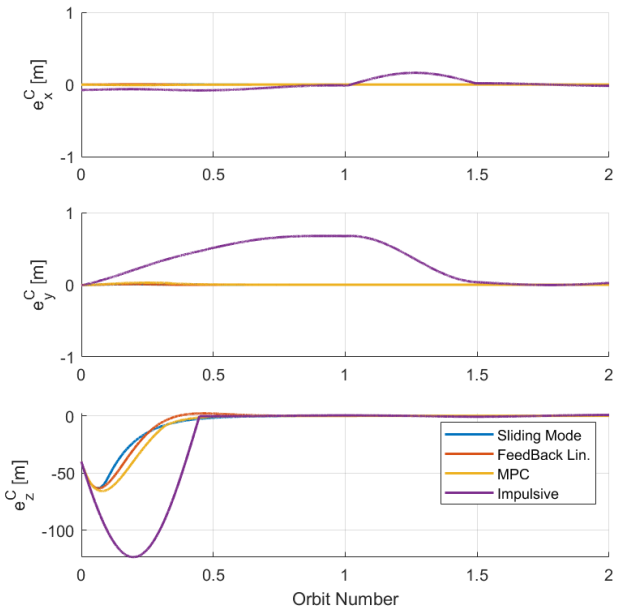

Fig. 13. The Tracking Errors in LVLH Frame of Chief for Rendezvous Mission with Error Case 3

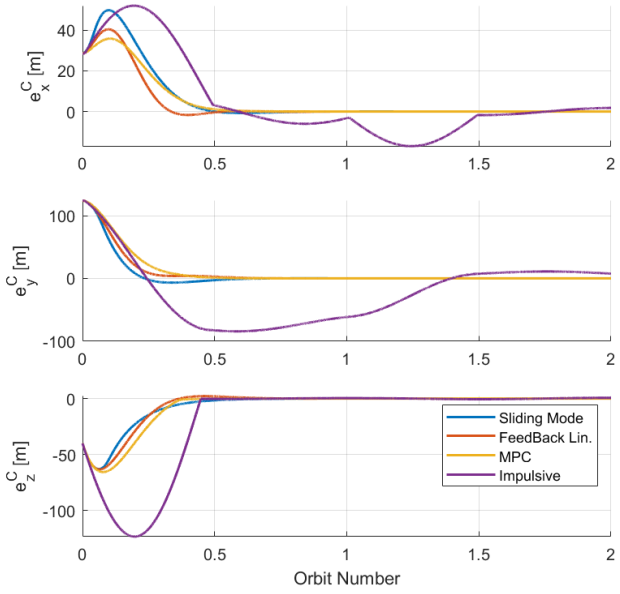

Fig. 14. The Tracking Errors in LVLH Frame of Chief for Rendezvous Mission with Error Case 4

gated.

As can be seen from the Tab. XXIV. The settling time trend was followed. Furthermore, the Δv consumption trend for rendezvous missions was also obeyed. The Sliding Mode had the highest Δv, which was approximately 2 times higher than that of the Impulsive Law, and the lowest RMSE, which was 2.3 times lower than that of the Impulsive Law. The Feedback Linearization's Δv was 1.5 times higher than that of the Impulsive Law and its RMSE was 2.2 times lower than that of the of Impulsive Law. The smallest Δv corresponded to MPC, which was 1.2 times higher than that of the Impulsive Law. However, its RMSE was 2 times lower than that of the benchmark method. In Fig. 14, it is seen that, all the controllers follow the same trend.

TABLE XXIV
THE COMPARISON OF THE VARIOUS CONTROLLER PERFORMANCES FOR RENDEZVOUS SCENARIO ERROR CASE 4 FOR 5 ORBITS

	Δv [m/s]	RMSE [m]	Max Error [m]	Settling Time [s]
Sliding Mode	0.61	20.60	0	2010
Feedb. Linear.	0.45	21.06	0	1639
MPC	0.36	22.99	0	1983
Impulsive	0.30	46.43	5.05	8098

V. DISCUSSION

The complicated nature of satellite formation flying was tried to be simplified by implementing and comparing different types of controllers with different types of approaches, namely Sliding Mode, Feedback Linearization, MPC and an Impulsive Control, in terms of Δv usage and tracking error for two different missions, a Relative Orbit Mission and Rendezvous Mission. Each controller, except Impulsive Control, was investigated, by changing different parameters and then compared with each other through different missions and error cases.

It was noticed that, the Impulsive Law had the lowest Δv for all the tests. The reason behind that was believed to be to the fact that, it depends on calculation of the best possible time to correct the error, which increases the efficiency. Even though, similar approach was implemented in MPC, the model was assuming circular orbit with no perturbations affecting the system, hence the fuel consumption was high. On the other hand, Sliding Mode and Feedback Linearization controllers were even though numerically optimized for a cost function, they did not have such an application, thus, their fuel consumption was also high.

To achieve a comparison, a numerical optimization algorithm was adapted for Sliding Mode and Feedback Linearization Controllers. It was seen that, in the literature, some of the optimization with ABC was done with 6000 to 10000 maximum cycles [90], [92], however, in some examples 1000 maximum cycles was also used [62], [65]. In order to assure that the local minimum was found for the controller gains, the same numerical optimization problem was solved twice. In the end both of the solutions gave approximately the same gain set. As a result, the gains of those two controllers were assumed to be the local minimum.

Even though the same numerical optimizations were applied to Sliding Mode and Feedback Linearization, their Δv usage and corresponding tracking error in terms of RMSE were different. The reason behind that was believed to be due to the different nature of the controllers. For the optimization of the cost function, the Sliding Mode Controller seemed to focus on errors rather than fuel, whereas, the Feedback Linearization

did the other way around.

Throughout the investigations, concerning both examining the control parameters, and observing the comparisons of controllers with each other, it was seen that the error produced was inversely proportional with the Δv. In other words, if tracking error was desired to be small or tried to be cancelled as soon as possible, then the fuel consumption will be high. For example, Impulsive Law offered by Schaub and Alfriend applies thrusts only three times throughout the orbit. Hence, its RMSE is higher with lower Δv usage.

In the Relative Orbit Mission with different error cases, the Sliding Mode Controller had the highest Δv, 2.5 to 3.5 times higher than that of the Impulsive Law, with lowest tracking error and steady state error. Its RMSE was 2.7 to 8.3 times lower than that of the Impulsive Law. The Feedback Linearization used 1.8 to 2.9 times higher Δv than that of the Impulsive Law for the same missions, and produced slightly higher errors compared to Sliding Mode, 2.6 to 7.8 times lower RMSE than that of the Impulsive Law. MPC, consumed similar amounts of Δv with Feedback Linearization, 1.7 to 3 times higher than that of the Impulsive Law and produced the highest RMSE compared to other methods, 2.2 to 5.9 times lower RMSE than that of the Impulsive Law.

The difficulty of having a relative orbit was that, as known, the gravity perturbations effect satellites differently throughout the mission. In rendezvous missions, even though the initial effect of the gravity perturbations were different, the finals were similar since the position difference is zero. As a result, the ranking of the controllers were almost the same for the different error cases for rendezvous mission. Furthermore, since the continuous controllers always tries to cancel the errors introduced by perturbations in the Relative Orbit Mission, the Δv of the rendezvous mission for the same error cases were lower, because when the rendezvous happens, the perturbation effects diminishes for the relative position. However, the RMSE of both of the mission was on the same order. This was because, controllers followed similar paths.

In Rendezvous mission, in terms of Δv, the Impulsive Law, again outperformed all the designed controllers. It was noticed that, on the contrary to the Relative Orbit Mission, MPC consumed the least amount of fuel with the highest RMSE, compared to designed controllers, for all the error cases. The Δv, of MPC was 1.2 to 1.9 times higher than that of the Impulsive Law. Whereas, the RMSE of MPC was 2 to 6.1 times lower than that of the Impulsive Law. The second highest Δv consumption was for Feedback Linearization, with the second highest RMSE. The Δv of it was 1.5 to 2.2 times higher than that of the Impulsive Law, and produced 2.2 to 7.2 times smaller RMSE. The Sliding Mode, again consumed the highest Δv, 2 to 2.6 times higher than that of the Impulsive Law, and its RMSE was 2.3 to 7.5 times smaller.

As expected, the Sliding Mode Controller consumed the highest amount of Δv with the smallest amount of RMSE for all the missions. As mentioned earlier, the robustness of the Sliding Mode comes with the cost of fuel. The MPC with the CW equations had variable performance for the Relative Orbit Mission, however, its Δv for the rendezvous mission was quite close to that of the Impulsive Law. Briefly, the optimization problem solved in MPC allows it to have close performance to the benchmark method. The Feedback Linearization, which lacks both the robustness and optimization features, was in the middle of those designed controllers.

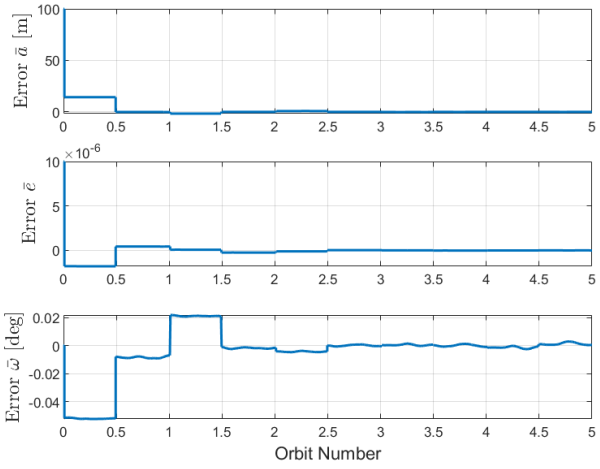

Fig. 15. Error of mean semi-major Axis, eccentricity and argument of periapsis for Relative Orbit Mission with initial error Case 4

It is noticed that the performance of the MPC with the CW model was improved in the Rendezvous mission. This was believed to be due to the fact that, the error of the model reduces with the decrease in formation distance [93]. As a result, the model becomes closer to reality, of course not exactly due to perturbances. Hence, the Δv was reduced more than for the other methods.

In the comparison for Relative Orbit Mission, the tracking error calculations of the Impulsive Law was obtained with a reference created with approximation. In this approximation, initial error was on the order of centimeters, however, after 5 orbits, the error was on the order of 20 meters, with an increasing trend. That means, the RMSE and maximum errors shared in Section IV-F has errors near in the order of tens of meters. However, in terms of mean orbital elements, the tracking error was quite low. Tracking error in terms of mean orbital elements was shared in Fig. 15 and 16 for Relative Orbit Mission error Case 4. This situation does not change the fact that, the Impulsive Law produces high amount of error. Because, in the Rendezvous mission, the Impulsive Law still had the highest RMSE among all the controllers.

Furthermore, the Low Thrust System implemented is a cold gas system, with a smaller specific impulse, near 3.5 times smaller than that of a hydrazine system. Which means that, 2 to 4 times higher Δv would mean 7 to 12 times higher fuel consumption. If an electrical thrusting system, with high specific impulse was adapted, then there is a possibility that the two systems, the low thrust and high thrust systems, would have similar levels of fuel consumption. However, it is out of scope of this thesis. In order to protect the environment while reducing fuel consumption, electrical propulsion systems with high specific impulse are thought to be beneficial.

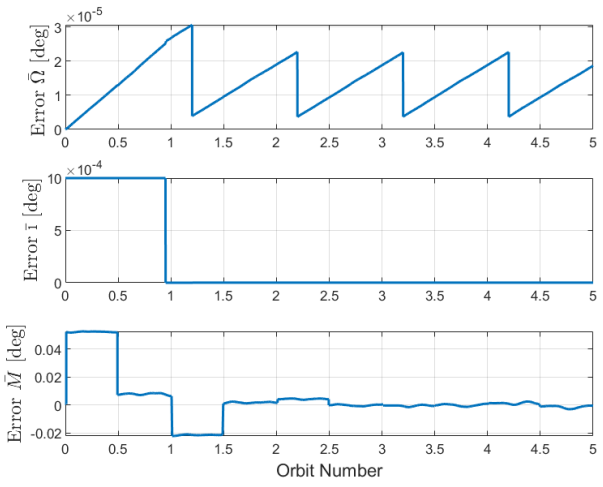

Fig. 16. Error of right ascension of the ascending node, inclination and mean anomaly for Relative Orbit Mission with initial error Case 4

VI. Conclusion

The complexity of the arrangement of the relative motion of the two identical satellites was tried to be reduced while investigating the Δv cost and tracking error of different control approaches.

This study shows how to apply different reference trajectory methods and different dynamical models to use for control of relative motion. The transformation of this reference trajectory to different Frames of Reference was implemented, and tracked with a continuous control approaches. A similar reference trajectory was created in terms of Mean Orbital Elements and tracked with an Impulsive Law offered by Schaub and Alfriend [81].

A slight difference in reference trajectories was observed between continuous control and impulsive laws for the relative orbit mission due to numerical operations. This introduced approximately 10 m of error for both root mean square error and maximum error in steady state. However, the same error was not observed for rendezvous mission. As a result, the reader should be careful while considering the tracking error of the impulsive law in the relative orbit mission.

The study showed that, there exists an inversely proportional relationship in between Δv and tracking error, as expected. The Impulsive law had the highest tracking error, both in terms of root mean square error and maximum error in the steady state, but, the smallest Δv. Similarly, Sliding Mode Controller had the highest Δv for all the test scenarios, and produced the smallest tracking error.

It was noticed that Model Predictive Control, working with Clohessy–Wiltshire equations, had Δv levels similar to the Impulsive law in the rendezvous mission. However, it had one of the highest Δv in the relative orbit mission. This showed that the Clohessy-Wiltshire equations should be approached with care while using them for formation flying missions where the perturbation effects are not negligible.

The LEO is a frequently used orbit for commercial and scientific satellites. LEO is becoming more and more populated with debris due to the collision happening in between them. This means, removal of debris from space is becoming more vital for the space missions. A rendezvous mission was investigated. It was shown that, both impulsive controllers and continuous controllers were able to diminish the relative position error.

More efficiency-oriented operation of impulsive law approaches allowed these types of controllers to be used in satellite formation flying. However, it is noticed that, it comes with the cost of tracking error. If low error rates are desired, the follow-up satellite system should be controlled continuously at each point in the orbit. But, it has been found that this type of control will also relatively increase the fuel consumption of the tracking satellite.

Management of energy is a fundamental ground for human welfare, economic development and poverty reduction and global demand for limited and constantly decreasing energy resources is growing rapidly day by day. Nevertheless, it should be remembered that energy systems also have important environmental effects such as causing environmental hazards and pollution. Considering that, if the mission can tolerate tracking errors, then the impulsive laws would offer better solutions in terms of economical end environmental causes, i.e. longer lifetime. If the mission demands high tracking accuracy, then a highly efficient electrical propulsion systems might be used to compensate for higher Δv requirements.

VII. Future Work

In this study it was seen that the Δv spent for a rendezvous mission was lower than that of the relative orbit mission for all the controllers, even though the initial errors were the same. However, the Δv of the MPC was reduced more than other controllers. This is thought to be related to the model used in MPC, which does not account for perturbations. Hence, this shows that due to model assumptions, the MPC performed badly when the perturbations were present. To improve the MPC, a model that is offered by [56] which covers J_2 effects can be implemented and compared with the MPC at hand.

It is known that Feedback Linearization control is vulnerable to model noise and uncertainties [94], [95]. The performances shared here for Feedback Linearization might not be reachable due to possible noise in the system. So, it might be beneficial to investigate the controller performances under noise, or thrust misalignment.

Additionally, in this study, the positions of each satellite was known with 100% accuracy. In reality, it is known that there are estimation algorithms to predict the position of the satellite through sensor measurements which include errors. Future work might involve the controller performances with an observer, or it might focus on that algorithm directly.

In this work, the boosters of the satellite was modeled as a continuous function that has a saturation limit only. In other words, it can create all the thrust up until the saturation limit. However, in general the thrust system does not have such a capability. To overcome that a Schmidt trigger design can be

implemented. Even more, this study can be redone with a high fidelity thrust model.

Furthermore, in this study the effect of the aerodynamics was ignored due to the altitude and satellites being aerodynamically identical. In the GRACE mission, which is at 500 km LEO, the satellites have the same shape, however, they have slightly different ballistic coefficient, 0.14% to 0.32% difference [33]. This is because of the attitude requirement of the mission. As a result, a future investigation might involve the atmospheric effects as perturbations or implement 6 Degree of Freedom model rather than a point mass model to investigate such effects.

ACKNOWLEDGMENT

First of all, I would like to express my appreciation for my supervisor, Dr. Gunnar Tibert for his guidance throughout this thesis. His comments and pinpoint accuracy helped me to locate the errors both in my point of view and in my study.

I would like to thank my intelligent and hardworking colleagues, Emre Ünal and Oğuz Han Altıntaş for discussing the details of both mechanics of space and control approaches. Those discussions allowed me to broaden my horizon. Also I would like to express my gratitude for Dr. Ahmet Sofyalı for his explanations about theoretical aspects of control approaches in space and Sarper Kumbasar for the discussions that we had for the control structures at hand. For grammar and translation help I am grateful to Mustafa Al-Janabi, Simon Mao and Hamish Keay for their dedication.

I would like to thank Roketsan Missiles Inc. which is more than a company to me. With the scholarship that I got, I was able to achieve that long time dream of mine. I would like to thank Dr. Özgür Ateşoğlu, for helping me to find this interesting topic.

I owe my greatest gratitude to my best friend and love of my life Yağmur Bulut. When there was no light, she shine like the sun. When there was no hope in the walls of my home, she held my hands and remind me who I am.

Finally, this thesis was dedicated to my family, my mother Mukadder Başaran and my father Dr. Abdulhadi Başaran. A mother who never knew the limits of self devotion for a better education of her son. A father, that never hesitated to help me even though he did not know the technical aspects of this study. Their dedication and devotion help me to survive throughout this pandemic, and focus on my study. It would be shame if I did not mention about the enjoyable talks that I had with my brother Yakup Başaran and my sister Sevde Başaran, which reminded me of my home.

APPENDIX A
TRANSFORMATION BETWEEN CLASSICAL ORBITAL ELEMENTS AND CARTESIAN COORDINATES

A. Cartesian Coordinates to Classical Orbital Elements

The input to the transformation is the Position, $\boldsymbol{r}$ and Velocity $\dot{\boldsymbol{r}}$ of the satellite with respect to ECI frame, with the gravitational constant of the primary, μ. This approach is taken from [96]. The angular momentum vector is calculated based on Eq. (127), and calculation of eccentricity vector $\boldsymbol{e}$ is in Eq. (128).

$$\mathbf{h} = \mathbf{r} \times \dot{\mathbf{r}} \tag{127}$$

$$\mathbf{e} = \frac{\dot{\mathbf{r}} \times \mathbf{h}}{\mu} - \frac{\mathbf{r}}{\|\mathbf{r}\|} \tag{128}$$

Calculation of vector $\boldsymbol{n}$ which points toward the ascending node and true anomaly f are in Eq. (129) and (130), respectively.

$$\mathbf{n} = (0, 0, 1)^{\mathrm{T}} \times \mathbf{h} = (-h_y, h_x, 0)^{\mathrm{T}} \tag{129}$$

$$f = \begin{cases} \arccos \frac{\langle \mathbf{e}, \mathbf{r} \rangle}{\|\mathbf{e}\|\|\mathbf{r}\|} & \text{for } \langle \mathbf{r}, \dot{\mathbf{r}} \rangle \geq 0 \\ 2\pi - \arccos \frac{\langle \mathbf{e}, \boldsymbol{r} \rangle}{\|\boldsymbol{\mu}\|\mathbf{r}\|} & \text{otherwise} \end{cases} \tag{130}$$

The inclination of the orbit is calculated with the z component of the angular momentum vector, namely $\boldsymbol{h}_z$, in Eq. (131).

$$i = \arccos \frac{h_z}{\|\mathbf{h}\|} \tag{131}$$

Calculation of the eccentricity e, which is the magnitude of the eccentricity vector, and the eccentric anomaly, E in Eq. (132).

$$e = \|\mathbf{e}\| \quad E = 2 \arctan \left(\frac{\tan \frac{f}{2}}{\sqrt{\frac{1+e}{1-e}}} \right) \tag{132}$$

Then the Right Ascension of the Ascending Node, Ω, and the Argument of Periapsis is calculated in Eq. (133) and (134)

$$\Omega = \begin{cases} \arccos \frac{n_x}{\|\mathbf{n}\|} & \text{for } n_y \geq 0 \\ 2\pi - \arccos \frac{n_x}{\|\mathbf{n}} & \text{for } n_y < 0 \end{cases} \tag{133}$$

$$\omega = \begin{cases} \arccos \frac{\langle \mathbf{n}, \mathbf{e} \rangle}{\|\mathbf{n}\|\|\mathbf{e}\|} & \text{for } e_z \geq 0 \\ 2\pi - \arccos \frac{\langle \mathbf{n}, \mathbf{e} \rangle}{\|\mathbf{n}\|\|\mathbf{e}\|} & \text{for } e_z < 0 \end{cases} \tag{134}$$

Calculation of the Mean Anomaly is in Eq. (135).

$$M = E - e \sin E \tag{135}$$

The final orbital element is the Semi-Major Axis, which is in Eq. (136).

$$a = \frac{1}{\frac{2}{\|\mathbf{r}\|} - \frac{\|\dot{\mathbf{r}}\|^2}{\mu}} \tag{136}$$

B. Classical Orbital Elements to Cartesian Coordinates

This formation takes the classical osculating orbital elements and produces the corresponding ECI position and velocity of the satellite. The approach is implemented from [97]. The first step is the calculation of the eccentric anomaly based on mean anomaly. This can be achieved with Newton–Raphson Method, shared in Eq. (137).

$$f(E) = E - e \sin E - M \tag{137}$$

$$E_{j+1} = E_j - \frac{f(E_j)}{\frac{\mathrm{d}}{\mathrm{d}E_j} f(E_j)} = E_j - \frac{E_j - e \sin E_j - M}{1 - e \cos E_j}$$

$$E_0 = M$$

Then the true anomaly, based on eccentric anomaly is calculated according to Eq. (138).

$$f(t) = 2 \cdot \arctan 2 \left(\sqrt{1+e} \sin \frac{E(t)}{2}, \sqrt{1-e} \cos \frac{E(t)}{2} \right) \tag{138}$$

where arctan2 calculates the correct quadrant of the angle, seen in Eq. (139).

$$\arctan 2(y,x) = \begin{cases} \arctan\left(\frac{y}{x}\right) & x > 0 \\ \arctan\left(\frac{y}{x}\right) + \pi & y \geq 0, x < 0 \\ \arctan\left(\frac{y}{x}\right) - \pi & y < 0, x < 0 \\ +\frac{\pi}{2} & y > 0, x = 0 \\ -\frac{\pi}{2} & y < 0, x = 0 \\ \text{undefined} & y = 0, x = 0 \end{cases} \tag{139}$$

The magnitude of the position from the main body to the satellite is calculated according to the Eq. (140).

$$r_c(t) = a(1 - e\cos E(t)) \tag{140}$$

Calculation of the position vector $\boldsymbol{o}(t)$ and velocity vector $\dot{\boldsymbol{o}}$ resolved in orbital frame are in Eq. (141) and (142), respectively.

$$\mathbf{o}(t) = \begin{pmatrix} o_x(t) \\ o_y(t) \\ o_z(t) \end{pmatrix} = r_c(t) \begin{pmatrix} \cos f(t) \\ \sin f(t) \\ 0 \end{pmatrix} \tag{141}$$

$$\dot{\mathbf{o}}(t) = \begin{pmatrix} \dot{o}_x(t) \\ \dot{o}_y(t) \\ \dot{o}_z(t) \end{pmatrix} = \frac{\sqrt{\mu a}}{r_c(t)} \begin{pmatrix} -\sin E \\ \sqrt{1-e^2}\cos E \\ 0 \end{pmatrix} \tag{142}$$

In order to resolve $\boldsymbol{o}(t)$ and $\dot{\boldsymbol{o}}$ in ECI, the DCM shared in Eq. (143) is applied.

$$\boldsymbol{C}_{IO} = \underline{\boldsymbol{R}}_z(-\Omega)\underline{\boldsymbol{R}}_x(-i)\underline{\boldsymbol{R}}_z(-\omega) \tag{143}$$

where $\underline{\boldsymbol{R}}_z$ denotes a DCM of pure rotation in z.

Appendix B
First Order Transformation Between Osculating Orbital Elements and Mean Orbital Elements

The method described here is the first-order truncated version of an infinite power series solution of the theories in [51] and [53], taken from [47]. This truncation means that with a simple sign change, the method can be used in both ways. The Classical Orbital Elements are used, the input is œ and the output is œ′. The mapping starts with the definition of the γ_2 as in Eq. (144).

$$\gamma_2 = \frac{J_2}{2}\left(\frac{r_e}{a}\right)^2 \tag{144}$$

which is suitable for the mapping from mean orbital elements to osculating elements. If the inverse mapping is desired, then a minus sign should be added to Eq. (144). The definition of $\eta = \sqrt{1-e^2}$ is used to define $\gamma_2^{'}$, in Eq. (145).

$$\gamma_2' = \frac{\gamma_2}{\eta^4} \tag{145}$$

Then the Mean Anomaly is transformed into Eccentric Anomaly with the use of Keplerian equation, $M = E - e\sin E$. The solution of this can be obtained with a Newton–Raphson method, in Eq. (137). Then the true anomaly, f is calculated with Eq. (146).

$$f = 2\arctan\left(\sqrt{\frac{1+e}{1-e}}\tan\left(\frac{E}{2}\right)\right) \tag{146}$$

The ratio of a/r is calculated with the Eq. (147).

$$\frac{a}{r} = \frac{1 + e\cos f}{\eta^2} \tag{147}$$

Then the transformed semi-major axis is calculated according to the Eq. (148).

$$\begin{aligned} a' =& a + a\gamma_2\Bigg(\left(3\cos^2 i - 1\right)\left(\left(\frac{a}{r}\right)^3 - \frac{1}{\eta^3}\right) + \\ & 3\left(1-\cos^2 i\right)\left(\frac{a}{r}\right)^3\cos(2\omega + 2f)\Bigg) \end{aligned} \tag{148}$$

The intermediate variables for the future calculations are shared below.

$$\delta e_1 = \frac{\gamma_2'}{8} e\eta^2 \left(1 - 11\cos^2 i - 40\frac{\cos^4 i}{1 - 5\cos^2 i}\right)\cos(2\omega) \tag{149}$$

$$\begin{aligned} \delta e =& \delta e_1 + \frac{\eta^2}{2}\Bigg\{\gamma_2\Bigg[\frac{3\cos^2 i - 1}{\eta^6}\Bigg(e\eta + \frac{e}{1+\eta} + 3\cos f \\ & + 3e\cos^2 f + e^2\cos^3 f\Bigg) + 3\frac{1-\cos^2 i}{\eta^6}\Bigg(e + 3\cos f \\ & + 3e\cos^2 f + e^2\cos^3 f\Bigg)\cos(2\omega + 2f)\Bigg] \\ & - \gamma_2'\left(1-\cos^2 i\right)\left(3\cos(2\omega + f) + \cos(2\omega + 3f)\right)\Bigg\} \end{aligned} \tag{150}$$

$$\begin{aligned} \delta i =& -\frac{e\delta e_1}{\eta^2\tan i} + \frac{\gamma_2'}{2}\cos i\sqrt{1-\cos^2 i}(3\cos(2\omega + 2f) \\ & + 3e\cos(2\omega + f) + e\cos(2\omega + 3f)) \end{aligned} \tag{151}$$

$$\begin{aligned} M' + \omega' + \Omega' =& \\ & M + \omega + \Omega + \frac{\gamma_2'}{8}\eta^3\left(1 - 11\cos^2 i - 40\frac{\cos^4 i}{1-5\cos^2 i}\right) \\ & - \frac{\gamma_2'}{16}\Bigg(2 + e^2 - 11\left(2 + 3e^2\right)\cos^2 i \\ & - 40\left(2 + 5e^2\right)\frac{\cos^4 i}{1 - 5\cos^2 i} - 400e^2\frac{\cos^6 i}{\left(1 - 5\cos^2 i\right)^2}\Bigg) \\ & + \frac{\gamma_2'}{4}\Bigg(-6\left(1 - 5\cos^2 i\right)(f - M + e\sin f) \\ & + \left(3 - 5\cos^2 i\right)(3\sin(2\omega + 2f) + 3e\sin(2\omega + f) \\ & + e\sin(2\omega + 3f))\Bigg) \\ & - \frac{\gamma_2'}{8}e^2\cos i\left(11 + 80\frac{\cos^2 i}{1 - 5\cos^2 i} + 200\frac{\cos^4 i}{\left(1 - 5\cos^2 i\right)^2}\right) \\ & - \frac{\gamma_2'}{2}\cos i\Bigg(6(f - M + e\sin f) \\ & - 3\sin(2\omega + 2f) - 3e\sin(2\omega + f) - e\sin(2\omega + 3f)\Bigg) \end{aligned} \tag{152}$$

$$
\begin{aligned}
(e\delta M) =& \frac{\gamma_2'}{8} e\eta^3 \left(1 - 11\cos^2 i - 40\frac{\cos^4 i}{1-5\cos^2 i}\right) \\
&- \frac{\gamma_2'}{4}\eta^3 \left\{ 2\left(3\cos^2 i - 1\right)\left(\left(\frac{a\eta}{r}\right)^2 + \frac{a}{r} + 1\right)\sin f \right. \\
&+ 3\left(1-\cos^2 i\right)\left[\left(-\left(\frac{a\eta}{r}\right)^2 - \frac{a}{r} + 1\right)\sin(2\omega + f) \right. \\
&\left.\left. + \left(\left(\frac{a\eta}{r}\right)^2 + \frac{a}{r} + \frac{1}{3}\right)\sin(2\omega + 3f)\right]\right\} \qquad (153) \\
\delta\Omega =& -\frac{\gamma_2'}{8} e^2 \cos i \left(11 + 80\frac{\cos^2 i}{1-5\cos^2 i} + 200\frac{\cos^4 i}{(1-5\cos^2 i)^2}\right) \\
&- \frac{\gamma_2'}{2}\cos i(6(f - M + e\sin f) - 3\sin(2\omega + 2f) \\
&- 3e\sin(2\omega + f) - e\sin(2\omega + 3f)) \qquad (154)
\end{aligned}
$$

Now the the transformation for the rest of the elements can be done with an additional definition, in Eq. (155).

$$
\begin{aligned}
d_1 &= (e + \delta e)\sin M + (e\delta M)\cos M \\
d_2 &= (e + \delta e)\cos M - (e\delta M)\sin M
\end{aligned} \qquad (155)
$$

Then the transformed Mean Anomaly is calculated by using Eq. (156).

$$
M' = \arctan\left(\frac{d_1}{d_2}\right) \qquad (156)
$$

The transformed eccentricity is calculated according to Eq. (157).

$$
e' = \sqrt{d_1^2 + d_2^2} \qquad (157)
$$

For the final orbital elements, a final definition, shared in Eq. (158) is used.

$$
\begin{aligned}
d_3 &= \left(\sin\left(\tfrac{i}{2}\right) + \cos\left(\tfrac{i}{2}\right)\tfrac{\delta i}{2}\right)\sin\Omega + \sin\left(\tfrac{i}{2}\right)\delta\Omega\cos\Omega \\
d_4 &= \left(\sin\left(\tfrac{i}{2}\right) + \cos\left(\tfrac{i}{2}\right)\tfrac{\delta i}{2}\right)\cos\Omega - \sin\left(\tfrac{i}{2}\right)\delta\Omega\sin\Omega
\end{aligned} \qquad (158)
$$

Then the rest of the transformation is from Eq. (159) to (161).

$$
\Omega' = \tan^{-1}\left(\frac{d_3}{d_4}\right) \qquad (159)
$$

$$
i' = 2\sin^{-1}(\sqrt{d_3^2 + d_4^2}) \qquad (160)
$$

$$
\omega' = (M' + \omega' + \Omega') - M' - \Omega' \qquad (161)
$$

REFERENCES

[1] R. Faller, A. Ohndorf, B. Schlepp, and S. Eberle, "Preparation, Handover, and Conduction of Prisma Mission Operations at GSOC," in *63rd International Astronautical Congress*, Mar 2014. [Online]. Available: https://www.researchgate.net/publication/312157380_Preparation_Handover_and_Conduction_of_PRISMA_Mission_Operations_at_GSOC

[2] J. Llorente, A. Agenjo, C. Carrascosa, C. D. Negueruela, A. Mestreau-Garreau, A. Cropp, and A. Santovincenzo, "Proba-3: Precise formation flying demonstration mission," *Acta Astronautica*, vol. 82, no. 1, p. 38–46, 2013, doi: 10.1016/j.actaastro.2012.05.029.

[3] G. Krieger, M. Zink, M. Bachmann, B. Bräutigam, D. Schulze, M. Martone, P. Rizzoli, U. Steinbrecher, J. W. Antony, F. D. Zan, and et al., "Tandem-x: A radar interferometer with two formation-flying satellites," *Acta Astronautica*, vol. 89, p. 83–98, 2013, doi : 10.1016/j.actaastro.2013.03.008.

[4] T. M. Sgobba, B. M. Kanki, J.-F. M. Clervoy, and G. M. Sandal, *Space Safety and Human Performance*. Elsevier/Butterworth-Heinemann, 2018.

[5] J.-C. Liou, N. Johnson, and N. Hill, "Controlling the growth of future leo debris populations with active debris removal," *Acta Astronautica*, vol. 66, no. 5-6, p. 648–653, 2010, doi : 10.1016/j.actaastro.2009.08.005.

[6] J. Credland, G. Mecke, and J. Ellwood, "The Cluster mission: ESA's spacefleet to the magnetosphere," *Space Science Reviews*, vol. 79, no. 1, pp. 33–64, Jan 1997, doi : 10.1023/A:1004914822769.

[7] W. Steyn and Y. Hashida, "In-Orbit Attitude Performance of the 3-Axis Stabilised SNAP-1 Nanosatellite," in *Small Satellite Conference*, 2001. [Online]. Available: https://digitalcommons.usu.edu/cgi/viewcontent.cgi?article=1982&context=smallsat

[8] Y. Zheng and M. Sweeting, "Initial mission status analysis of 3-axis stable Tsinghua-1 microsatellite," in *Small Satellite Conference*, 2000. [Online]. Available: https://digitalcommons.usu.edu/smallsat/2000/All2000/6/

[9] NASA, "GRACE launch, press kit," 2002. [Online]. Available: https://www.jpl.nasa.gov/news/press_kits/gracelaunch.pdf

[10] G. L. Stephens, D. G. Vane, R. J. Boain, G. G. Mace, K. Sassen, Z. Wang, A. J. Illingworth, E. J. Oconnor, W. B. Rossow, S. L. Durden, and et al., "The Cloudsat mission and the A-Train," *Bulletin of the American Meteorological Society*, vol. 83, no. 12, p. 1771–1790, 2002, doi : 10.1175/bams-83-12-1771.

[11] C. Frémeaux, "ESSAIM Cluster Disposal: Orbit Management," *SpaceOps 2012 Conference*, 2012, doi : 10.2514/6.2012-1266472. [Online]. Available: https://arc.aiaa.org/doi/pdf/10.2514/6.2012-1266472

[12] The Air Force Research Laboratory, "XSS-11 Micro Satellite," 2011. [Online]. Available: https://www.kirtland.af.mil/Portals/52/documents/AFD-111103-035.pdf?ver=2016-06-28-110256-797

[13] Defense Advanced Research Projects Agency, "Orbital express fact sheet," 2007. [Online]. Available: https://upload.wikimedia.org/wikipedia/commons/7/78/Orbita_Express_fact_sheet.pdf

[14] ESA, "Fastrac." [Online]. Available: https://earth.esa.int/web/eoportal/satellite-missions/f/fastrac

[15] ——, "Tdx." [Online]. Available: https://earth.esa.int/web/eoportal/satellite-missions/t/tandem-x

[16] W. Xiang and J. L. Jorgensen, "Formation flying: A subject being fast unfolding in space." [Online]. Available: https://www.dlr.de/iaa.symp/Portaldata/49/Resources/dokumente/archiv5/0309P_WangXiang.pdf

[17] NASA, "Magnetospheric multiscale," 2015, press Kit. [Online]. Available: https://www.nasa.gov/sites/default/files/files/MMS_PressKit.pdf

[18] Z. Singleton, "AggieSat4 / Bevo-2 Orbital Debris Assessment Report (ODAR)," 2014. [Online]. Available: https://apps.fcc.gov/els/GetAtt.html?id=147772&x=

[19] NASA, "GRACE-FO Launch Press Kit," 2018. [Online]. Available: https://www.jpl.nasa.gov/news/press_kits/grace-fo/download/grace-fo_launch_press_kit.pdf

[20] B. Harvey, *China in space: the great leap forward*, 2nd ed. Springer, 2019.

[21] D. Galano, D. Jollet, K. Mellab, J. Villa, L. Penin, R. Rougeot, and J. Versluys, "Proba-3 precise formation flying mission," in *10th International Workshop on Satellite Constellations and Formation Flying*, 07 2019, doi : 10.1016/j.actaastro.2012.05.029.

[22] R. Burns, C. A. McLaughlin, J. Leitner, and M. Martin, "Techsat 21: formation design, control, and simulation," in *2000 IEEE Aerospace Conference. Proceedings (Cat. No.00TH8484)*, vol. 7, 2000, pp. 19–25 vol.7, doi : 10.1109/AERO.2000.879271.

[23] P. Ferguson, F. Busse, B. Engberg, M. TillersonNick, A. Richards, and R. Twiggs, "Formation flying experiments on the Orion-Emerald mission," 08 2001, doi : 10.2514/6.2001-4688.

[24] D. Escorial, I. Tourne, F. Reina, J. Gonzalo, and B. Garrido, "FUEGO: A dedicated constellation of small satellites to detect and monitor forest fires," *Acta Astronautica - ACTA ASTRONAUT*, vol. 52, pp. 765–775, 05 2003, doi : 10.1016/S0094-5765(03)00052-3.

[25] H. Lübberstedt, D. Koebel, F. Hansen, and P. Brauer, "MAGNAS-Magnetic Nanoprobe SWARM," *Acta Astronautica*, vol. 56, pp. 209–212, 01 2005, doi : 10.1016/j.actaastro.2004.09.030.

[26] B. Fejer, C. Swenson, and J. Sahr, "The ION-F Satellite Constellation Science Mission," in *EGS General Assembly Conference Abstracts*, ser. EGS General Assembly Conference Abstracts, Jan. 2002, p. 3316.

[27] C. Swenson and B. Fejer, "The Ionospheric Nanosatellite Formation, Exploring Space Weather," 2002. [Online]. Available: https://digitalcommons.usu.edu/cgi/viewcontent.cgi?article=1944&context=smallsat

[28] P. Duchon, "Max: Formation flying for nuclear astrophysics," *Experimental Astronomy*, vol. 20, pp. 483–495, 12 2005, doi : 10.1007/s10686-006-9070-1.

[29] M. Bavdaz, D. H. Lumb, and A. J. Peacock, "XEUS mission reference design," in *UV and Gamma-Ray Space Telescope Systems*, G. Hasinger and M. J. L. Turner, Eds., vol. 5488, International Society for Optics

and Photonics. SPIE, 2004, pp. 530 – 538, doi : 10.1117/12.552928. [Online]. Available: https://doi.org/10.1117/12.552928

[30] P. D'Arrigo and S. Santandrea, "APIES: A mission for the exploration of the main asteroid belt using a swarm of microsatellites," *Acta Astronautica*, vol. 59, no. 8-11, pp. 689–699, 2006, doi : 10.1016/j.actaastro.2005.07.011.

[31] E. Gill, M. Steckling, and P. Butz, "Gemini: A milestone towards autonomous formation flying," in *ESA Workshop on on-board Autonomy*, vol. 419. Noordwijk: ESTEC, 2001.

[32] A. Leger and T. Herbst, "DARWIN mission proposal to ESA," 2007. [Online]. Available: https://arxiv.org/abs/0707.3385

[33] M. Kirschner, O. Montenbruck, and S. Bettadpur, *Flight Dynamics Aspects of The GRACE Formation Flying*, Jan 2001. [Online]. Available: https://www.researchgate.net/publication/224782021_FLIGHT_DYNAMICS_ASPECTS_OF_THE_GRACE_FORMATION_FLYING

[34] C. P. Escoubet, M. Fehringer, and M. Goldstein, "The Cluster mission," *Annales Geophysicae*, vol. 19, p. 1197–1200, 2001, doi : 10.5194/angeo-19-1197-2001. [Online]. Available: https://www.researchgate.net/publication/234236368_The_Cluster_mission

[35] S. Bandyopadhyay, G. P. Subramanian, R. Foust, D. Morgan, S.-J. Chung, and F. Hadaegh, "A review of impending small satellite formation flying missions," *53rd AIAA Aerospace Sciences Meeting*, 2015, doi : 10.2514/6.2015-1623.

[36] E. Kyle, "2019 launch vehicle/site statistics," Dec 2019. [Online]. Available: https://www.spacelaunchreport.com/log2019.html

[37] ——, "2014 launch vehicle/site statistics," Dec 2014. [Online]. Available: https://www.spacelaunchreport.com/log2014.html

[38] ——, "2015 launch vehicle/site statistics," Dec 2015. [Online]. Available: https://www.spacelaunchreport.com/log2015.html

[39] ——, "2016 launch vehicle/site statistics," Dec 2016. [Online]. Available: https://www.spacelaunchreport.com/log2016.html

[40] ——, "2017 launch vehicle/site statistics," Dec 2017. [Online]. Available: https://www.spacelaunchreport.com/log2017.html

[41] ——, "2018 launch vehicle/site statistics," Dec 2018. [Online]. Available: https://www.spacelaunchreport.com/log2018.html

[42] S. Damico, E. Gill, and O. Montenbruck, "Relative Orbit Control Design for the PRISMA Formation Flying Mission," *AIAA Guidance, Navigation, and Control Conference and Exhibit*, 2006, doi : 10.2514/6.2006-6067.

[43] S. Damico, J.-S. Ardaens, and R. Larsson, "Spaceborne autonomous formation-flying experiment on the PRISMA mission," *Journal of Guidance, Control, and Dynamics*, vol. 35, no. 3, p. 834–850, 2012, doi : 10.2514/1.55638.

[44] S. D. Florio and S. D'Amico, "Optimal autonomous orbit control of remote sensing spacecraft," 2009.

[45] J. Mueller, J. Ziemer, R. Hofer, R. Wirz, and T. O'Donnell, "A survey of micro-thrust propulsion options for microspacecraft and formation flying missions," in *5th Annual CubeSat Developers Workshop San Luis Obispo, CA*, 2008.

[46] J. Atchison and M. Peck, "Length scaling in spacecraft dynamics," *Journal of Guidance, Control, and Dynamics*, vol. 34, pp. 231–246, 01 2011, doi : 10.2514/1.49383.

[47] H. Schaub and J. Junkins, *Analytical Mechanics of Space Systems*, ser. AIAA education series. American Institute of Aeronautics and Astronautics, Incorporated, 2014, doi : 10.2514/4.102400.

[48] K. Alfriend, S. R. Vadali, P. Gurfil, J. How, and L. Breger, *Spacecraft formation flying: Dynamics, Control and Navigation*. Elsevier, 2009, vol. 2, doi : 10.1016/C2009-0-17485-8.

[49] D. A. Vallado, *Fundamentals of astrodynamics and applications*. Springer Science & Business Media, 2001, vol. 12.

[50] Y. Kozai, "The motion of a close earth satellite," *The Astronomical Journal*, vol. 64, p. 367, 1959, doi : 10.1086/107957.

[51] D. Brouwer, "Solution of the problem of artificial satellite theory without drag," Yale Univ. New Haven CT. United States, Tech. Rep., 1959, doi : 10.1086/107958.

[52] H. G. Walter, "Conversion of osculating orbital elements into mean elements," *The Astronomical Journal*, vol. 72, p. 994, 1967, doi : 10.1086/110374.

[53] R. H. Lyddane, "Small eccentricities or inclinations in the brouwer theory of the artificial satellite," *The Astronomical Journal*, vol. 68, p. 555, 1963, doi : 10.1086/109179.

[54] H. Khalil, *Nonlinear Control, Global Edition*. Pearson Education Limited, 2015.

[55] R. G. Melton, "Time-explicit representation of relative motion between elliptical orbits," *Journal of Guidance, Control, and Dynamics*, vol. 23, no. 4, p. 604–610, 2000, doi : 10.2514/2.4605.

[56] S. A. Schweighart and R. J. Sedwick, "High-fidelity linearized J_2 model for satellite formation flight," *Journal of Guidance, Control, and Dynamics*, vol. 25, no. 6, p. 1073–1080, 2002, doi : 10.2514/2.4986.

[57] T. E. Carter, "New form for the optimal rendezvous equations near a keplerian orbit," *Journal of Guidance, Control, and Dynamics*, vol. 13, no. 1, pp. 183–186, 1990, doi : 10.2514/3.20533.

[58] K. Yamanaka and F. Ankersen, "New state transition matrix for relative motion on an arbitrary elliptical orbit," *Journal of Guidance, Control, and Dynamics*, vol. 25, no. 1, p. 60–66, 2002, doi : 10.2514/2.4875.

[59] H. Schaub, "Relative orbit geometry through classical orbit element differences," *Journal of Guidance, Control, and Dynamics*, vol. 27, no. 5, p. 839–848, 2004, doi : 10.2514/1.12595.

[60] H. Schaub and K. T. Alfriend, "J_2 invariant relative orbits for spacecraft formations," *Celestial Mechanics and Dynamical Astronomy*, vol. 79, no. 2, pp. 77–95, 2001, doi : 10.1023/A:1011161811472.

[61] D.-W. Gim and K. T. Alfriend, "State transition matrix of relative motion for the perturbed noncircular reference orbit," *Journal of Guidance, Control, and Dynamics*, vol. 26, no. 6, p. 956–971, 2003, doi : 10.2514/2.6924.

[62] D. Karaboga and B. Basturk, "A powerful and efficient algorithm for numerical function optimization: artificial bee colony (ABC) algorithm," *Journal of Global Optimization*, vol. 39, no. 3, pp. 459–471, Nov 2007, doi : 10.1007/s10898-007-9149-x. [Online]. Available: https://doi.org/10.1007/s10898-007-9149-x

[63] K. Deb, "An introduction to genetic algorithms," *Sadhana*, vol. 24, no. 4-5, pp. 293–315, 1999, doi : 10.1007/BF02823145.

[64] S. Sivanandam and S. Deepa, *Introduction to Particle Swarm Optimization and Ant Colony Optimization*. Berlin, Heidelberg: Springer Berlin Heidelberg, 2008, pp. 403–424, doi : 10.1007/978-3-540-73190-0_11.

[65] D. Karaboga and B. Basturk, "On the performance of artificial bee colony (ABC) algorithm," *Applied Soft Computing*, vol. 8, no. 1, pp. 687 – 697, 2008, doi : 10.1016/j.asoc.2007.05.007.

[66] A. Muthiah and R. Rajkumar, "A Comparison of Artificial Bee Colony algorithm and Genetic Algorithm to Minimize the Makespan for Job Shop Scheduling," *Procedia Engineering*, vol. 97, p. 1745–1754, 2014, doi : 10.1016/j.proeng.2014.12.326.

[67] V. R. Kulkarni and V. Desai, "ABC and PSO: A comparative analysis," in *2016 IEEE International Conference on Computational Intelligence and Computing Research (ICCIC)*, 2016, pp. 1–7, doi : 10.1109/ICCIC.2016.7919625.

[68] D. Scharf, F. Hadaegh, and S. Ploen, "A survey of spacecraft formation flying guidance and control. part ii: control," *Proceedings of the 2004 American Control Conference*, 2004, doi : 10.23919/acc.2004.1384365.

[69] P. Wang, F. Hadaegh, and K. Lau, "Synchronized formation rotation and attitude control of multiple free-flying spacecraft," *Journal of Guidance Control and Dynamics*, vol. 22, 01 1999, doi : 10.2514/2.4367.

[70] M. Mesbahi and F. Y. Hadaegh, "A robust control approach for the formation flying of multiple spacecraft," *1999 European Control Conference (ECC)*, 1999, doi : 10.23919/ecc.1999.7099774.

[71] V. Manikonda, P. O. Arambel, M. Gopinathan, R. K. Mehra, and F. Y. Hadaegh, "A model predictive control-based approach for spacecraft formation keeping and attitude control," in *Proceedings of the 1999 American Control Conference (Cat. No. 99CH36251)*, vol. 6, 1999, pp. 4258–4262 vol.6.

[72] A. Robertson, G. Inalhan, and J. P. How, "Formation control strategies for a separated spacecraft interferometer," in *Proceedings of the 1999 American Control Conference (Cat. No. 99CH36251)*, vol. 6, 1999, pp. 4142–4147 vol.6.

[73] F. Bauer, J. Bristow, D. C. Folta, K. Hartman, D. Quinn, and J. How, *Satellite formation flying using an innovative autonomous control system (AutoCon) environment*, doi : 10.2514/6.1997-3821. [Online]. Available: https://arc.aiaa.org/doi/abs/10.2514/6.1997-3821

[74] D. C. Folta, L. Newman, and T. Gardner, *Foundations of formation flying for Mission to Planet Earth and New Millennium*, doi : 10.2514/6.1996-3645. [Online]. Available: https://arc.aiaa.org/doi/abs/10.2514/6.1996-3645

[75] D. C. Folta and D. Quinn, "A 3-D method for autonomously controlling multiple spacecraft orbits," in *1998 IEEE Aerospace Conference Proceedings (Cat. No.98TH8339)*, vol. 1, 1998, pp. 51–60 vol.1, doi: 10.1109/AERO.1998.686672.

[76] H. Liu, J. Li, and B. Hexi, "Sliding mode control for low-thrust Earth-orbiting spacecraft formation maneuvering," *Aerospace Science and Technology*, vol. 10, no. 7, pp. 636 – 643, 2006, doi : 10.1016/j.ast.2006.04.008. [Online]. Available: http://www.sciencedirect.com/science/article/pii/S1270963806000848

[77] D. C. Redding, N. J. Adams, and E. T. Kubiak, "Linear-quadratic stationkeeping for the STS orbiter," *Journal of Guidance, Control, and*

Dynamics, vol. 12, no. 2, pp. 248–255, 1989, doi : 10.2514/3.20398. [Online]. Available: https://doi.org/10.2514/3.20398

[78] A. Sparks, *Linear control of satellite formation flying*, doi : 10.2514/6.2000-4438.

[79] S. Starin, A. Sparks, and R. Yedavalli, *Spacecraft formation flying maneuvers using linear-quadratic regulation with no radial axis inputs*, doi : 10.2514/6.2001-4029. [Online]. Available: https://arc.aiaa.org/doi/abs/10.2514/6.2001-4029

[80] L. Breger and J. P. How, "Gauss's Variational Equation-Based Dynamics and Control for Formation Flying Spacecraft," *Journal of Guidance, Control, and Dynamics*, vol. 30, no. 2, pp. 437–448, 2007, doi : 10.2514/1.22649. [Online]. Available: https://doi.org/10.2514/1.22649

[81] H. Schaub and K. T. Alfriend, "Impulsive feedback control to establish specific mean orbit elements of spacecraft formations," *Journal of Guidance, Control, and Dynamics*, vol. 24, no. 4, pp. 739–745, 2001, doi : 10.2514/2.4774. [Online]. Available: https://doi.org/10.2514/2.4774

[82] Y. Choi, S. Mok, and H. Bang, "Impulsive formation control using orbital energy and angular momentum vector," *Acta Astronautica*, vol. 67, no. 5, pp. 613 – 622, 2010, doi : 10.1016/j.actaastro.2010.04.008. [Online]. Available: http://www.sciencedirect.com/science/article/pii/S0094576510001256

[83] J. Scharnagl, P. Kremmydas, and K. Schilling, "Model predictive control for continuous low thrust satellite formation flying," *IFAC-PapersOnLine*, vol. 51, no. 12, pp. 12 – 17, 2018, iFAC Workshop on Networked Autonomous Air Space Systems NAASS 2018 doi : 10.1016/j.ifacol.2018.07.081. [Online]. Available: http://www.sciencedirect.com/science/article/pii/S2405896318308243

[84] E. N. Hartley, P. A. Trodden, A. G. Richards, and J. M. Maciejowski, "Model predictive control system design and implementation for spacecraft rendezvous," *Control Engineering Practice*, vol. 20, no. 7, pp. 695 – 713, 2012, doi : 10.1016/j.conengprac.2012.03.009. [Online]. Available: http://www.sciencedirect.com/science/article/pii/S0967066112000664

[85] G. Inalhan, M. Tillerson, and J. P. How, "Relative dynamics and control of spacecraft formations in eccentric orbits," *Journal of Guidance, Control, and Dynamics*, vol. 25, no. 1, pp. 48–59, 2002, doi : 10.2514/2.4874. [Online]. Available: https://doi.org/10.2514/2.4874

[86] B. Kouvaritakis and M. Cannon, "Model predictive control," *Switzerland: Springer International Publishing*, 2016.

[87] A. S. Yamashita, P. M. Alexandre, A. C. Zanin, and D. Odloak, "Reference trajectory tuning of model predictive control," *Control Engineering Practice*, vol. 50, pp. 1 – 11, 2016, doi : 10.1016/j.conengprac.2016.02.003. [Online]. Available: http://www.sciencedirect.com/science/article/pii/S0967066116300168

[88] M. Tavakoli and N. Assadian, "Model predictive orbit control of a low earth orbit satellite using gauss's variational equations," *Proceedings of the Institution of Mechanical Engineers, Part G: Journal of Aerospace Engineering*, vol. 228, pp. 2385 – 2398, 2014.

[89] A. Bemporad, L. Chisci, and E. Mosca, "On the stabilizing property of SIORHC," *Automatica*, vol. 30, no. 12, pp. 2013 – 2015, 1994, doi : 10.1016/0005-1098(94)90064-7. [Online]. Available: http://www.sciencedirect.com/science/article/pii/0005109894900647

[90] B. Akay and D. Karaboga, "Parameter tuning for the artificial bee colony algorithm," in *Computational Collective Intelligence. Semantic Web, Social Networks and Multiagent Systems*, N. T. Nguyen, R. Kowalczyk, and S.-M. Chen, Eds. Berlin, Heidelberg: Springer Berlin Heidelberg, 2009, pp. 608–619.

[91] M. Mahooti, "High precision orbit propagator," 2020, MATLAB Central File Exchange. Retrieved July 23, 2020. [Online]. Available: https://www.mathworks.com/matlabcentral/fileexchange/55167-high-precision-orbit-propagator

[92] D. Karaboga and B. Basturk, "Artificial Bee Colony (ABC) Optimization Algorithm for Solving Constrained Optimization Problems," in *Foundations of Fuzzy Logic and Soft Computing*, P. Melin, O. Castillo, L. T. Aguilar, J. Kacprzyk, and W. Pedrycz, Eds. Berlin, Heidelberg: Springer Berlin Heidelberg, 2007, pp. 789–798, doi : 10.1007/978-3-540-72950-1_77.

[93] Yue Hang, G. Xu, D. Wang, and Eng Kee Poh, "Comparison study of relative dynamic models for satellite formation flying," in *2008 2nd International Symposium on Systems and Control in Aerospace and Astronautics*, 2008, pp. 1–6, doi : 10.1109/ISSCAA.2008.4776195.

[94] O. E. Ramos, "A Comparison of Feedback Linearization and Sliding Mode Control for a Nonlinear System," in *2019 IEEE Sciences and Humanities International Research Conference (SHIRCON)*, 2019, pp. 1–4, doi : 10.1109/SHIRCON48091.2019.9024871.

[95] D. Lee, H. Jin Kim, and S. Sastry, "Feedback linearization vs. adaptive sliding mode control for a quadrotor helicopter," *International Journal of Control, Automation and Systems*, vol. 7, no. 3, pp. 419–428, Jun 2009, doi : 10.1007/s12555-009-0311-8. [Online]. Available: https://doi.org/10.1007/s12555-009-0311-8

[96] R. Schwarz, "Cartesian state vectors to keplerian orbit elements," 2017. [Online]. Available: https://downloads.rene-schwarz.com/download/M002-Cartesian_State_Vectors_to_Keplerian_Orbit_Elements.pdf

[97] ——, "Keplerian orbit elements to cartesian state vectors," 2014. [Online]. Available: https://downloads.rene-schwarz.com/download/M001-Keplerian_Orbit_Elements_to_Cartesian_State_Vectors.pdf